Identification of Candidate Biomarkers by Combining Laser Capture Microdissection and Mass Spectrometry

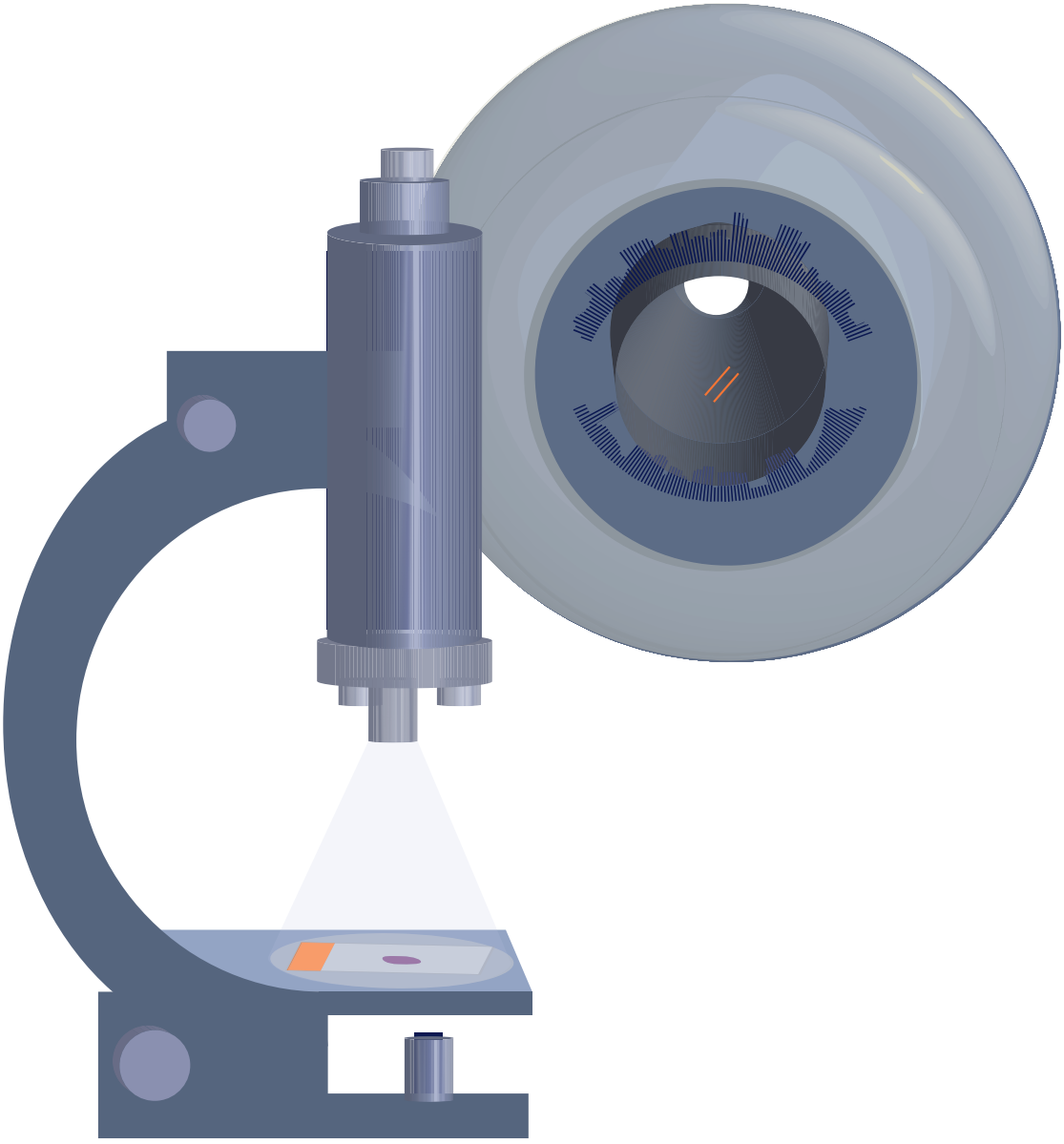

Coşkun Güzel

Identification of Candidate Biomarkers by Combining Laser Capture Microdissection and Mass Spectrometry

Coşkun Güzel

The financial support for the printing of this thesis was kindly provided by the Erasmus MC, Rotterdam, the Netherlands.

ISBN: 978-94-6380-971-9
Cover design & layout by: Fenna Schaap (www.fennaschaap.nl)
Printed by: ProefschriftMaken
eBook: https://www.globalacademicpress.com/ebooks/coskun_guzel/

Identification of Candidate Biomarkers by Combining Laser Capture Microdissection and Mass Spectrometry

Identificatie van kandidaat-biomarkers door de combinatie van laser capture microdissectie en massaspectrometrie

Proefschrift

ter verkrijging van de graad van doctor aan de
Erasmus Universiteit Rotterdam
op gezag van de rector magnificus
Prof. dr. R.C.M.E. Engels
en volgens het besluit van het College voor Promoties.
De openbare verdediging zal plaatsvinden op

woensdag 7 oktober 2020 om 15:30 uur

door

Coşkun Güzel

geboren te Çayıralan, Turkije

Erasmus University Rotterdam

Promotiecommissie

Promotoren
Prof. dr. P.A.E. Sillevis Smitt
Prof. dr. E.A.P. Steegers

Overige leden
Prof. dr. J.M. Kros
Prof. dr. ir. G. W. Jenster
Prof. dr. S.A. Scherjon

Co-promotor
Dr. T.M. Luider

Table of contents

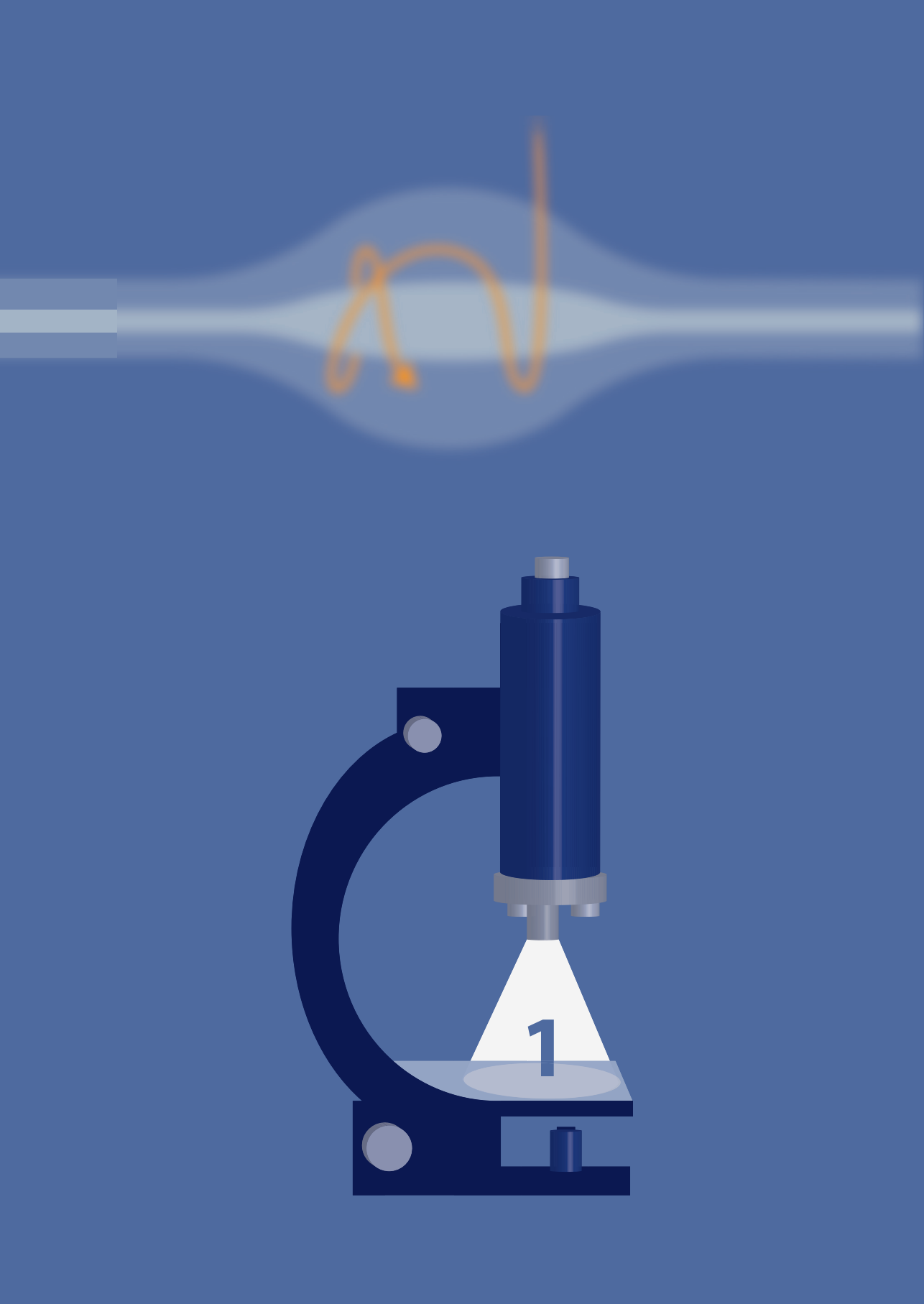
1

Chapter 1
General introduction

Adapted from:

Coşkun Güzel, Christoph Stingl, Frank Klont, Roel Tans, Esther Willems, Rainer Bischoff, Alain J. van Gool, Theo M. Luider, and the Biomarker Development Center Consortium. *Parts of this chapter have been published for a book entitled 'Targeted Proteomics for Absolute Quantification of Protein Biomarkers in Serum and Tissues' in the series Handbook for Biomarkers in Precision Medicine (CRC Press). In press April 2019.*

Treatment of a disease would be most probably more successful if the onset of the disease is diagnosed before clinical manifestation. Unsuccessful treatment can be a result of late diagnosis (1, 2). In this thesis, we choose a method to analyze affected tissue to find potential biomarker candidates and subsequently focus on these biomarkers in body fluids.

In biomarker analysis different molecular-based assays are used, e.g. ligand binding assays (LBAs) and enzyme-linked immunosorbent assays (ELISAs). Advantages of immunoassay technology are the high selectivity and sensitivity (e.g., plasma detection limits in the low pictograms per milliliter range) (3) and the ease with which they can be performed in a high-throughput format. However, immunoassays have limitations such as the high development cost for sensitive and well-characterized antibodies as well as cross-reactivity with other proteins or interference from other ligands bound to the target protein (4). In most cases, the primary structure of the antibody is not available (5). Although multiplexing is possible with immunoassays (e.g. flow cytometry), analytical quality generally suffers from applicability issues because the analytical conditions need to be a compromise between the reagents of all components of a multiplex set (6, 7). Most importantly, the often-limited specificity of antibodies that are crucial components of immunoassays limits their use in biomarker analysis, which requires optimal specificity in addition to sensitivity. In many cases, differential behavior of protein biomarkers cannot be confirmed in follow-up studies (8) and requires a more robust analytical method to quantify these target proteins.

Mass spectrometry (MS) has emerged as an alternative analytical method to quantify proteins and protein isoforms (including splice variants). Protein analysis favors the use of liquid chromatography (LC) coupled with MS, based on well-established ionization principles. The various proteomics methods can roughly be classified in bottom-up proteomics (focusing on identification of protein fragments following proteolytic digestion), top-down proteomics (focusing on intact proteins), and targeted proteomics (focusing on quantifying preselected peptides or proteins). The latter has received much attention for biomarker analysis, validation, and further evaluation (9, 10).

In this thesis we describe the advantages of using laser capture microdissection combined with MS technology to find potential candidate biomarkers for diagnostic and prognostic purposes in two diseases, preeclampsia and cervical cancer. We present both a bottom-up and a targeted proteomics technique using affected tissue followed by validation in biomaterial for preeclampsia and cervical cancer, respectively (Figure 1).

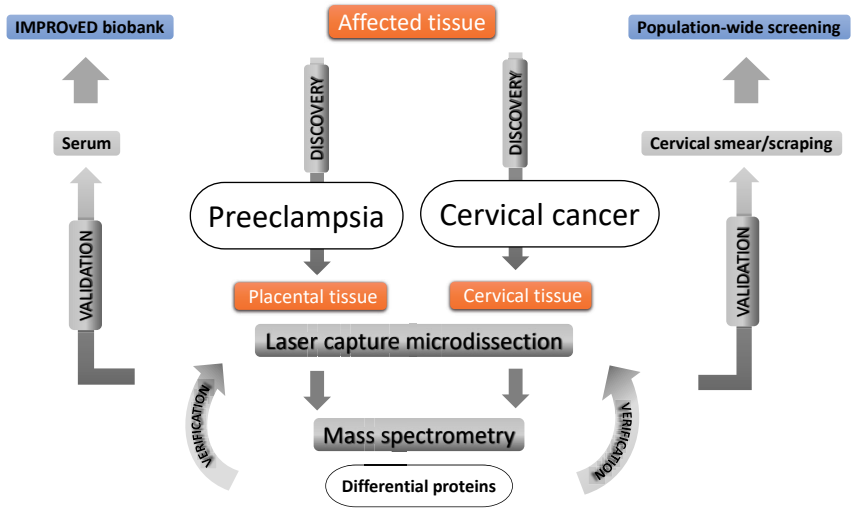

Figure 1. The proteomics workflow for biomarker discovery and validation for two examples, preeclampsia and cervical cancer. IMPROvED=Improved Pregnancy Outcomes by Early Detection (11).

1.1 Preeclampsia

Preeclampsia is one of the four hypertensive pregnancy disorders that is accompanied by high blood pressure (≥140/90 mmHg) and proteinuria (≥0.3 gram/24 hour) after 20 weeks of gestation (Figure 2) (12).

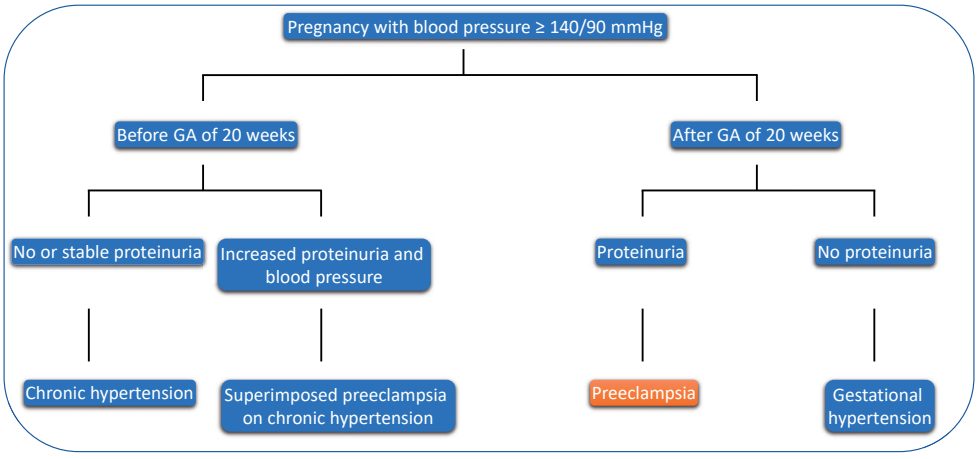

Figure 2. The diagnosis of preeclampsia among hypertensive disorders in pregnant women. GA=gestational age.

The exact cause of preeclampsia is unknown, but it is thought to be related to reduced blood flow and reduced trophoblast cell invasion into the decidua and myometrium, which leads to placental dysfunction. In preeclamptic women, the endovascular remodeling and invasion of the spiral arteries are incomplete, which results in reduced and irregular placental perfusion (13). Notably, for preeclamptic placenta syncytial knots of trophoblast cells that are surrounded on chorion villi are observed compared to at term control placenta (Figure 3) (14, 15).

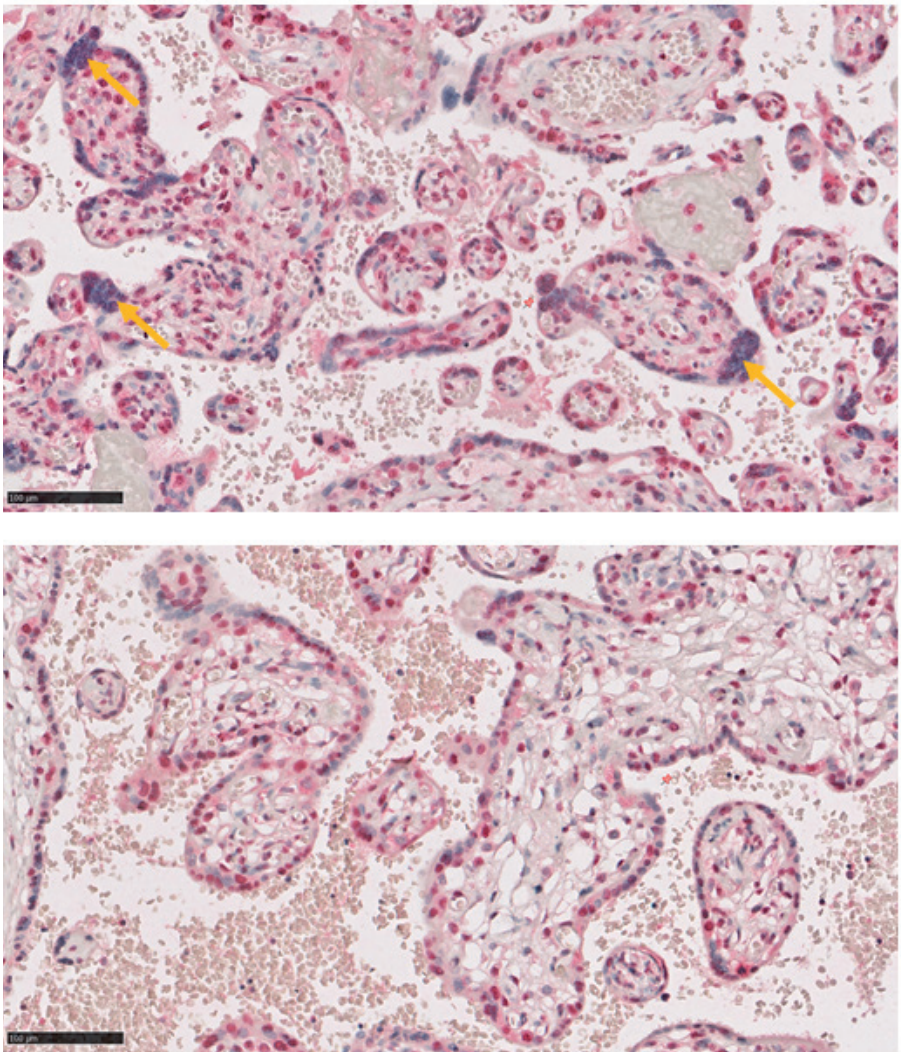

Figure 3. *S100A6* staining of syncytial knots (indicated with arrows) of trophoblast cells typically observed in placental tissue from a preeclampsia patient shown in the top panel, and from a healthy pregnant woman in the lower panel.

Several angiogenic factors such as VEGF, PIGF, endoglin, sFlt-1, sEng that might be involved in preeclampsia have been described in literature (16). However, none of these factors was used to diagnose preeclampsia before the disease was clinically manifest. A variety of interventions (e.g., rest, exercise, reduced salt intake, antioxidants) to prevent and to manage preeclampsia showed insufficient evidence to be recommended (17).

1.2 Cervical cancer

Cervical cancer is a disease that is caused by infection (99%) of different types of human papillomaviruses (HPV). Despite population-wide screening and vaccination programs in developed countries, cervical cancer is still the fourth most common female cancer in the world. HPV-types 16-18 are responsible for 70% of all cervical cancer starting with precancerous stages, also known as cervical intraepithelial neoplasia (CIN) lesions (Figure 4).

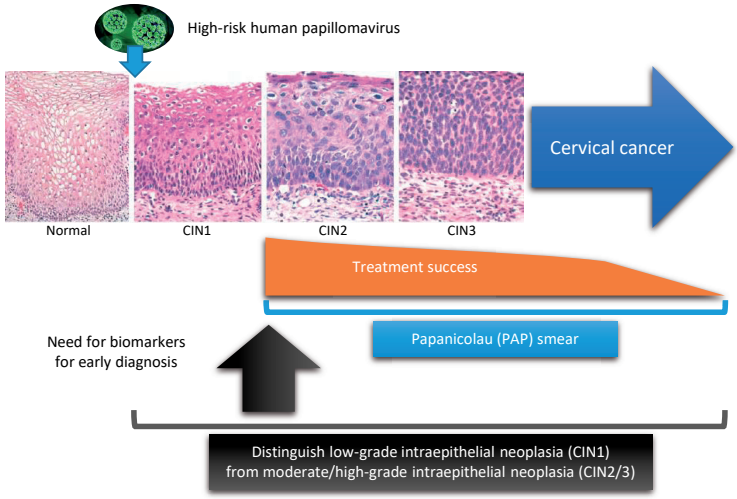

Figure 4. Progression of cervical cancer development from normal to invasive CIN3 after high-risk HPV (hrHPV) infection into cervical cancer. Women with CIN1 diagnosis is usually left untreated. The treatment of most women with CIN2 diagnosis can be successful and may further decrease in the more severe stages.

On a morphological level, the progression from healthy cervical tissue via the well-defined precancerous lesions of mild (CIN1), to moderate neoplastic (CIN2) to severe neoplastic (CIN3) lesions followed by (metastasized) cervical cancer can be well-distinguished (18). In most cases, CIN2+ lesions will progress to cancer if left untreated, and CIN1 will revert to normal without any treatment. Therefore, there is a medical need for effective biomarkers to detect cervical cancer in early stage CIN1 accurately in, for example, cervical smear or scraping material.

Currently, the PAP smear test (cells that are taken from the uterine cervix for cytological analysis) is used worldwide to detect cell abnormalities in an early stage. A high-risk HPV (hrHPV) screening test in which DNA of the virus is detected is used serial or parallel to the cytology test. Current screening test to diagnose cervical cancer at an early stage (CIN2+) of the disease shows low sensitivity of ~50% for cytology-based testing and specificity of ~85% for hrHPV testing as shown in Figure 5 (19, 20). Combining both tests (co-testing), higher specificity, and sensitivity (exact values are not known) can be reached. However, it is still far from ideal. In the Netherlands approximately 800,000 women are yearly invited for screening, in which 60% are attending, and 48,000 diagnosed positive for a CIN lesion. One percent is diagnosed with CIN2+ (i.e., grade 2 or worse), the cut-off for the risk of developing cancer, because most CIN1 lesions regress to normal (~9%). Women who are negatively diagnosed for hrHPV are asked to return five years later (Figure 5) (20-22).

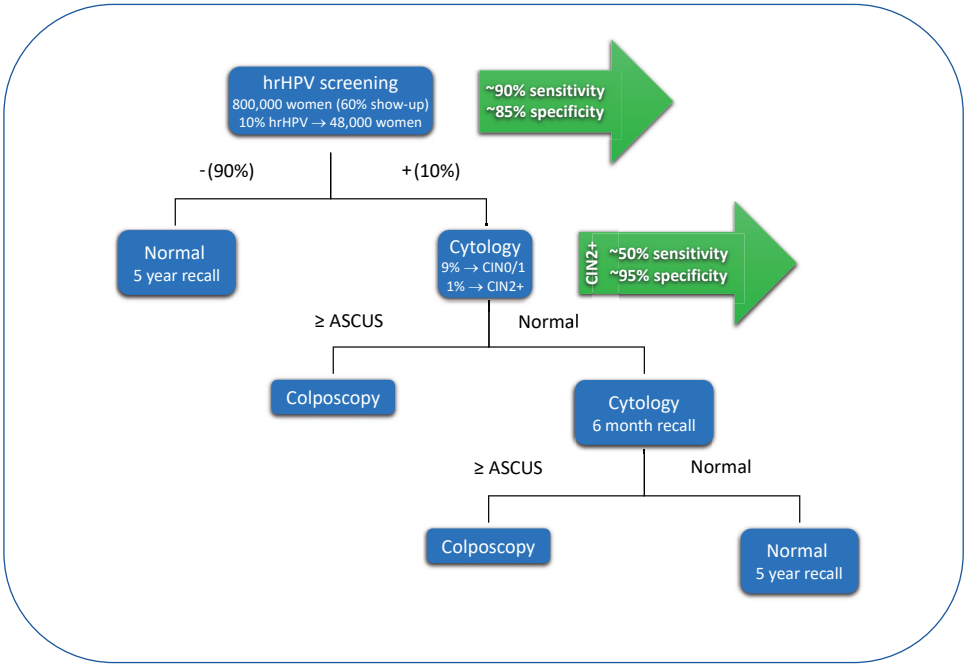

Figure 5. Flow chart of Dutch population-based screening for cervical cancer (2018). ASCUS=Atypical Squamous Cells of Undetermined Significance.

Only hrHPV-positive women will be invited for follow-up testing using conventional cytology-based PAP smear tests. Many women will show false-positive test results which will lead to unnecessary referrals (~66%), anxiety, and higher costs for the health-care system (20,

23-25). To reduce the risk of developing cervical cancer, several countries, including the Netherlands have started with hrHPV vaccination programs in young women. This vaccine will only protect against hrHPV-16 and 18 (covering 70% of the infections) and will, therefore, not prevent all hrHPV-induced cervical cancers. The population-wide screening will remain necessary to be analyzed in the coming decades to demonstrate the effectiveness of these vaccine programs.

1.3 Shotgun/bottom-up proteomics

In this thesis we describe the detection of proteins by shotgun proteomics applied on affected cells in tissue obtained from placenta of preeclampsia patients presented in our study (26) and cervical cancer tissue (**Chapter 6**). In this proteomics workflow proteolytic-peptides are matched with a protein database and eventually identified. Most of the peptides produced by this workflow have a length in a range of 4–26 amino acids. This length corresponds to a mass range of approximately 450–3000 Da, which is ideal for analysis with MS. We hypothesized that differential proteins might be found in comparing diseased and non-diseased (healthy) tissue and that a part of these differential proteins can also be found in biofluids.

1.4. Laser capture microdissection

To reduce complexity and to minimize covering by high abundant proteins in biofluids we considered another method for analyzing proteomes on tissue level as the starting point to find differentially expressed proteins. Laser capture microdissection (LCM) is a technique that has been used successfully as a tool for the isolation of cells (27-31). Cells are dissected on a microscopic scale with a laser beam (infrared or ultraviolet) to collect biological material and subsequently used in proteomics and genomics platforms. With the laser beam cells are excised from a defined area into a collection tube. Well-defined regions of cells can be selected precisely (<1 µm) and visualized by a microscope. LCM is utilized to extract precisely the cells or tissue structures of interest and has the possibility to collect the volume of tissue for comparison accurately. A disadvantage of this approach is the more time-consuming nature of this technology compared to whole extraction of tissue, notably when a large number of cells (i.e. >5,000 cells) is required to be collected per sample. Proteins can be lost during processing procedures such as fixation and staining. Moreover, commercial LCM devices are not able to keep cryosections at low temperature during microdissection (not applicable for paraffinized tissue). LCM approach can be very challenging due to the minimal amount of tissue available for analysis. For example, we showed by peptide sequencing the identification of proteins characteristic for preeclampsia using a few hundred cells (26). A few thousand proteins can be identified from about 8,000 isolated cells from cervical tissue (**Chapter 6**). A successful LCM approach relies on the accurate capturing of cells or tissue structures that are readily distinguishable from surrounding cells, and that is sensitive enough to measure proteins at nanograms level.

1.5 Selected and Parallel Reaction Monitoring mass spectrometry

In the field of targeted proteomics Selected Reaction Monitoring (SRM) has emerged as the most widely used experimental MS approach to quantify peptides in biological samples and thereby determine corresponding protein levels (32-37). However, interferences in complex biological samples often limit sensitivity in comparison with immunoassays unless appropriate sample preparation is performed (38-40). Co-eluting peptides with a precursor ion mass close to the peptide of interest may result in fragment ions that overlap with the targeted transitions, resulting in considerable chemical noise. Such noise limits the sensitivity of detection and contributes to diminished accuracy and precision. Besides, it is challenging to quantify low levels of proteins in biological samples like serum or tissue due to the limited sensitivity and dynamic range of MS detectors and finite loading capacity of LC columns as well as insufficient resolution for separating interfering compounds.

Parallel Reaction Monitoring (PRM) using high-resolution MS goes beyond SRM. It provides data with higher mass accuracy (41, 42), thus reducing interferences caused by co-eluting compounds with similar but not identical mass transitions (41, 43, 44). The higher selectivity allows covering a wider dynamic concentration range (41). Moreover, PRM methods for individual peptides are easier to set up because all transitions are monitored. Optimal transitions in terms of sensitivity and specificity can be retrieved and combined *in silico* after analysis (45). Literature on PRM shows the feasibility of the approach for quantification of proteins in complex biological samples after proteolytic digestion (43, 46, 47). Notably, Domon and coworkers published on the use of PRM in large-scale experiments (48-51). However, reaching the nanograms per milliliter level in body fluids without using affinity binders (e.g., immunoglobulins) remains a challenge also for PRM approaches. Measuring low protein levels (nanograms per milliliter) in trypsin-digested and fractionated serum in a reproducible manner is possible (44). As an example (**Chapter 5**), we targeted *HSP90α,* a protein that is up-regulated in various cancers and is thus pursued as a target for anticancer therapy (52, 53). We compared the concentration of *HSP90α* in 43 sera from healthy subjects measured by SRM, by PRM and by a commercially available ELISA concerning their comparability, repeatability, and sensitivity (44). In this study we demonstrated a reproducible, robust, and sensitive PRM assay to determine *HSP90α* concentrations in strong cation exchange (SCX)-fractionated sera at low nanograms per milliliter levels. The sensitivity of the PRM assay aligned with data obtained by ELISA and showed better repeatability. In SRM and especially PRM, the quality of measurement can easily be assessed by an aberrant ratio between transitions. In ELISA results caused by aberrations in the assay are much more difficult to recognize as outliers. If fractionation of biological samples is technically feasible, PRM can be used as an attractive alternative to immunoassays to quantify multiple proteins at the nanograms per milliliter level in complex protein mixtures, including serum. The major analytical advantages of MS include the more specific detection and the excellent

technical reproducibility that can be reached (coefficient of variation (CV) lower than 5%). Reaching picograms per milliliter levels of biofluid remains challenging by PRM, although it highly depends on sample preparation.

To use PRM and SRM peptides of interest ought to be chosen according to a set of criteria. The peptides selected must be unique for the protein targeted (proteotypic peptides) and the peptide must not be too short (less than seven amino acids) or too long (more than 20 amino acids) to prevent loss of specificity and sensitivity, respectively. One should avoid ragged ends that could lead to partial enzymatic digestion and, ideally, they should contain no amino acids that are prone to chemical modifications, such as oxidation (methionine, histidine, tryptophan moieties), deamidation (asparagine, glutamine residues), or N-terminal cyclization of glutamine and glutamate and N-terminal carboxymethylation of cysteine. Moreover, N- and C-terminal peptides are in general more prone to degradation and should be avoided if possible. Additionally, one should be aware of protein-specific amino acid polymorphisms, post-translational modifications (e.g., methylation, phosphorylation, glycosylation), and other natural variants resulting in different proteoforms. Publicly available databases such as the SRMAtlas compendium (http://www.srmatlas.org), Uniprot, ENSEMBLE or dbsnip are imperative in that respect. Most software programs (e.g., Skyline) incorporate build-in libraries and filters to exclude peptides with specific amino acids features, as outlined above, to facilitate target selection. Nonetheless, unexpected modification or loss of peptides due to natural cleavage or degradation of protein subunits can introduce aberrant ratios between peptides within one protein. It is therefore encouraged to select at least two peptides per protein for adequate quantification and the use of corresponding recombinant proteins if possible (36, 54).

1.5.1 Sample preparation

Sample preparation for analysis both in SRM and PRM remains a point of specific concern. Most often, sample preparation is performed stepwise: lysis and denaturation; followed by reduction and alkylation of sulfhydryl (thiol) groups; and finally, proteolytic (predominately tryptic) digestion. Because the peptides targeted by PRM and SRM are mostly selected in such a way that sulfhydryl groups are not present in these peptides, it is not necessary to use reducing and alkylation reagents that may produce adverse effects. Undesired side reactions with an alkylating reagent (e.g. iodoacetamide) can occur. Additionally, without enrichment both methodologies generally remain less sensitive as compared with immunoassays. The combination of highly selective MS with an affinity purification to obtain optimal sensitivity would be a golden combination. Several possibilities exist using various binders, e.g. antibodies (including Stable Isotope Standards and Capture by Anti-Peptide Antibodies (SISCAPA)) and affimers. In general, without sample fractionation both SRM and PRM can reach micrograms protein of interest per milliliter serum. However, with sample fractionation affinity enrichment by antibodies or different separations (e.g., ion

exchange columns or metal bound chromatography (such as Ni^{2+}-IMAC, TiO_2)) sensitivities of nanograms per mL serum (44, 55, 56) or nanograms per gram of total protein in tissue can be reached (57, 58).

1.6 Absolute quantitation

Stable isotope-labeled peptides are essential references for targeted MS to obtain absolute quantitation and reliability of the measurements performed. We can divide the function of these stable isotope-labeled peptides in two directions: (1) correction for variation introduced, for instance, by the matrix of a patient sample; and (2) calibrants to correct for non-linearity. The use of references for bioassays is described in detail by the FDA (http://www.fda.gov) and in the EMI guidelines (http://www.ema.europa.eu). These reference peptides give information about analytical performance (recovery and reproducibility) (59, 60).

Stable isotope-labeled peptides can be added in various steps of sample preparation during the method development to provide detailed information for each stage and potential problems that may occur. Ideally, the stable isotope-labeled peptide is spiked at the start of the sample preparation but not necessarily. Nonspecific cleavage during digestion can be assessed to a certain level by adding peptides with specific enzyme cleavage sites. There may be biological reasons that spiking of the references can be difficult, for instance, due to the presence of enzymatic activity affecting the spiked peptide or a sample preparation step aiming to remove small molecules (e.g., precipitation). Most ideally, the protein of interest is spiked as a stable isotope-labeled protein; this is often difficult and expensive to realize, and even recombinant proteins are chemically not precisely comparable to endogenous proteins in a complex sample environment. This problem, obtaining the ideal reference standard, is comparable to immunoassay techniques and it is not specific for MS. MS gives the possibility to standardize in a specific way because more than one peptide of a protein can be selected and a thorough assessment for correct measurement among the different peptides can be performed. The use of pure endogenous proteins or corresponding recombinant proteins can help considerably in that respect. In complex samples, such as serum and tissue, one observes that disagreements between peptides for the same protein can exist. However, after additional sample preparation these measurements often align much better, but not always. The use of a quantifying peptide and a qualifier peptide cannot solve the gap between peptides from the same protein. The ultimate problem is that if sample preparation cannot reduce the complexity of the peptide or protein mixture significantly, quantitative results are less accurate.

The signal-to-noise ratio of SRM and PRM measurements depends on the quadrupole characteristics. In quadrupoles of different vendors, mass windows may be adjusted to different mass widths (ranging from 0.2 to 2 *m/z*) that have a pronounced effect on sensitivity and selectivity. One can imagine that, if the mass window is too wide, many interfering

compounds will pass the quadrupole, generating possibly interfering fragment ions. However, if the window of the quadrupole is too small, fewer ions will pass, and sensitivity will suffer. Because the quadrupole window has a large effect on the signal-to-noise characteristics of measurements, the combination of a high-resolution mass analyzer for the fragment ions with a quadrupole mass filter for precursor ion selection can significantly improve selectivity by reducing chemical noise without necessarily decreasing sensitivity. An optimal width of the quadrupole settings with high-resolution fragment ion analysis will decrease the lower limit of detection significantly.

The analysis of SRM and PRM data can be performed in a dedicated program such as Skyline software (61). For correct annotation and integration of the peaks manual inspection is still recommended after automatic data processing. For assessment of a larger number of samples, specific algorithms can be used to streamline this process. The Skyline software is supported by all major MS vendors and is maintained and kept at a continuously high level.

1.7 Future perspectives in multiplexing in targeted proteomics

SRM and PRM have the potential to measure and quantify multiple proteins of interest (up to ~100 peptides per run) including specific mutations and modifications without using antibodies. As such, it has matured to a powerful method for specific analysis of protein and peptide biomarkers. For serum proteins in the micrograms per milliliter range, this has been illustrated by the Borchers group that developed a 30-min targeted MS method to quantify 67 plasma proteins in several clinical studies (62).

A further innovation is needed to apply SRM and PRM to a large number of samples in routine diagnostic laboratories and population studies. Preferably, in a bioassay the measurement of a sample should take only a few minutes per sample. SRM or PRM protein measurements may be performed in a few minutes in exceptional cases. However, longer time frames of up to 1 hour exist, which is much longer than compared with immunoassays with a low minute scale per analysis. Immunoassays can be applied in automated high-throughput technology. Technically, MS can measure on a second-minute timescale. However, in a multiplex analysis of multiple peptides, chromatography remains the bottleneck concerning increasing throughput. In contrast, in SRM mode the dwell time (the duration in which each *m/z* ion signal is collected) can become a limiting factor. Technically and theoretically improvement in throughput might be achievable based on robust, fast and parallelized chromatography approaches (63) benefiting the multiplex possibility of this technique.

Recently, profiling of mass peaks by data-independent acquisition (DIA) MS received quite some interest (64). Using this approach in which the precursor isolation window is typically 20-25 Da, biological samples are profiled in an unbiased manner, usually using ultra-high resolution QTOF mass spectrometers, yielding a data-rich profile of tryptic peptides.

Through a subsequent data-dependent acquisition (DDA), one can focus on a predefined set of peptide biomarkers. This avoids the time- and labor-intensive step of peptide-specific assay development, as discussed above in SRM and PRM. The same laboratory workflow is used for analysis of samples from the same matrix. For comparative studies this is a potentially powerful approach. However, DIA-DDA MS will only provide semi-quantitative data at best, so it is currently unsuitable for absolute quantitation of biomarker peptides. Further innovation is needed through a combination of DIA-DDA MS with multiplex labeling techniques to fully realize the potential of MS as a high-throughput, multiplex analytical technique. Although this may come at the cost of increased complexity, decreased sensitivity, and higher costs, it might open alternative avenues for clinically applicable quantification of multiple proteins in complex clinical samples.

Scope of this thesis

This thesis describes a method to use affected tissue as a source to find potential biomarker candidates that may be used diagnostically in biofluids and for biochemical knowledge. As a proof of principle, two examples are used (preeclampsia and cervical cancer) by using laser capture microdissection to isolate relevant cells. After verification in relevant tissue we developed a targeted mass spectrometric assay to quantify and validate serum from women who were diagnosed with preeclampsia and in tissue material obtained from women with a risk to develop cervical cancer.

In **Chapter 2**, we investigated whether it was possible to quantify proteins at the cellular level in FFPE placenta of preeclamptic patients. We described a targeted MS approach to quantify calcyclin (*S100A6*) that was differentially found in preeclampsia. Laser capture microdissected placental FFPE tissue from preeclampsia patients were compared with women with preterm delivery. We showed that targeted MS of laser microdissected material from formalin-fixed paraffin-embedded tissue resulted in finding higher *S100A6* levels in placental trophoblast cells from preeclamptic patients compared to trophoblast cells from control pregnants.

In **Chapter 3**, we confirmed the observation mentioned in Chapter 2 with immuno-histochemistry in a larger cohort**.** This confirmation was performed on formalin-fixed paraffin-embedded placental tissue. *S100A6* expression was blindly compared between women with early-onset preeclampsia and non-hypertensive controls. Significantly more *S100A6* staining was present in trophoblast cells from early-onset preeclamptic patients compared to trophoblast cells from control pregnants.

In **Chapter 4**, based on our research on placental tissue we hypothesized that protein *S100A6* activates interacting protein *HSP90. S100A6* levels were determined in serum from women with and without preeclampsia transversally collected in all trimesters of pregnancy using

PRM methodology. The interacting protein *HSP90* was measured to investigate whether *S100A6* and *HSP90* behave differently in patients with preeclampsia compared to pregnant normotensive controls. We observed that HSP90 was significantly increased in the third trimester of preeclamptic patients.

In **Chapter 5**, we described the technical aspects between MS-based measurements SRM, PRM, and an ELISA immunoassay as a gold standard. To better understand factors governing variability and sensitivity in targeted MS compared to immunoassay *HSP90α* protein was taken as an example. We were able to quantify *HSP90α* in serum at the low nanogram per milliliter level with all three methods (SRM, PRM, and ELISA). PRM measurements reduced variation and showed comparable sensitivity to immunoassay.

In **Chapter 6**, we investigated whether specific protein networks assigned to tumor mechanisms become active during the early stage of cervical cancer. We performed a shotgun MS approach to analyze significant differential proteins between cervical cancer tissues and healthy subjects and subsequently determined abundances of some of these proteins with PRM measurements.

Finally, the obtained results as described in this thesis are summarized and discussed in **Chapter 7**.

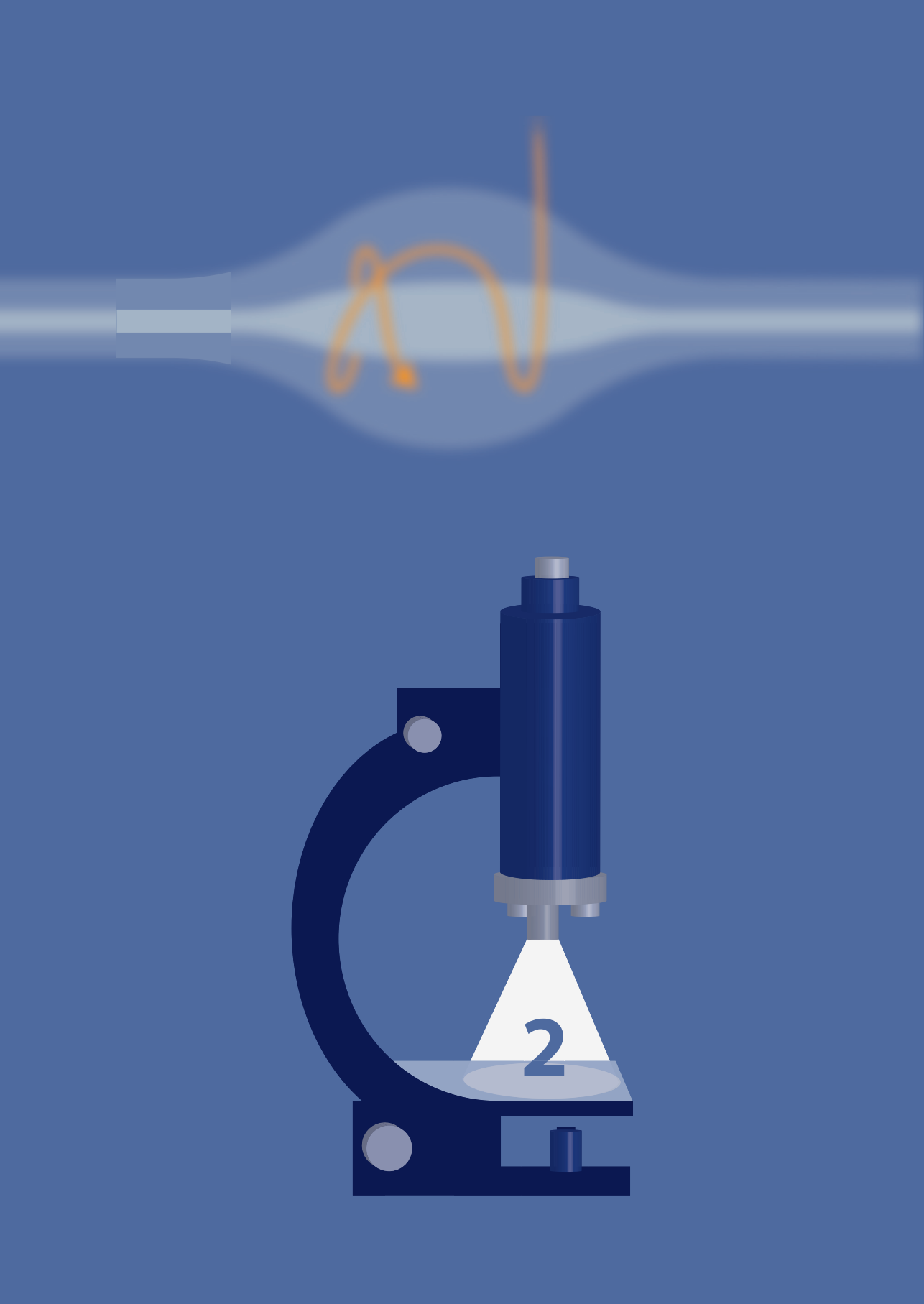
2

Chapter 2

Multiple reaction monitoring assay for preeclampsia related calcyclin peptides in formalin-fixed paraffin-embedded placenta

Coşkun Güzel[1], Nicolette T. C. Ursem[2], Lennard J. Dekker[1], Pieter Derkx[3], Jos Joore[4], Evert van Dijk[4], Gerard Ligtvoet[4], Eric A. P. Steegers[2], and Theo M. Luider[1]

[1]Department of Neurology, Erasmus MC, Rotterdam, the Netherlands
[2]Department of Obstetrics and Gynaecology, Division of Obstetrics and Prenatal Medicine, Erasmus MC, Rotterdam, the Netherlands
[3]Department of Pathology, Erasmus MC, Rotterdam, the Netherlands
[4]Pepscan Presto BV, Lelystad, the Netherlands

J Proteome Res. 2011 Jul 1;10(7):3274-82. doi: 10.1021/pr1010795

Summary

Although the cause of preeclampsia during pregnancy has not been elucidated yet, it is evident that placental and maternal endothelial dysfunction is involved. We previously demonstrated that in early-onset preeclampsia placental calcyclin (*S100A6*) expression is significantly higher compared to controls (De Groot *et al*. Clin. Proteomics 2007, 1, 325). In the current study, the results were confirmed and relatively quantified by using Multiple Reaction Monitoring (MRM) on two peptide fragments of calcyclin. Cells were obtained from control (n=5) and preeclamptic placental (n=5) tissue collected by laser capture microdissection (LCM) from formalin-fixed paraffin-embedded (FFPE) material treated with a solution to reverse formalin fixation. Two calcyclin peptides with an extra glycine inserted in the middle of the amino acid sequence were synthesized and used as an internal reference. Data presented, show that MRM on laser microdissected material from FFPE tissue material is possible. The developed MRM assay to study quantitative levels of proteins in FFPE laser microdissected cells using non-isotopic labeled chemical analogs of mass tagged internal references showed that in preeclamptic patients elevated levels of calcyclin is observed in placental trophoblast cells compared to normal trophoblast cells. By immunohistochemistry, we were able to confirm this observation in a qualitative manner.

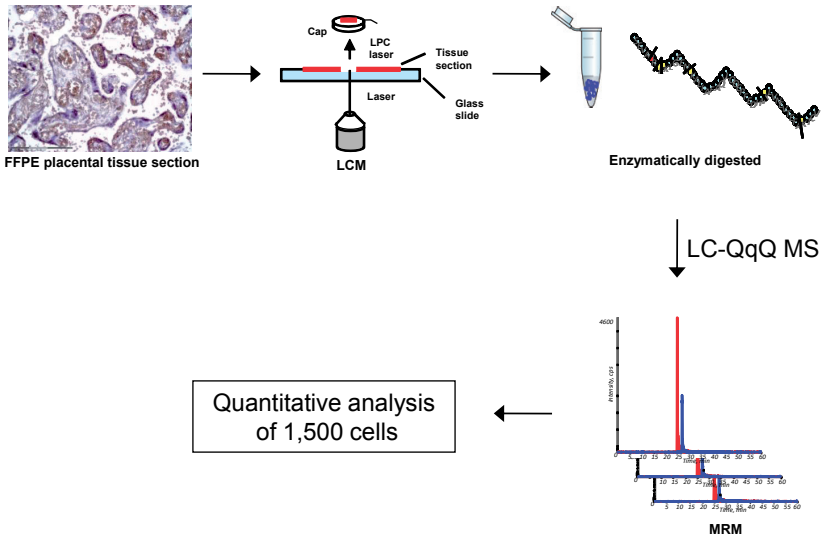

Introduction

Preeclampsia is a pregnancy-specific syndrome that complicates 2-8% of pregnancies (13). Various theories have been described as to why preeclampsia arises, but no cause has been proven yet (13). The syndrome is characterized by new-onset hypertension (diastolic blood pressure of ≥90 mmHg) and substantial proteinuria (300 mg protein / 24h) at or after the 20th week of pregnancy (13). It is a leading cause of maternal mortality in developed countries and increases perinatal mortality up to five-fold (65). It can be subclassified into early- and late-onset, and mild and severe PE (66, 67). Although its pathogenesis is not yet understood, it is evident that disturbed placental function in early pregnancy, which contributes to placental oxidative stress and abnormalities of the maternal vascular endothelium, plays an important role. In normal placentation, spiral arteries that provide blood supply to the placenta undergo striking modifications. The arteries lose their elastic lamina and smooth muscle and become greatly dilated, and trophoblast plugs are resolved by the migration of the trophoblast (68, 69). In preeclamptic women, the endovascular remodeling and invasion of the spiral arteries is impaired, which results in reduced and irregular placental perfusion. This could lead to production of reactive oxygen species (ROS) leading to placental oxidative stress, resulting in endoplasmic reticulum stress and impaired protein synthesis (70). High production of nitric oxide, carbon monoxide and peroxynitrite could negatively affect trophoblast differentiation and vascular remodeling (68, 71-74). Furthermore, it has been described that placental oxidative stress causes apoptosis and/or necrosis of the syncytiotrophoblast and release of various components into the maternal circulation, stimulating production of inflammatory cytokines (75, 76).

Previously, we reported that proteins such as calcyclin (*S100A6*), choriomammotropin precursor (CSH) and surfeit locus protein (SURF4), identified by nano-LC and FT-ICR mass spectrometry were related to early-onset preeclampsia (27, 28). Calcyclin (*S100A6*), a member of the S100 family, is a Ca^{2+} binding protein. It acts as a signal-transducer in intracellular processes (77). It is known that it is highly expressed in human epithelial cells, fibroblasts and involved in various forms of cancer(78). Agents evoking oxidative stress and exposure to ionizing radiation to induce generation of ROS resulted in an up-regulation of calcyclin in cancer cells. This suggests a role for calcyclin in the cellular stress response (79, 80).

Recently, studies have shown that it is possible to retrieve proteins from formalin-fixed paraffin-embedded (FFPE) tissue collections after laser capture microdissections that can be used for proteomics analyses (81-83). FFPE material has not been routinely used yet for mass spectrometry due to its crosslinking property caused by formaldehyde. Prieto *et al.*, 2005 described that they extracted peptides from FFPE tissue using the liquid tissue method and identified specific proteins related to colon cancer by TOF mass spectrometry (84). FFPE tissue processing is commonly used in pathology laboratories worldwide and used in histopathology due to its excellent morphology preservation. FFPE tissue can easily be

stored at room temperature without any loss of stability (85) and would be an ideal source for proteomics studies.

Selected Reaction Monitoring method is increasingly used for targeted mass spectrometric quantification of proteins in various frozen tissue samples (27, 86-89). In this study, we extracted proteins obtained from control and preeclamptic placental tissue collected from formalin-fixed paraffin-embedded (FFPE) material after laser capture microdissection. Calcyclin levels were quantified using Multiple Reaction Monitoring (MRM) on two calcyclin peptides. As an internal reference, two calcyclin peptides with a glycine insertion in the middle of the amino acid were synthesized. We correlated positive immunohistochemistry with the obtained MRM results and demonstrated that the technique could be used for relative quantitation of calcyclin concentrations in trophoblast and stroma cells.

Experimental procedures and methods

Placental samples

A total of 10 placental tissues were provided by the Department of Pathology, Erasmus MC. Of these 10 placentas, five were obtained from women who experienced early-onset preeclampsia (before 34 wk gestation) and five women with preterm delivery of unknown cause (Table 1).

The two groups were matched for gestational age. Preeclampsia was defined as the occurrence after 20 weeks of gestation of blood pressure of 140/90 mmHg or more and proteinuria of 300 mg protein/24h or more. The hemolysis, elevated liver enzymes, low platelets (HELLP) syndrome was defined as the simultaneous occurrence of a platelet count of less than 100×10^9/L and serum aspartate aminotransferase and serum alanine aminotransferase concentrations greater than 30 units/L. The Medical Ethics Review Board of the Erasmus MC, Rotterdam, approved the protocol.

FFPE tissue processing

Placental tissues were formalin-fixed paraffin-embedded (FFPE) according to standard routine guidelines provided by the Department of Pathology, Erasmus MC. Pieces of placenta parenchyma were cut and put into a fixation solution within 1 hour. The tissues were fixated in 10% phosphate-buffered formalin (Klinipath BV, Duiven, NL) for maximal 3 hours at room temperature. Subsequently, the tissues were processed by automation using an embedding station (Shandon Excelsior Tissue Processor (Thermo Electron, Breda, NL)), the process started with another extra hour formalin fixation, in five consecutive steps the fixated tissues were dehydrated in alcohol at 37°C (total time 5 hours), followed by three separated incubation steps in xylene at 40°C for a total of 2.5 hours. After that, the dehydrated fixated tissues were transferred into paraffin (Klinipath BV) at 60°C. The whole process takes 709

Table 1. Clinical information of samples.

#	Diagnosis	Maternal age (yr)	Gr	P	Blood pressure (mmHg)	Proteinuria (mg/24h)	GA at delivery (days)	HELLP	Birth weight (g)	Birth weight centiles [90]	Placenta weight (g)	G
1	PE	33	3	0	205/95	289	204	yes	930	p5	223	M
2	PE	20	3	0	170/100	137*	219	no	1430	p40	NK	F
3	PE	34	2	1	160/100	828	224	yes	1150	p5	240	F
4	PE	30	1	0	180/120	466	184	yes	690	p20	163	F
5	PE	29	2	0	160/105	771	203	yes	1070	p15	238	M
6	Control	22	1	0	100/70	0	223	no	2100	p75	450	M
7	Control	20	1	0	120/80	0	194	no	1010	p50	252	M
8	Control	37	6	2	110/70	0	199	no	1200	p20	291	M
9	Control	33	2	1	130/80	0	198	no	855	p10	560	F
10	Control	40	2	0	130/75	0	213	no	1050	p15	212	F

*PE= early-onset preeclampsia; Control=preterm delivery; Blood pressure=systolic/diastolic blood pressure at admission; Gr=gravidity; P=parity; GA=gestational age; NK=not known; proteinuria = 300 mg/24h or more; G=gender; F=female, M=male; *=exception; value recorded as g/L.*

minutes of transfer time. Subsequently, the processed tissues were manually embedded into paraffin blocks. After tissue processing, sections of 10 µm thickness were cut and mounted on to Director laser microdissection slides (Expression Pathology, MD, USA). Prior to laser microdissection, the slides were hydrated in xylene (3x) for 5 min, 1 min 100% alcohol (3x), 1 min 70% alcohol, 1 min 50% alcohol followed by 30 seconds in deionized water and 1 min in hematoxylin, respectively.

Frozen tissue processing

From placental parenchyma, trophoblast containing tissue was dissected. Subsequently, the dissected tissue was embedded in Cryoblock tissue medium (Klinipath BV) using liquid nitrogen-cooled iso-pentane. Then, sections of 10 µm were mounted on to a polyethylene naphthalate (PEN) membrane (1.35 mm) as recommended by the manufacturer (Carl Zeiss Micro Imaging, Göttingen, Germany). After that, the sections were hydrated in 100% alcohol for 5 min, 1 min 70% alcohol, 1 min 50% alcohol followed by 30 seconds in deionized water, and 2 min in hematoxylin, respectively. Subsequently, the slides were dehydrated in 1 min 50% alcohol, 1 min 70% alcohol, and 1 min 100% alcohol.

Laser capture microdissection

Laser Microdissected trophoblastic as well as stromal cells were collected from FFPE placental parenchyme tissue sections obtained from pregnancies complicated by early-onset preeclampsia (n=5) and from normotensive control women after preterm delivery of unknown cause (n=5) (Table 1). Five thousand cells were microdissected by a P.A.L.M laser microdissection system (Carl Zeiss MicroImaging, Munich, Germany) (Figure 1). Per MRM experiment, 1,500 cells were used.

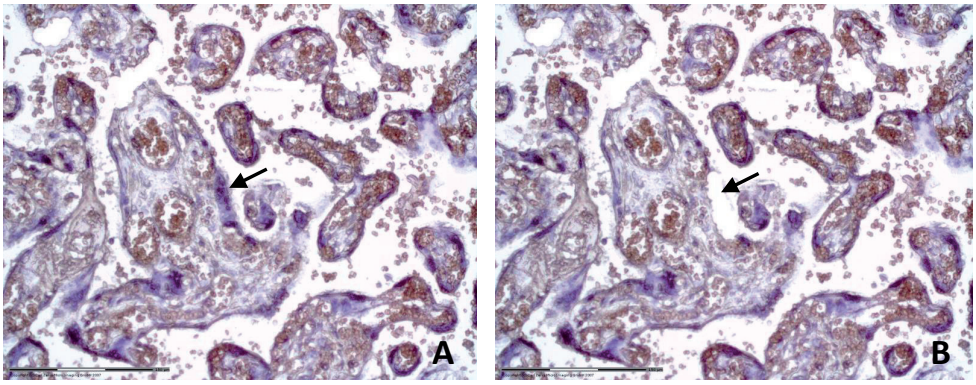

Figure 1. Laser Capture Microdissected trophoblast cells obtained from FFPE placenta (#2) tissue. A) before and B) after Laser Pressure Catapulting. Laser microdissected trophoblast cells are indicated with arrows.

Sample preparation

Laser captured microdissected cells, trophoblast as well as stroma cells, were collected in Liquid Tissue Buffer (LTB) (Expression Pathology, Gaithersburg, MD, USA) and subsequently heated at 95°C for 90 minutes. After centrifugation, LCM samples were sonicated for 1 min at 80% by an Ultrasonic Disruptor Sonifier (II, Model W-250/W-450 (Bransons Ultrasonics)). Enzymatic digestion was performed by adding 0.5 µg of trypsin (Proteomics Grade) (Expression Pathology) to the solutions and incubated overnight (16 hours) at 37°C. The digestion reaction was stopped and reduced by incubating with 2.5 mM DTT (Reduction Reagent, Expression Pathology).

LC-MRM-MS

Enzymatic digests of approximately 1,500 microdissected trophoblast and stroma cells were spiked with two synthetic glycine inserted calcyclin peptides of each 750 atto-mole (internal reference) (PepScan, Lelystad, the Netherlands) and separated for 60 min on a dual-gradient defined Ultimate nano-LC system (Dionex, Sunnyvale, CA, USA) prior to ESI analysis. The analytic nano-column was a PepMap C-18 (75 µm×250 mm) used with a trap column. The gradient elution with a flow rate of 300 nL/min started from 0 to 5 min at 100% A and followed by 45% B from 5 min to 60 min, 90% B from 61 min to 66 min and equilibrated at 100% A to 80 min (A=2% ACN/ 0.1% formic acid in HPLC grade water, B=80% ACN/0.08% formic acid in HPLC grade water). All separations were performed on a single column that was only used for these experiments. Subsequently, MRM measurements were performed by a 4000 QTrap (ESI-QqQ) (AB Sciex, Foster City, CA, USA) mass spectrometer. Positive ion mode was used to record MRM signals for each calcyclin double-charged peptide, i.e., LMEDLDR (446.211>647.297) and LQDAEIAR (458.244>674.302) as well as for the two synthetic peptides with a glycine insertion (bold G in following primary structures, i.e., LME**G**DLDR and LQDA**G**EIAR, $[M+H]^+$ 948 Da and 972 Da, respectively). The following parameters were set using a nanosource III: curtain gas 10 psi, capillary voltage 3500 V, GS1 10 psi, IHT 150°C. The MRM signals were integrated using the algorithm of MultiQuant software (version 2.0, AB Sciex). The observed MRM expression levels were compared to the findings obtained by immunohistochemistry. Commercially available antibodies specific for calcyclin (P06703, Sigma–Aldrich, St. Louis, USA) were used for validation by IHC according to the recommendation of the manufacturers. Immunohistochemistry is a semi-quantitative method, we used classes of intensity; - = no staining, +/- = very faint staining, + = staining but very low, ++ = normal staining, +++ = intense staining.

Orbitrap Mass spectrometry

Trypsin digests of tissue extracts were analyzed by LC-MS/MS using an Ultimate 3000 nano-LC system (Dionex, Germering, Germany) online coupled to a hybrid linear ion trap/Orbitrap mass spectrometer (LTQ Orbitrap XL; Thermo Fisher Scientific, Bremen, Germany). Five microliters of each digest were loaded onto a C18 trap column (C18 PepMap, 300µm ID

x 5mm, 5µm particle size, 100 Å pore size; Dionex, the Netherlands) and desalted for 10 minutes using a flow rate of 20 µL /min. The trap column was switched online with the analytical column (PepMap C18, 75 µm ID x 150 mm, 3 µm particle and 100 Å pore size; Dionex, the Netherlands) and peptides were eluted with the following binary gradient: 0% - 25% eluent B for 120 min and 25% - 50% eluent B for further 60 minutes, where eluent A consisted of 2% acetonitrile and 0.1% formic acid in ultra-pure water and eluent B consisted of 80% acetonitrile and 0.08% formic acid in water. The column flow rate was set to 300 nL/min. For MS/MS analysis a data-dependent acquisition method was used: a high-resolution survey scan from 400 – 1800 *m/z* was performed in the Orbitrap (automatic gain control (AGC) 106, resolution 30,000 at 400 *m/z*; lock mass set to 445.120025 *m/z* [protonated (Si(CH3)2O)6])(28). Based on this survey scan the five most intense ions were consecutively isolated (AGC target set to 104 ions) and fragmented by collision-activated dissociation (CAD) applying 35% normalized collision energy in the linear ion trap. Once a precursor had been selected, it was excluded for 3 minutes.

Orbitrap-MS/MS data processing

From the raw data files of the FT tandem mass spectrometer, MS/MS spectra were extracted by Mascot Deamon version 2.2.2 using the Xcalibur extract msn tool (version 2.07) into mgf files. All mgf files were analyzed using Mascot (Matrix Science, London, UK; 2.2). The mascot was set up to search the UniProt-database (version 56.0, human taxonomy (20069 entries)), assuming trypsin digestion. The Mascot search engine was used with a fragment ion mass tolerance of 0.50 Da and a parent ion tolerance of 10 ppm. Oxidation of methionine was specified in Mascot as a variable modification. The Mascot server was set-up to display only peptide identifications with Mascot ion scores greater than 25.

Scaffold (version Scaffold_2_02_03, Proteome Software Inc., Portland, OR) was used to summarize and filter the MS/MS-based peptide and protein of all the measurement results obtained by Mascot Deamon. Peptide identifications were accepted if they could be established at greater than 95.0% probability as specified by the Peptide Prophet algorithm. Protein identifications were accepted if they could be found at greater than 99.0% probability and contained at least two identified peptides.

Results

By Orbitrap mass spectrometry protein extracts from equal areas of microdissected paired FFPE and frozen tissue were compared. A number of 2,500 laser microdissected trophoblast cells were extracted from 3 paired (PE #1, #2, and control #1, Table 1) frozen and FFPE material. A comparable number of proteins, on average, 141 proteins that had at least two peptides with significant Mascot scores) between similar frozen and FFPE tissue (p=0.7260). We observed an overlap of 60% (on average) of identified proteins. This was in agreement with the variation observed in proteins identified in LCM experiments in a previous study on

esophagus tissue (91). We determined by a Bland-Altman plot that there was no significant difference between the number of proteins and their corresponding identified peptides obtained from fresh frozen and FFPE tissue (Figure 7). Additional information about the identification of proteins and overlap of proteins and peptides among samples is presented in Supporting Information that can be opened by publicly available viewer Scaffold (http://www.proteomesoftware.com).

Data and MRM analysis

The MRM signals were integrated using MultiQuant software. Using the software, the relative levels of calcyclin for preeclampsia patients and controls were calculated. MRM quantitative assessment of calcyclin was performed by means of the two synthetic peptides that were spiked into the enzymatic digests (Figure 2). Ionization efficiency experiments of the peptides with and without the glycine insertion showed comparable MRM intensity signals (Figure 3).

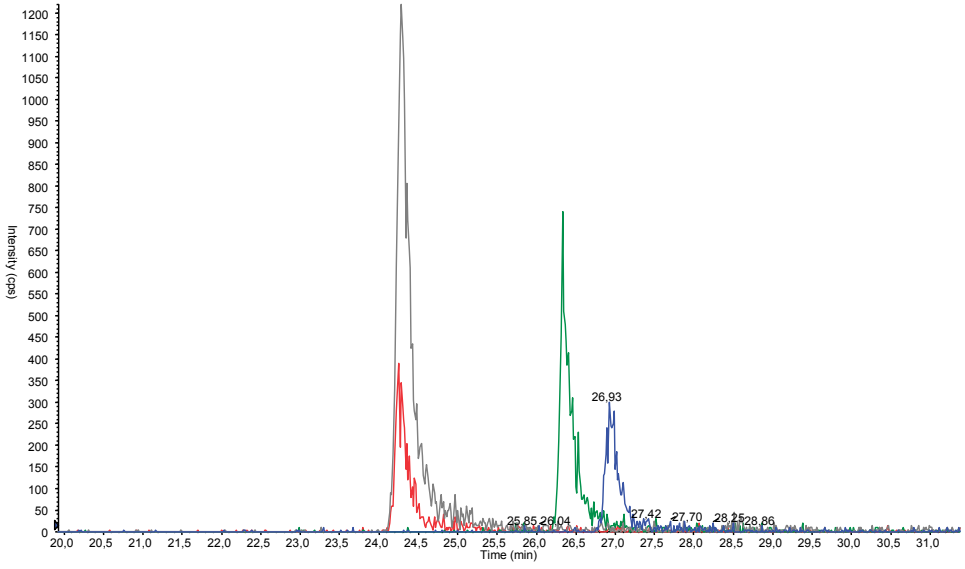

Figure 2. MRM transitions for double-charged peptide, i.e., LQDAEIAR (458.244>674.302) and LMEDLDR (446.211>647.297) part of calcyclin are represented in red and blue, respectively. The remaining two MRM signals (grey and green) represent the mass tagged internal references, respectively.

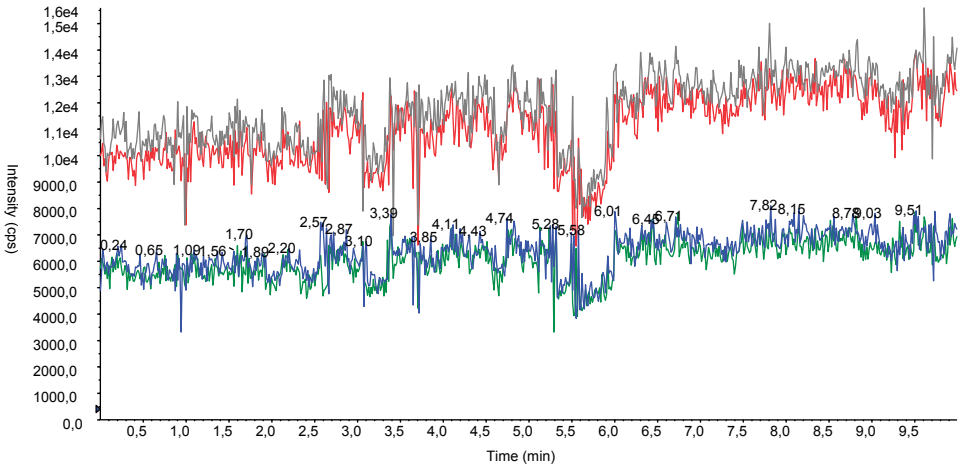

Figure 3. MRM signal of two analytes and their references. The upper two signals represent *m/z* 915 Da (analyte, grey) and *m/z* 972 Da (reference, red). The *m/z* 891 Da (analyte, green) and *m/z* 948 Da (reference, blue) show almost pairwise equal intensities.

The analytes LMEDLDR and LQDAEIAR and references LME**G**DLDR and LQDA**G**EIAR were spiked together into an equivalent of 1,500 trophoblast and stromal cells from FFPE placental tissue (PE#2, Table 1). Calibration curves of the two analytes and their two internal references with a concentration range of 0.2–5 fmol/µL (3 measurements per concentration) showed a linear correlation ($R^2 \geq 0.97$). The slopes of the analytes and internal references indicate that the response in the mass spectrometer between the analyte and reference peptides is similar (Figure 4).

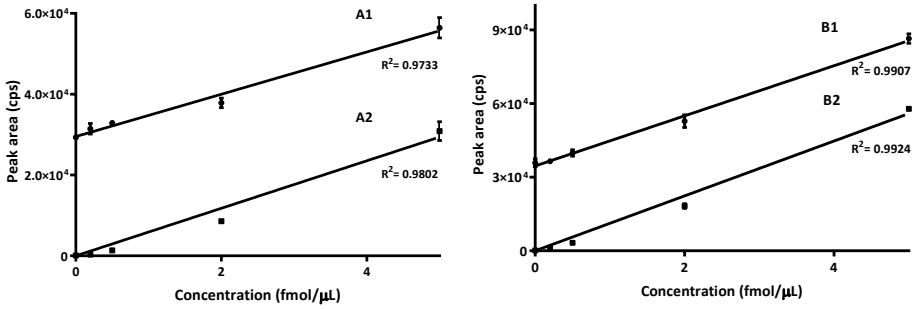

Figure 4. The correlation coefficients (R^2) of the two internal references, i.e., LME**G**DLDR and LQDA**G**EIAR references and LMEDLDR and LQDAEIAR analytes, are represented in A and B, respectively. The concentration range of spiked peptides was between 0.2-5 fmol/µL (3 measurements per concentration spiked peptide).

In addition, the MRM peaks for the LMEDLDR and LQDAEIAR analytes compared to the LME**G**DLDR and LQDA**G**EIAR references showed similar intensities, respectively.

We also determined the influence of variation in the matrix tissue on MRM signals. Calibration curves of the two internal references with a concentration range of 0.05–5 fmol/µL (4 measurements per concentration) showed a linear correlation ($R^2 \geq 0.97$) (Figure 5).

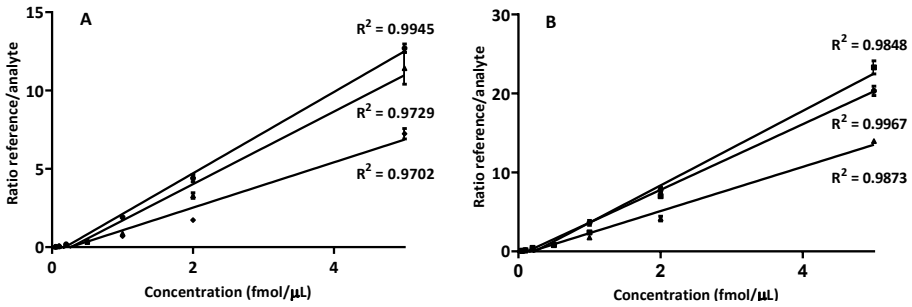

Figure 5. Three LCM experiments on three independent placenta tissue sections of sample #2 are presented. The internal reference peptides were spiked into an equivalent of a mixture of 1,500 trophoblast and stromal cells from placental tissue. Each line represents a different sample part of the tissue. The correlation coefficients (R^2) of the two internal references, i.e., LME**G**DLDR and LQDA**G**EIAR, [M+H]+ 948 Da and 972 Da, are represented in A and B, respectively. The concentration range of spiked peptides was between 0.05-5 fmol/µL (4 measurements per concentration spiked peptide). Linearity and reproducibility in the measurements were observed.

This result was obtained for three independent LCM experiments obtained among different consecutive tissue sections. The mean ratio of all CVs over the concentration range of 0.05-5 fmol/µL as a function of the reference and analyte ratio was 7.2% (range 2.0–25.1%) and 6.3% (range 1.4–24.6%) for LMEDLDR and LQDAEIAR, respectively.

The MRM transitions for each calcyclin double-charged peptide, i.e., LMEDLDR (446.211>647.297) and LQDAEIAR (458.244>674.302) were measured in microdissected trophoblast and stromal cells from preeclamptic patients and controls (Table 2).

Table 2. Quantification of two calcyclin peptides in trophoblast and stromal cells by MRM.

LMEDLDR	1,500 (t) (in fmol)	1,500 (s) (in fmol)	LQDAEIAR	1,500 (t) (in fmol)	1,500 (s) (in fmol)
PE #1	1.33	0.05	PE #1	0.76	0.03
PE #2	3.20	0.11	PE #2	1.73	0.08
PE #3	7.99	3.24	PE #3	5.95	2.11
PE #4	2.73	0.27	PE #4	1.59	0.07
PE #5	0.50	0.15	PE #5	0.40	0.12
Control #6	0.93	0.08	Control #6	0.44	0.05
Control #7	0.56	0.11	Control #7	0.54	0.24
Control #8	0.25	0.15	Control #8	0.21	0.12
Control #9	1.04	0.11	Control #9	0.54	0.07
Control #10	0.40	0.09	Control #10	0.30	0.10

PE = early-onset preeclampsia, Control = preterm control; t = trophoblast cells; s = stroma cells.

Calcyclin levels were significantly (p=0.0171, using unpaired t-test) higher in trophoblast cells of preeclampsia patients compared to controls. For stroma cells, the difference was not considered to be statistically significant (p=0.1652). On average, for both calcyclin peptide analytes 2.6 and 0.6 fmol per 1,500 trophoblast and stromal cells obtained from preeclamptic FFPE placental tissue (#1-5) were calculated, respectively. For preterm controls (#6-10), it was 0.5 and 0.1 fmol per 1,500 trophoblast and stromal cells, respectively. We assumed in this calculation that the composition of the internal references was ideal (no deviation from the amino acid composition or weighing errors).

Validation of calcyclin by immunohistochemistry

Trophoblast cells from placental samples of preeclamptic patients showed stronger positive staining compared to stromal cells (Figure 6). Table 3 represents data of expression levels of calcyclin in the early-onset preeclampsia and preterm controls.

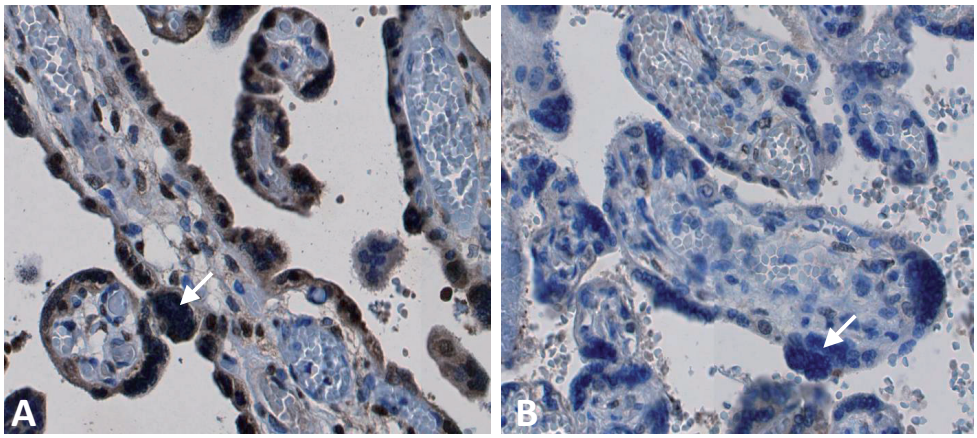

Figure 6. Immunohistochemistry of calcyclin in placenta of early-onset preeclampsia versus preterm controls. The arrows illustrate trophoblast cells. Preeclamptic trophoblast cells stain heavily with antibodies specific for calcyclin (*S100A6*) (#3, panel A) in contrast to preterm (#10, panel B). Some staining is observed in cells within the stroma as well for both preeclamptics and preterm controls (magnification 40x).

Table 3. Immunohistochemistry.

No.	Study samples	Expression level (*S100A6*) in trophoblast cells	Expression level (*S100A6*) in stroma cells
1	PE	+++	+
2	PE	++	+
3	PE	++	+
4	PE	+++	+/-
5	PE	+	+/-
6	Control	+/-	+/-
7	Control	+	+
8	Control	+/-	+/-
9	Control	++	+/-
10	Control	-	-

Samples used for immunohistochemistry. (–) no staining; (+/-) very faint staining; (+) staining but very low; (++) normal staining; (+++) intense staining. The sample numbers correspond to the numbers presented in Table 1.

Discussion

This study quantifies calcyclin levels in preeclamptic placental tissue by means of Multiple Reaction Monitoring (MRM) of two calcyclin peptides from laser microdissected cells that were obtained from control and preeclamptic trophoblast cells collected from formalin-

fixed paraffin-embedded (FFPE) material and confirms earlier obtained data (28). The use of FFPE tissue has been largely limited for proteomic analyses due to problems associated with covalent crosslinking formed by formaldehyde (92). Hood *et al*., 2005 described a successful MS-based proteome analysis of FFPE. Using LTB according to a protocol of Expression Pathology (USA), it is now possible to extract proteins and reverse the crosslinking in FFPE tissue comprehensively.

By Bland-Altman plotting, we compared the two methods (FFPE and frozen) and observed that no significant difference is observed for the peptides identified per protein (Figure 7).

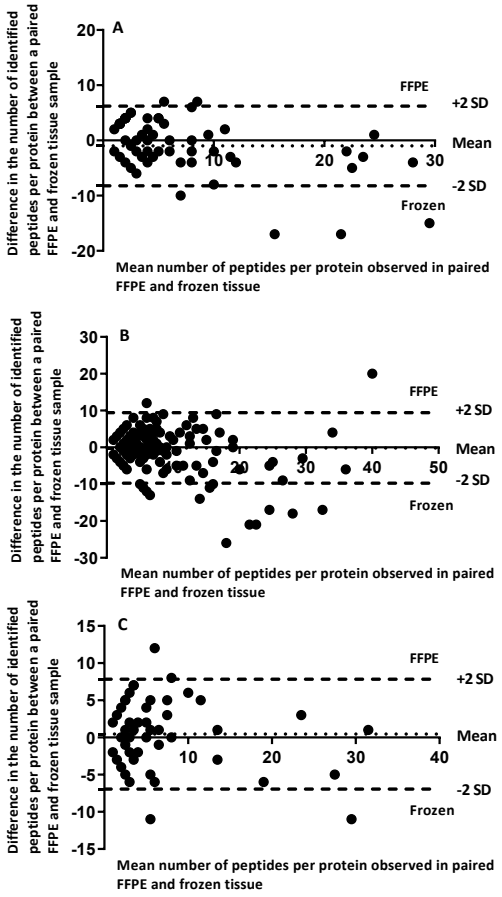

Figure 7. Bland-Altman plots. Plotting of the number of identified peptides per protein obtained from FFPE and frozen tissue for paired samples PE#1, PE#2, and control#1 are represented in A, B, and C, respectively. No significant difference was observed between FFPE or frozen tissue processing.

We conclude that after treatment of LTB, the effect of formalin crosslinking can be reversed and results in a number of identified proteins comparable with fresh frozen material. An overlap of 60% between identified proteins extracted from FFPE and frozen placental tissue performed by Orbitrap (Supporting Information) was observed. However, this variation is in agreement between variation observed in frozen tissue as described by Stingl *et al.*, 2010. Also, the number of identified proteins in FFPE or frozen tissues did not show a significant difference ($p>0.05$).

As an internal reference, two calcyclin peptides with a glycine insertion in the middle of the amino acid sequence were used for quantification. This approach was used as an alternative compared to isotopically labeled peptides as an internal reference. We have shown that the influence of glycine insertion on its ionization efficiency is neglectable for the peptides used (Figure 3 and Figure 4).

The custom synthesized reference peptides related to a purity of >94% (for all four synthetic peptides used) as observed by HPLC. A direct infusion step was performed to determine the ionization efficiency of the analyte and reference. Our experiments suggest that analytes and their glycine inserted reference peptides show comparable TICs (Figure 3). The correlation coefficient and the covariance of the two internal references obtained from three independent LCM experiments (Figure 5) revealed that we attained high reproducibility and linearity. The CVs for both internal references in three experiments measured over the concentration range of the spiked peptides were, on average less than 7.3%. The MRM signal for the spiked internal reference peptide LQDA**G**EIAR (0.750 fmol) was higher with a factor of on average 1.9 ± 0.36 (18.5% CV) compared to reference peptide LME**G**DLDR. On the other hand, for the ratio of the peptides measured for the analyte (LQDAEIAR/LMEDLDR), we observed a value of 1.34 ± 0.35 (26% CV). So, the values of LQDAEIAR are probably underestimated with a factor of 1.5 (1.9 divided by 1.34), resulting in corrected values that are overlapping better for both peptides as described in Table 2. An exact amino acid composition and purity determination would give the possibility to come to absolute quantification.

Many experiments of extracting proteins and subsequent MS-based proteome analyses from frozen biopsies are presented in the literature (reviewed by Ahmed *et al*., 2009). Because of its relatively simple snap-frozen fixation and minimal exposure to fixatives, it is an appreciated way. However, from a practical point of view FFPE fixated material is even more favorable because archive material could be used without the disadvantages of frozen material (less morphology, stability of tissue, storage advantages by room temperature).
The MRM signals with regard to peak areas for the calcyclin peptides were on average nine times higher in trophoblast cells of preeclamptic patients compared to controls. The MRM findings supported the immunohistochemistry result where preeclamptic trophoblast cells

stained intensely with antibodies specific for calcyclin in contrast to preterm controls (Figure 6). A good correlation was observed between MRM and IHC. However, the highest calcyclin concentration by MRM presented in sample #3 was not observed as the most intensive staining. This could be explained by the qualitative aspect of IHC. Control sample #9 showed relatively higher MRM values compared to other samples, as well as higher expression levels observed by IHC. The clinical data of this control sample (Table 1) showed that this patient was admitted to hospital due to intrauterine growth restriction of the fetus. This might explain the elevated value observed in this sample. Table 2 shows that calcyclin levels were lower in stroma cells in general compared to trophoblast cells and were not significantly statistically different. The elevated value in stroma cells from preeclamptic sample #3 represented weak positive expression performed by IHC (Table 3). We have no explanation for this discrepancy.

Calcyclin is one of the 20 small acidic proteins which belongs to the S100 family of EF-hand calcium-binding proteins (93). It is involved in various intracellular processes such as cell cycle progression, signal-transduction, exocytosis, cytoskeleton rearrangement and has been reported as significantly different in a variety of cancer (94-98). Lesniak *et al*., 2009 described that calcyclin levels were elevated in different cell cultures by the effects of adding agents such as cadmium, curcumin, and $H_2O_{2,}$ which evoke oxidative stress. The fact that we observed higher levels of calcyclin in placental trophoblast cells of preeclamptic women compared with those of preterm controls suggests possible involvement of oxidative stress (68).

In conclusion, we demonstrated that reliable relative quantification of calcyclin at the cellular level is possible in FFPE material and opens ways to determine in general quantitative protein abundances at the cellar level through LCM technology.

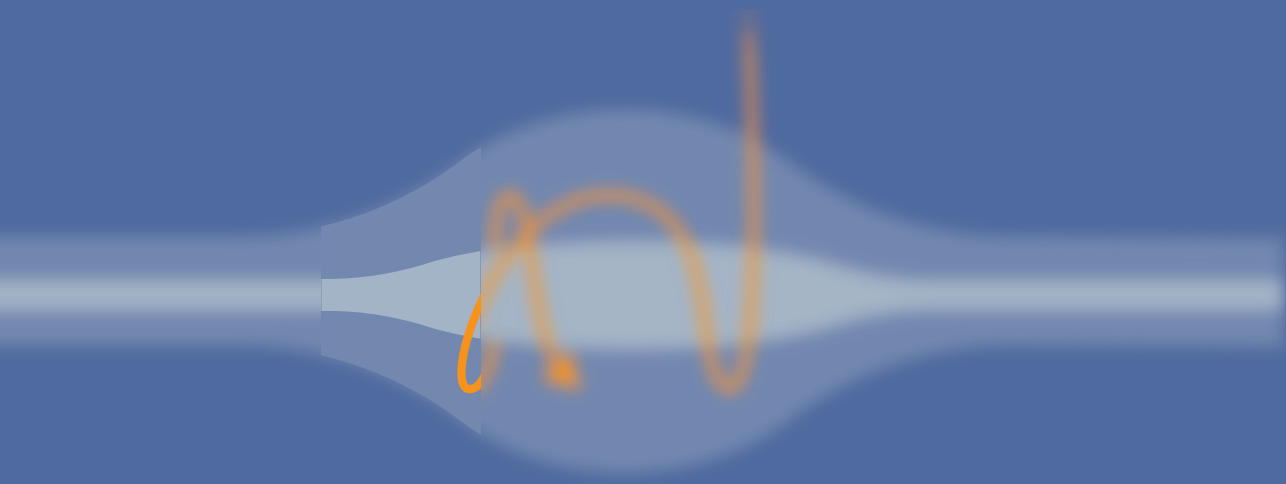

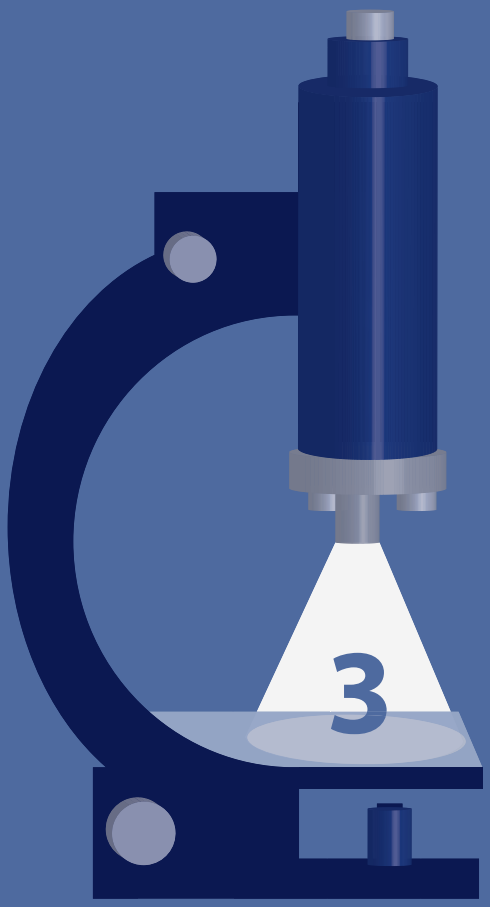
3

Chapter 3

Trophoblast calcyclin is elevated in placental tissue from patients with early preeclampsia

P.B.B. Schol[a,b,c], C. Güzel[a], E.A.P. Steegers[b], R.R. de Krijger[c] , T.M. Luider[a]

[a] Dept. of Neurology; Erasmus MC PO Box 2040, 3000 CA Rotterdam, the Netherlands
[b] Dept. of Obstetrics and Gynaecology; Division of Obstetrics and Prenatal Medicine, Erasmus MC PO Box 2040, 3000 CA Rotterdam, the Netherlands
[c] Dept. of Pathology; Erasmus MC PO Box 2040, 3000 CA Rotterdam, the Netherlands

Pregnancy Hypertens. 2014 Jan;4(1):7-10. doi: 10.1016/j.preghy.2013.11.003

Abstract

The aetiology of preeclampsia is thought to originate from aberrant spiral artery remodelling and invasion evoking cellular oxidative stress. Previously, we discovered differentially expressed proteins in trophoblast cells of preeclamptic pregnancies. One of these proteins is calcyclin (*S100A6*), a Ca^{2+}-binding protein associated with cellular stress response. By immunohistochemistry on formalin-fixed paraffin-embedded placental tissue, calcyclin expression was compared between women with early preeclampsia (n=72) and non-hypertensive controls (n=66) (χ^2, p=0.006) blindly by two observers. Significantly more intense staining was seen in trophoblast cells of preeclamptic pregnancies compared to control placentas suggesting that trophoblast calcyclin is elevated in early pregnancy.

Introduction

The aetiology of preeclampsia is currently unknown. The pathology is thought to originate from aberrant spiral artery remodelling (13). The uterine spiral arteries undergo remodelling through endovascular cytotrophoblast invasion, which change from narrow, high resistance vessels into wide, low resistance vessels (13). However, in preeclampsia these changes occur partially or not at all, causing insufficient low-pressure spiral arteries and therefore disturbed placental perfusion, which results in oxidative stress, endoplasmic reticulum stress and endothelial dysfunction (13).

We discovered previously differentially expressed proteins in trophoblast cells of preeclamptic pregnancies compared to trophoblast cells of healthy placental control tissue (26, 27, 99). One of these proteins is calcyclin (*S100A6*); a Ca^{2+}-binding protein belonging to the S100 family associated with cellular stress response, in which calcyclin is up-regulated (78, 100). In this study, we confirm by immunohistochemistry that trophoblast calcyclin is related to preeclampsia and discuss its role within the aetiology and its possible role as a marker for preeclampsia.

Methods

Formalin-fixed paraffin-embedded (FFPE) placental tissues were collected from the pathology archives at the Erasmus MC. Preeclampsia was defined as new-onset hypertension (≥140/≥90 mmHg) and proteinuria (≥0.3 g/ 24 hours) at or after 20 weeks of gestation. Eligible patients (n=76) were defined as women who delivered between 20 to 34 weeks of gestation with a clinical diagnosis of preeclampsia. The control group (n=75) was defined as women who delivered between 20 to 34 weeks without preeclampsia or any other hypertensive pregnancy disorder (Table 1). Only singleton pregnancies were included.

Table 1. Comparison of clinical characteristics of patients and control population.

		Mean (±SD)	Statistical value	dF	P-value
Age	P(n=72)	31.68 (4.964)	t= -1.496	121.281	0.137
	C(n=66)	30.20 (6.505)			
GA	P(n=72)	29.351 (2.371)	t= -3.632	136	0.000
	C(n=66)	27.845 (2.499)			
Gravid	P(n=72)	2.15 (1.307)	t= 1.509	110.384	0.134
	C(n=66)	2.59 (2.000)			
Parity	P(n=72)	0.61 (0.943)	t= 1.760	136	0.081
	C(n=66)	0.94 (1.239)			
Birth weight	P(n=72)	1075.25 (333.327)	t= 1.580	122.651	0.117
	C(n=66)	1179.08 (428.050)			
SBP	P(n=72)	162.69 (20.169)	t= -16.801	118.382	0.000
	C(n=66)	114.75 (12.519)			
DBP	P(n=72)	101.24 (11.759)	t= -18.857	130.638	0.000
	C(n=66)	67.34 (9.138)			

P=patients, C=controls, t=independent samples test, SD=standard deviation, dF=degrees of freedom, P-value=significance, GA=gestational age, SBP=systolic blood pressure, DBP=diastolic blood pressure). Birth weight in grams, age in years, GA in weeks, SBP, and DBP in mmHg.

The FFPE tissues were cut in 4 µm sections, mounted on glass slides and were automatically incubated with anti-calcyclin mouse antibody (*Sigma S5049, 1:25, Sigma-Aldrich, MO, USA*) using the Ventana Bench Mark Ultra (*Ventana, AZ, USA)* and its amplification step according to the manufacturer's instructions (*Ventana*). Slides were counterstained with haematoxylin-eosin.

Per patient, two slides of mid-placental tissue were analysed. The entire slides were blindly evaluated by two observers and grouped in 5 subcategories (++/+/+-/-/--, Table 2) at 100x and 400x magnification under auspice of a pathologist.

Table 2. Non-parametric test immunohistochemistry.

		--	-	+/-	+	++	χ2 value	dF	P-value
Median									
Trophoblasts	**P(n=72)**	0	4	14	38	16	14.292	4	0.006
	C(n=66)	2	8	17	37	2			
Stroma	**P(n=72)**	0	27	34	11	0	7.038	3	0.071
	C(n=66)	0	13	39	12	2			
Observer 1									
Trophoblasts	**P(n=72)**	2	2	18	27	23	12.599	4	0.013
	C(n=66)	3	9	14	32	8			
Stroma	**P(n=72)**	9	26	25	12	0	6.339	4	0.175
	C(n=66)	4	18	28	13	3			
Observer 2									
Trophoblasts	**P(n=72)**	0	6	36	26	4	25.728	4	0.000
	C(n=66)	3	16	42	4	1			
Stroma	**P(n=72)**	0	36	36	0	0	5.591	2	0.061
	C(n=66)	0	22	42	2	0			

P=patients, C=controls, χ2 value=non-parametric test, dF=degrees of freedom, P-value=significance

Slides exhibiting extreme heterogeneity in staining, indicating poor fixation by formalin were excluded. Results were averaged, and in case of a difference no greater than one subcategory, the highest given staining score was used.

Data were analysed using SPSS18. The immunohistochemistry data were analysed with a chi-square test (2-tailed). General characteristics of the study population tests were compared using a two-tailed independent t-test. Interobserver variation with paired data was determined through a Sign test. Results were considered statistically significant if $p<0.05$.

Results

Calcyclin staining intensity (Figures A and B) in trophoblasts was significantly higher in preeclamptic patients than in controls (χ^2 = 14.292, p=0.006).

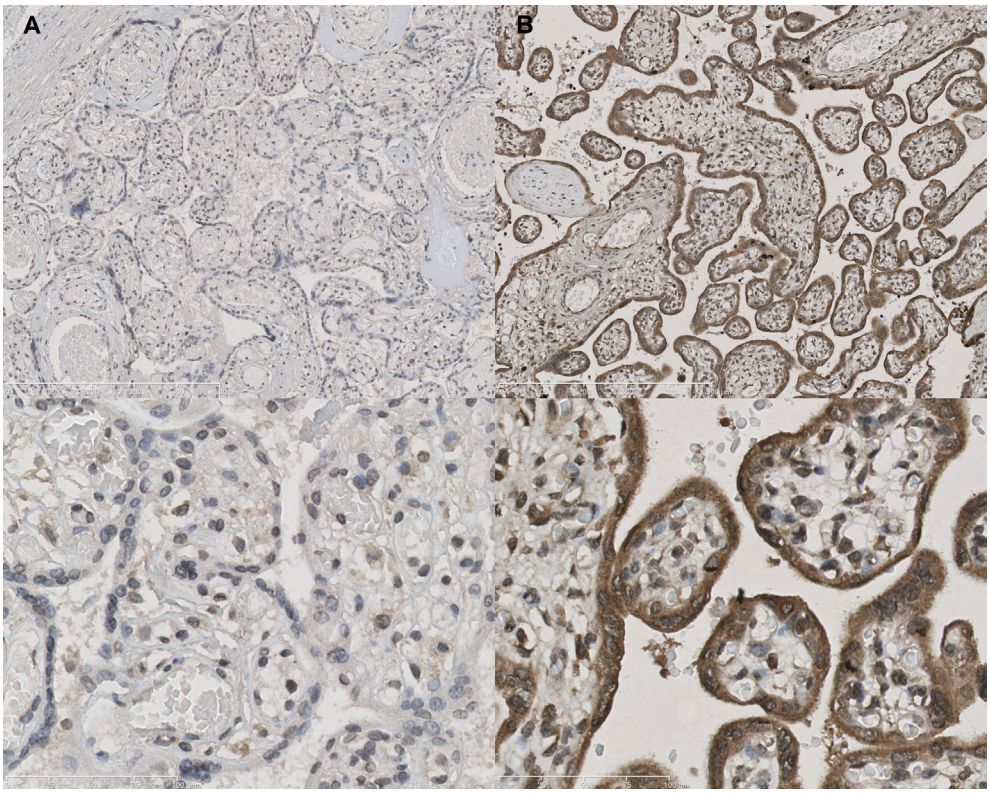

Figures A and B. Placental trophoblast staining. (A) No staining in trophoblast cells and faint staining in stromal cells from a control. Image 100x (upper panel), and 400x magnification (lower panel). (B) Intense staining in trophoblast cells and faint staining in stromal cells from a preeclampsia patient. Image 100x (upper panel), and 400x magnification (lower panel).

No significant difference was found in stromal cells (χ^2 = 7.038, p=0.071). When results were analysed per reviewer independently, significantly more intense staining was seen in trophoblast cells of preeclamptic women in comparison to control trophoblast cells (χ^2 = 12.599, p=0.013/χ^2 = 25.728, p=0.0000, Ob1 and Ob2 respectively). Staining of *S100A6* in stromal cells remained non-significant (χ^2 = 6.339, p=0.175/χ^2 = 5.591, p=0.061). There was a significant interobserver variation within trophoblast scoring but not in stromal scoring (Z = -7.11, p=0.00; Z = -1.51, p=0.131) (Table 2).

From 151 samples, 13 samples showed extreme heterogeneity and were excluded from analysis because these samples did not reach the technical criteria of homogeneous staining. No significant differences in general characteristics were found between both groups with the exception of systolic and diastolic blood pressure and gestational age (GA), which were lower for the control group. A scatter plot (not shown) showed no clustering of staining intensity, making gestational age unlikely as a confounder.

Discussion

This study confirms an association between trophoblast calcyclin expression and early preeclampsia by immunohistochemistry.

The placenta in a preeclamptic pregnancy suffers from oxidative stress, endothelium dysfunction, and endoplasmic reticulum stress. In these three biological processes, calcyclin is known to be up-regulated (78, 79, 100).

Intracellular calcyclin plays a pivotal role in cell-to-cell communication and intracellular signal transduction: it is a regulator of cell proliferation, has an active role in cytoskeleton morphology, and has an antioxidant effect (78, 79, 100).

Calcyclin stimulates the tumour suppressor protein p53 and the heat shock proteins (HSP) HSP70 and *HSP90* (100-102). Heat shock proteins are induced by stress stimuli to maintain cell integrity and viability. HSP70 is known to be elevated in preeclamptic pregnancies (103). Intracellular HSP70 acts as an anti-inflammatory and improves recovery after cellular stress. In contrast, extracellular HSP70 has the opposite effect. It stimulates an immune response (104).

It can be speculated that calcyclin stabilises the damaged cell, giving it time to repair, but when ineffective, it triggers apoptosis. Therefore, calcyclin may have a link to preeclampsia within a stress response.

With regard to the methodology, immunohistochemistry is a semi-quantitative method and subject to interobserver variation as also observed in this study. Even though interobserver variation exists, the individual observer data showed significant differences in trophoblast staining of preeclamptic pregnancies versus non-preeclamptic pregnancies in both groups independently. These results seem to be shifted per observer by just one group and are consistent with the results of the pooled data. Positive stromal cells, although not significant per observer and in the pooled data are more likely to be stained when reviewed by observer 1, which shows the sensitivity of immunohistochemistry to interobserver variation. To eliminate interobserver variation, a quantitative method like immunofluorescence or mass spectrometry could be thought of, although these techniques have drawbacks in calibration on tissue and sensitivity, respectively.

In conclusion, the concentration of calcyclin at delivery is elevated in preeclamptic trophoblast cells compared to non-preeclamptic trophoblast cells. Calcyclin may be related to the pathophysiology of preeclampsia. When released during apoptosis, it might be a serum candidate biomarker for the early prediction of early-onset preeclampsia. Early detection of preeclampsia may contribute to an early start of management and possibly will decrease adverse outcomes by better monitoring of the disease. Some promising biomarkers have been described, but none of these have been widely implemented clinically yet (105). To find these biomarkers we reasoned that affected trophoblast cells in placenta could be a source to find such candidate biomarkers.

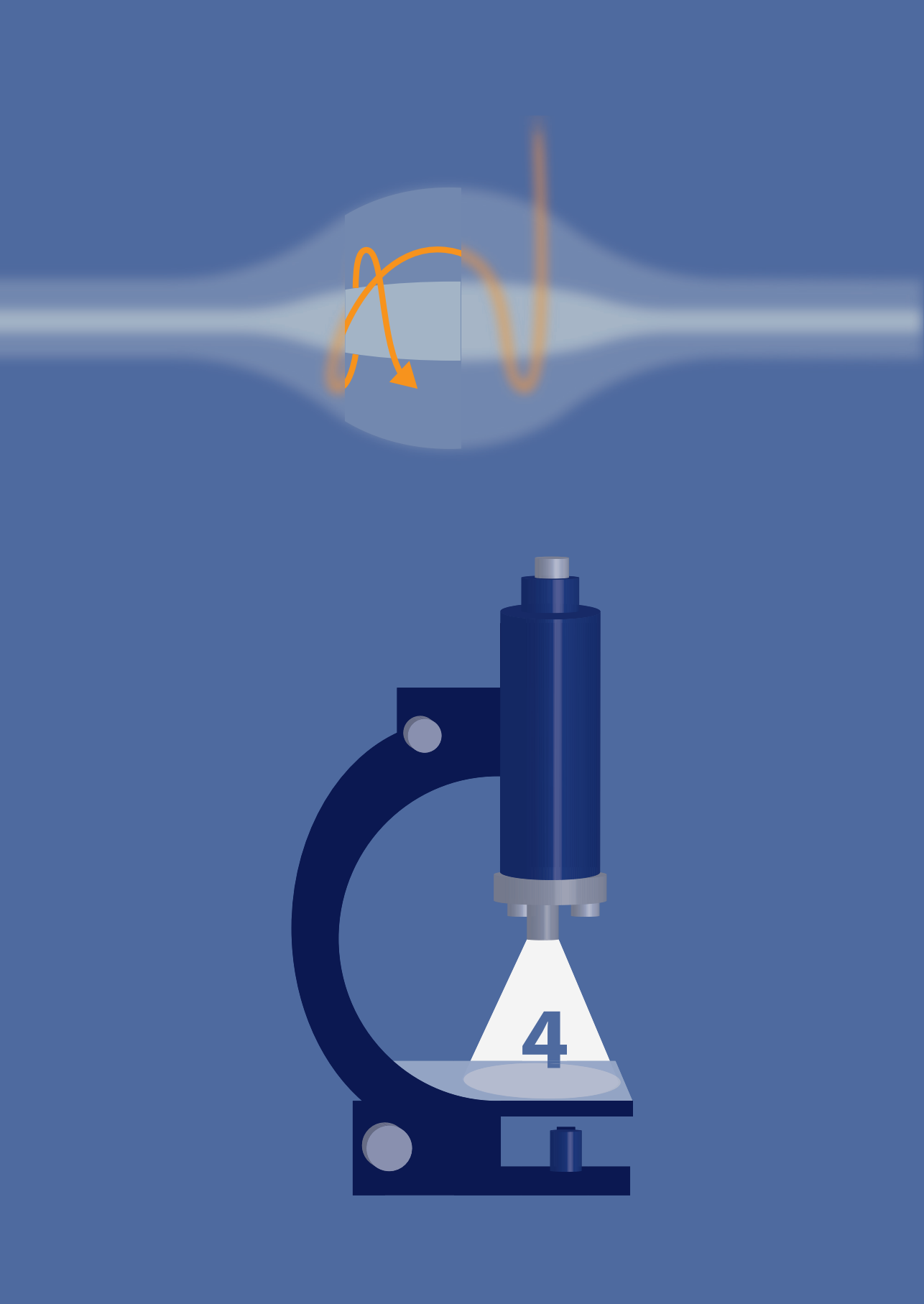
4

Chapter 4

Quantification of calcyclin and heat shock protein 90 in sera from women with and without preeclampsia by mass spectrometry

Coşkun Güzel[1], Caroline B. van den Berg[2], Johannes J. Duvekot[2], Christoph Stingl[1], Thierry P.P. van den Bosch[3], Marcel van der Weiden[3], Eric A.P. Steegers[2], Regine P.M. Steegers-Theunissen[2], Theo M. Luider[1]

[1] Laboratory of Neuro-Oncology/Clinical & Cancer Proteomics, Department of Neurology, Erasmus University Medical Center Rotterdam, the Netherlands

[2] Departments of Obstetrics and Gynecology, Erasmus University Medical Center Rotterdam, the Netherlands

[3] Department of Pathology, Erasmus University Medical Center Rotterdam, the Netherlands

Proteomics Clin Appl. 2018 Nov 11:e1800181. doi: 10.1002/prca.201800181

Abstract

We previously showed that the protein calcyclin (*S100A6*) was significantly elevated in placental tissue of patients with preeclampsia. The presence of *S100A6* in relation to an interacting *HSP90* binding was studied in a unique set of transversally collected serum samples of preeclamptic patients. Maternal serum levels of *S100A6* and *HSP90* were cross-sectionally compared throughout pregnancy from the first trimester till term among women with preeclampsia (n=43) and age-matched normotensive pregnant controls (n=46). A serum-based 2D LC/MS PRM assay was used to quantify both proteins. Serum levels of *S100A6* were significantly lower in patients with preeclampsia in the second trimester of pregnancy as compared to controls ($p<0.05$), while serum levels of *HSP90* were significantly higher in patients with preeclampsia in the third trimester of pregnancy ($p<0.001$). In addition, localization of both proteins in placental tissue was observed by double immunofluorescence staining. Results showed that *S100A6* and *HSP90* were partially colocalized. In this hardly accessible sample set, we used a sensitive and repeatable PRM technique with low variation levels (CV<5%) for both *S100A6* and *HSP90* proteins.

Significance of the study

We compared serum levels of *S100A6* and *HSP90* throughout pregnancy from the first trimester till term among women with preeclampsia and age-matched normotensive pregnant controls. A serum-based online 2D LC/MS PRM assay was used to quantify these literature-known interacting proteins. Partial colocalization of both proteins was observed in trophoblast cells from placental tissue. Both proteins were notably changed in serum of preeclamptic patients as compared to controls. However, there was no association with the onset of preeclampsia. *S100A6* was already significantly decreased before the onset of preeclampsia in the second trimester of pregnancy and *HSP90* was strongly (significant) increased in the third trimester. This suggests that these two proteins may play a role in the pathogenesis of preeclampsia.

Introduction

Preeclampsia (PE) is a pregnancy-specific multi-organ disorder that is diagnosed by new-onset hypertension and proteinuria after 20 weeks of gestation (13). It affects 2-8% of all pregnancies and is one of the leading causes of maternal mortality worldwide (13, 106). Also, perinatal mortality is five times higher in women with PE (106). The exact cause of PE remains unknown but most likely is the result of abnormal placentation during the first trimester of pregnancy usually observed in early-onset PE. During normal pregnancies, cytotrophoblast cells promote arteriolar dilation by invading the uterine spiral arteries. In PE, cytotrophoblast cells do not invade the spiral arteries adequately, resulting in reduced placental blood flow leading to excessive placental oxidative stress (107, 108). Signs of pending PE may be expected to be notable early in pregnancy before the onset of the clinical disease. Studying serum markers may lead to an understanding of the pathogenesis of PE at a protein level. The latter may contribute to better screening, monitoring, and possible prevention of this disorder.

Previously, we reported significantly discriminating peptide patterns between trophoblast and stromal cells by laser capture microdissection (LCM) (27, 28). We also demonstrated by immunohistochemistry that *S100A6* was significantly more abundant in placentas of preeclamptic women as compared to controls (109). By Multiple Reaction Monitoring (also known as SRM) we showed significantly elevated levels of *S100A6* in formalin-fixed paraffin-embedded (FFPE) preeclamptic placentas compared to controls by LCM (35). Concentrations of serum *S100A6* in healthy non-pregnant persons were known to be low (~2-8 ng/mL) (110, 111). S100 proteins, including *S100A6*, interact with the tetratricopeptide repeat (TPR) domains of the *HSP70* and *HSP90* (*HSP70*/*HSP90*)-organizing protein (*Hop*) in a Ca^{2+}-dependent manner. After interacting with *S100A6*, *HSP70,* and *HSP90* dissociates from *Hop-HSP70* and *Hop-HSP90* complex and blocks binding to other partner proteins (112, 113).

Based on our previous research on placental tissue and the hypothesis that *S100A6* activates *HSP90* via the *HOP* protein as a result of oxidative stress, it is suggested that *HSP90* might also play a role in the pathophysiology of PE. For this purpose, a cross-sectional study was performed with hard to acquire a set of maternal serum samples transversally collected during the first, second, and third trimester of pregnancy. We investigated whether these two proteins behave differently in patients with PE as compared to pregnant normotensive controls. A serum-based 2D LC/MS PRM assay (114) was used to quantify both proteins. In addition, we developed a double immunofluorescence staining with antibodies against *S100A6* and *HSP90* to show that both proteins *S100A6* and *HSP90* are present in trophoblast cells.

Materials and methods

Study design

A case-control study was conducted at the Department of Obstetrics and Gynecology of the Erasmus MC, Rotterdam, the Netherlands. Serum samples from two different studies were used: a nested case-control study embedded in the Rotterdam Periconceptional Cohort (Predict study) (115), a prospective tertiary hospital-based study, and the Lepra Study (116), a retrospective tertiary hospital-based case-control study focused on brain involvement during PE. Both studies were approved by the local Medical Ethical and Institutional Review Board of Erasmus MC (MEC-2004-227 and MEC 2007-086). At admission, participants gave written informed consent for participation. Serum samples were available of 43 patients with PE, consisting of 20 early-onset and 23 late-onset PE, and 46 normotensive controls. Sixty-three percent of the samples were collected in the first trimester (<14 weeks), 17 percent in the second trimester (14-27 weeks) and 20 percent in the third trimester (≥28 weeks) of pregnancy. These percentages did not differ between cases and controls. Cases and controls were matched for maternal age, geographic origin, parity and gestational age at sampling. PE was defined as systolic blood pressure ≥140 mmHg or diastolic blood pressure ≥90 mmHg on at least two occasions four hours apart after 20 weeks of gestation with proteinuria (protein/creatinine ratio of ≥30 mg/mmol) following the ISSHP guidelines. Clinical data were obtained from questionnaires and medical records. An independent set consisting of ten placental tissues that were provided by the department of Pathology, Erasmus MC, were used for immunofluorescence studies. Five were obtained from women who experienced early-onset PE and five from women with spontaneous preterm delivery without hypertension.

Sample preparation by SCX chromatography

Seven µL of each serum sample was diluted 47-times in 0.01% RapiGest (Waters, Milford, MA) dissolved in 50 mM ammonium bicarbonate, reduced using 15 mM DTT followed by alkylation using 15 mM iodoacetamide (IA) and subsequently enzymatically digested by adding 30 µL trypsin (100 µg/mL dissolved in 3 mM Tris-HCl pH 8.8) (Gold, Mass Spectrometry Grade, Promega, Madison, WI) at 37°C overnight. The enzymatic reaction was stopped by adding 50% of formic acid (FA) to reach a final concentration of 0.5 - 1.0% FA. All digested sera were spiked with 40 fmol of both *S100A6* and *HSP90* stable isotope-labeled (SIL) peptides (Thermo Fisher Scientific, Bremen, Germany; purity of >97% as stated by the manufacturer (Ultimate-grade)), followed by desalting by Solid Phase Extraction (Discovery DSC-18 SPE 96-well Plate, Sigma Aldrich, the Netherlands). Subsequently, digested samples were fractionated by SCX chromatography to measure relatively low levels (ng/mL) of *S100A6* and *HSP90* in sera from PE patients. All samples were off-line fractionated with a Luna 5 µm, 150 × 2 mm SCX column (Phenomenex, Torrance, CA) that was connected to a nano-LC system (Thermo Fisher Scientific, Germering, Germany) using the following conditions: buffer A (14 mM KH_2PO_4, 24 mM H_3PO_4, pH 2.5, adjusted with 37% (w/w) HCl)

in 25% (v/v) acetonitrile (HPLC grade; Biosolve, Valkenswaard, the Netherlands) in Milli-Q water; buffer B (buffer A containing 350 mM KCl); linear gradient from 100% buffer A to 40% buffer B in 40 minutes, followed by a wash with 100% buffer B until 45 minutes at a flow rate of 200 µL/min and equilibration of the column in buffer A for 17 minutes. All chemicals used for SCX fractionation were purchased from Sigma-Aldrich (St Louis, MO). As shown previously (114), fifty µL fractions (180 fractions in total for each serum sample) were automatically collected in 384-well plates (VWR, Amsterdam, the Netherlands) and sealed with an adhesive aluminum foil (VWR, Amsterdam, the Netherlands). Fractions were dried down in SpeedVac concentrator (RVT4104, Scientific Savant, San Jose, CA) and subsequently stored at -20°C until further analysis. Only fractions containing the two peptides (on average eight) were reconstituted in 0.1% FA prior PRM measurements.

PRM in serum and placental tissue

A PRM assay was developed for quantitative measurements of *S100A6* and *HSP90* levels in serum using SIL peptides serving as internal standards, i.e., LQDAEIAR ($^{13}C_6{}^{15}N_4$) for *S100A6* and YIDQEELNK ($^{13}C_6{}^{15}N_2$) related to both isoforms *HSP90*α and *HSP90*β. *HSP90*β was not analyzed, because it is known from literature that very low levels (~1-2 ng/mL) of *HSP90*β were usually measured in serum (117, 118).

For *S100A6*, a relatively low molecular weight protein (~10 kDa) only the single signature peptide LQDAEIAR was used because other tryptic *S100A6* peptides contain amino acids that are prone to oxidation (methionine, cysteine), acetylation, phosphorylation or are too long, i.e., more than 20 amino acids. The single signature peptide YIDQEELNK was used for *HSP90* measurements because almost identical results were obtained for another *HSP90* peptide DQVANSAFVER as explained in our previous paper (114). In this study, we also showed an agreement between ELISA and PRM results for *HSP90*.

PRM signals for *S100A6* were recorded for doubly-charged endogenous and SIL peptide LQDAEIAR precursor ions with *m/z* of 458.25 and *m/z* 463.25, respectively. For *HSP90*, *m/z* 576.28 and *m/z* 580.29 were taken for YIDQEELNK, respectively. PRM measurements were carried out on a nano-LC system (Thermo Fisher Scientific, Germering, Germany) online coupled to an Orbitrap Fusion mass spectrometer (Thermo Fisher Scientific, San Jose, CA, US). Three microliters of each SCX-fractionated sample were loaded on to a trap column (PepMap C18, 300 µm ID × 5 mm length, 5 µm particle size, 100 Å pore size; Thermo Fisher Scientific), washed and desalted for five minutes using 0.1% TFA in water as loading solvent. The trap column was then switched in-line with the analytical column (PepMap C18, 75 µm ID × 250 mm, 2 µm particle and 100 Å pore size, Thermo Fisher Scientific). Peptides were eluted with a binary gradient from 12 to 25% solvent B in 14.7 minutes, where solvent A consisted of 0.1% FA in water, and solvent B consisted of 80% acetonitrile and 0.08% FA in water. The column flow rate was set to 250 nL/min and oven temperature to 40°C. All LC

solvents were UHPLC grade and purchased at Biosolve, Valkenswaard, the Netherlands. For electrospray ionization, nano ESI emitters (New Objective, Woburn, MA) were used and a spray voltage of 1.8 kV was applied. For PRM of the doubly charged precursor ions of LQDAEIAR and YIDQEELNK (endogenous and SIL), we used the targeted MS/MS mode set up as follows: isolation width 1.4 Da, HCD fragmentation at a normalized collision energy of 25%, ion injection time was set to 512 ms (by setting the AGC target to 500,000 ions), Orbitrap resolution of 240,000. Selection of the precursor ions was time scheduled and each duty cycle consisted of two targeted MS/MS scans (endogenous and SIL form of a peptide) yielding a scan rate of approximately 0.83 Hz. Fluoranthene (202.0777 Da) was infused as lock mass (Easy IC option active).

The PRM data have been deposited to the ProteomeXchange Consortium via the PRIDE (119) partner repository with the dataset identifier PXD009025.

We determined placental abundances of *S100A6* and *HSP90*; whole tissue lysates were collected from placentas of six preeclamptic patients, five age-matched preterm controls, and four term controls. Collected tissue pieces were collected in 200 µL 0.1% Rapigest SF detergent, sonicated for 3 minutes using a horn sonifier bath (Ultrasonic Disruptor Sonifier II, Branson Ultrasonics, Danbury, CT, USA) at 85% amplitude and heated for 5 minutes at 99°C for protein denaturation. Fifty out of the 200 µL tissue lysates were each spiked with 1 fmol of *S100A6* and *HSP90* SIL peptides prior to enzymatic digestion. Samples were digested by adding 2 µg trypsin at 37°C overnight. PRM measurements were carried out on an Orbitrap Lumos (Thermo Fisher Scientific, Germering, Germany) instrument as described above with an adjustment of the gradient condition (from 4 to 38% solvent B in 30 minutes) to quantify protein levels of *HSP90*, and *S100A6*. Measured data were normalized based on UV data obtained during online LC-MS measurements of the tissue taken for each sample.

Data analysis

The PRM signals were integrated and analyzed using Skyline (61). The linearity, LOD, and LOQ of the assay were determined for *S100A6* and *HSP90* peptides according to our previous work (114) by spiking five different concentrations in triplicate into an SCX-separated serum digest. For each protein, the linear regression data including reproducibility of the serial dilutions of SIL peptide standards (expressed as %CV), LOD and LOQ are represented in Supporting Information, Excel data 1.

The SCX-fractionated serum digests were measured in a single run whereas ratios between endogenous and SIL peptides of *S100A6* and *HSP90* were calculated to determine the concentrations. Only fractions containing the highest *S100A6* or *HSP90* concentration were considered for further analysis. Statistical differences between serum levels of *S100A6* and *HSP90* in the total PE group, in the subgroups of early- and late-onset, and control

group during the first, second, and third trimester were calculated with an unpaired t-test. A probability below 0.05 was considered to be significant. Serum levels were tested for normality using Kolmogorov-Smirnoff and Shapiro-Wilk tests. Natural log (ln)-transformed values were used for statistical testing if data were not normally distributed. To evaluate the repeatability and reproducibility of the PRM assay, for both peptides three technical (three PRM measurements of an identical sample (quality control) throughout the assay run) and three methodological (three independently prepared replicates of an SCX-fractionated serum sample) replicates were measured and CVs as percentages calculated, respectively.

For statistical analysis of clinical characteristics independent students' T-tests (normally distributed data) or Mann-Whitney U tests (non-normal distributed data) were used for continuous variables and Chi-square tests or Fisher's exact tests were used for categorical variables.

Unsupervised hierarchical cluster analysis was performed to illustrate whether the proteins *S100A6* and *HSP90* were correlated with various metadata (Supporting Information, Excel data 2) of the investigated subjects. The following parameters were set using PermutMatrix 1.9.3. (http://www.atgc-montpellier.fr/permutmatrix): Pearson distance for dissimilarity, Wards' method, as a clustering method, and Bipolarization seriation (120, 121).

Double immunofluorescence microscopy

FFPE placental material from an independent set consisting of five preeclamptic women and five age-matched preterm delivered controls (26-32 weeks; used for routine procedures according to our department of Pathology and 'Code of Conduct for Responsible use' by the FEDERA, http://www.federa.org) were used for immunofluorescence with antibodies against *S100A6* and *HSP90*. Tissues were cut in 4 µm sections and routinely processed. Immunofluorescence assays were performed on a VENTANA BenchMark Discovery automated staining instrument (Ventana Medical Systems), using VENTANA reagents except as noted, according to the manufacturer's instructions. Slides were deparaffinized using EZ Prep solution (cat # 950–102) for 16 minutes at 72°C. Epitope retrieval was accomplished with CC1 solution (cat # 950–224) at high temperature 97°C for a period of time 36 min. Mouse-anti-S100A6 (clone CACY-100, Sigma Aldrich), was manually applied for 1 hour and 4 minutes at 37°C followed by second antibody UMAP anti-mouse conjugated with horseradish peroxidase for 12 minutes followed by 0.01% H_2O_2 and Red 610-tyramide detection (cat # 760-245). Next, the antibody denature step was done at 97°C for 12 minutes with CC2 solution (cat # 950-223). Subsequently, mouse-anti-HSP90 (clone D7a, Abcam) was manually applied and incubated for 40 minutes at 37°C. Then conjugated by second antibody UMAP anti-mouse with horseradish peroxidase for 12 minutes, followed by the application of 0.01% H_2O_2 and FAM-tyramide detection (cat #760-243). The slides were counterstained with DAPI Vectashield (Vector Laboratories, Burlingame, Ca) and imaged using the LSM 700 (Carl Zeiss, Germany) laser scanning confocal microscope.

Results

Clinical characteristics of study groups

Clinical characteristics (Table 1) did not statistically differ between the study groups, except for 'chronic hypertension' and 'PE in a previous pregnancy', which was present expectedly more often in the cases.

Table 1. Clinical characteristics

General characteristics [a]	PE (n=43)	Normotensive control (n=46)	P-value*
Maternal age, years	33 (5)	33 (5)	0.820
Geographical origin			0.800
Western	29 (67.4%)	28 (62.2%)	
Non-Western	14 (32.6%)	17 (37.8%)	
Study cohort			
Predict study	30 (70%)	22 (48%)	
Lepra study	13 (30%)	24 (52%)	
Index pregnancy			
Nulliparous	23 (53.5%)	24 (52.2%)	0.901
Preconception BMI, kg/m^2	27 (5)	25 (6)	0.237
Smoking (during pregnancy)	3 (7.5%)	0 (0%)	0.215
Highest systolic blood pressure, mmHg	155 (17)	126 (10)	<0.001
Highest diastolic blood pressure, mmHg	100 (9)	77 (6)	<0.001
Proteinuria (gram/24 hours)	0.54	NA	
Protein/Creatinine-ratio	63	NA	
Gestational diabetes	1 (2.3%)	2 (4.3%)	1.000
Twin pregnancy	3 (7%)	3 (6.5%)	1.000
Serum sampling			
Gestational age in weeks	12 (6-31)	10 (6-31)	0.608
Gestational age in days	87 (46-117)	75 (45-117)	0.464
Trimester comparison			0.982
Number of samples			
First trimester	27 (62.8%)	29 (63.0%)	
Second trimester	7 (16.3%)	8 (17.4%)	
Third trimester	9 (20.9%)	9 (19.6%)	
Medical history			
Chronic hypertension	13 (30.2%)	0 (0%)	<0.001
Insulin Dependent Diabetes Mellitus	1 (2.3%)	1 (2.2%)	1.000
Obstetric history			
Recurrent miscarriages	0 (0.0%)	5 (10.9)	0.056
PE in previous pregnancy	13 (30.2%)	2 (4.3%)	<0.05

General characteristics [a]	PE (n=43)	Normotensive control (n=46)	P-value*
Previous Caesarean delivery	8 (18.6%)	10 (21.7%)	0.713
Phenotypes preeclampsia			
HELLP	13 (30.2%)	NA	NA
Early-onset PE [b]	20 (8[d], 4[e], 8[f]) (47.6%)	NA	NA
Late-onset PE [b]	23 (19[d], 3[e], 1[f]) (52.4%)	NA	NA
Severe PE [b]	21 (50%)	NA	NA
Clinical symptoms			
Headache	21 (51.2%)	2 (4.3%)	<0.001
Visual complaints	10 (24.4%)	2 (4.3%)	<0.05
Upper abdominal pain	15 (36.6%)	1 (2.2%)	<0.001
Nausea	11 (26.8%)	2 (4.3%)	<0.05
General discomfort	6 (14.6%)	0 (0%)	<0.05
Dyspnea	3 (7.3%)	1 (2.2%)	0.339
Neonatal characteristics [c]			
Birth weight, gram	2335 (1410-2845)	3310 (2940-3675)	<0.001
Birth weight<10th percentile	9 (20%)	2 (4.2%)	<0.05
Male gender	25 (54.3%)	20 (41.7%)	0.219

[a] *Data are presented as n (%), mean with standard deviation (SD) or median with range.* [b] *These definitions are according to the ISSHP guidelines, see reference (122).* [c] *Due to five twin pregnancies with living children (n=94).* [d] *Number of samples in the first trimester,* [e] *Second trimester,* [f] *Third trimester. * For comparisons between groups independent students' T-tests, Mann-Whitney U tests, Chi-square tests, and Fisher's exact tests were used. NA = not applicable.*

Women with PE had higher blood pressure and lower birth weight of the neonate. Women with PE reported more often complaints of headache, visual disturbances, upper abdominal pain, nausea, and general discomfort.

Serum S100A6 and HSP90 levels

Table 2 shows the results of comparisons between patients with PE and controls at different gestational ages for *S100A6* and *HSP90* measured by PRM.

Table 2. *S100A6* and *HSP90* serum levels measured by PRM of women with PE and pregnant normotensive controls from the first (1st), second (2nd) and third (3rd) trimester of pregnancy. Statistical comparisons were made using an unpaired t-test. Serum levels were not normally distributed and therefore an ln-transformation was used to normalize the data. A probability value below 0.05 was considered to be significant.

S100A6 trimester	PE (n=43) concentration in ng/mL (median; IQR)	CO (n=46) concentration in ng/mL (median; IQR)	p-value
1st (n=56)	59.3 (34.0 - 68.6)	63.2 (47.3 - 92.0)	NS
2nd (n=15)	41.7 (36.6 - 47.2)	75.6 (54.5 - 143.4)	<0.05
3rd (n=18)	113.2 (68.7 - 191.2)	171.8 (63.4 - 781.7)	NS
all (n=89)	59.8 (36.8 - 78.0)	80.6 (49.7 - 102.2)	<0.05
HSP90 trimester			
1st (n=56)	100.1 (80.8 - 118.9)	96.7 (76.9 - 140.7)	NS
2nd (n=15)	91.9 (66.0 – 101.3)	105.4 (63.9 - 132.5)	NS
3rd (n=18)	194.2 (116.8 - 412.4)	62.6 (53.7 - 79.0	<0.001
all (n=89)	103.3 (83.0 - 157.6)	93.7 (65.0 - 125.8)	<0.05

PE=preeclampsia; CO=pregnant normotensive controls; IQR=interquartile range; NS=not significant.

Serum levels were not normally distributed and for this reason, the ln-transformed values were used for statistical testing. A complete overview of *S100A6* and *HSP90* levels measured in PE and control is illustrated in Figure 1 by plotting each protein level against the trimester group.

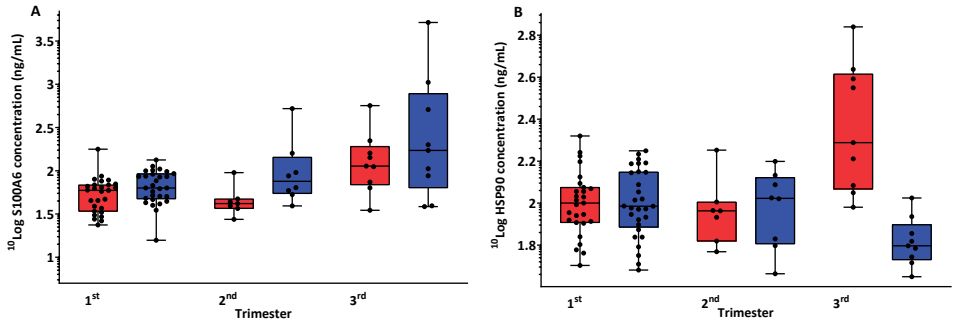

Figure 1: Serum levels of A) *S100A6* and B) *HSP90* were measured (for individual concentrations per trimester, see Table 2) for each PE (red) and control (blue) group obtained from the first, second, and third trimesters. In the second trimester, *S100A6* was significantly lower in serum of patients with PE compared to controls. Serum levels of *HSP90* were significantly elevated in the third trimester.

Serum levels of *S100A6* were overall lower in patients with PE compared to controls (Table 2, 59.8 ng/mL versus 80.6 ng/mL, $p<0.05$) analyzed for all three trimesters together. When analyzing the trimesters separately, it was observed that during the second trimester *S100A6* was significantly lower in patients with PE (Table 2, 41.7 ng/mL versus 75.6 ng/mL, $p<0.05$). In the other two trimesters, an increasing not significant trend was observed.

Serum levels of *HSP90* were overall significantly higher in patients with PE compared to controls (Table 2, 103.3 ng/mL versus 93.7 ng/mL, $p<0.05$). When analyzing the trimesters separately *HSP90* was significantly higher in serum of cases only in the third trimester (Table 2, 194.2 ng/mL versus 62.6 ng/mL, $p<0.001$).

The LOD and LOQ for *S100A6* that was based on peptide LQDAEIAR was 0.3 ng/mL and 0.8 ng/mL, respectively. The LOD and LOQ for *HSP90* were 2.8 and 8.6 ng/mL, respectively.

The CV for repeatability and reproducibility calculated for the *S100A6* peptide LQDAEIAR was 3.6% and 2.0%, respectively. In the case of *HSP90*, the CV was 2.1% and 6.8% for YIDQEELNK, respectively.

Sensitivity analysis of the *S100A6* and *HSP90* serum levels individually analyzed per trimester and for all three trimesters together did not reveal any significant difference between early- and late-onset PE. Furthermore, we investigated by unsupervised hierarchical clustering that various parameters were correlated with *S100A6* and *HSP90*. The patient and control group were separated completely (Supporting Information, Figure S1).

The abundances of S100A6 and HSP90 in placental tissue measured by PRM

Results showed that *S100A6* (Supporting Information, Figure S2A) was significantly different between preeclamptics and term controls ($p=0.0381$). Comparing the preeclampsia group with the preterm control group was not significant ($p=0.7619$). For *HSP90* (Supporting Information, Figure S2B), we did not find significant differences between preeclamptics and term controls ($p=0.9307$). Comparing the preeclampsia group with the preterm control group was also not significant ($p=0.0519$) (borderline).

Colocalization of S100A6 and HSP90 in placentas by immunofluorescence staining

Using immunofluorescence staining, it was observed that *S100A6* and *HSP90* were partially colocalized in cytoplasm of trophoblast cells from placental tissue of preeclamptic patients ($n=5$) and preterm matched controls ($n=5$). Figure 2 is an example of immunofluorescence trophoblast staining for *S100A6* and *HSP90* in placenta of a PE case and age-matched preterm control.

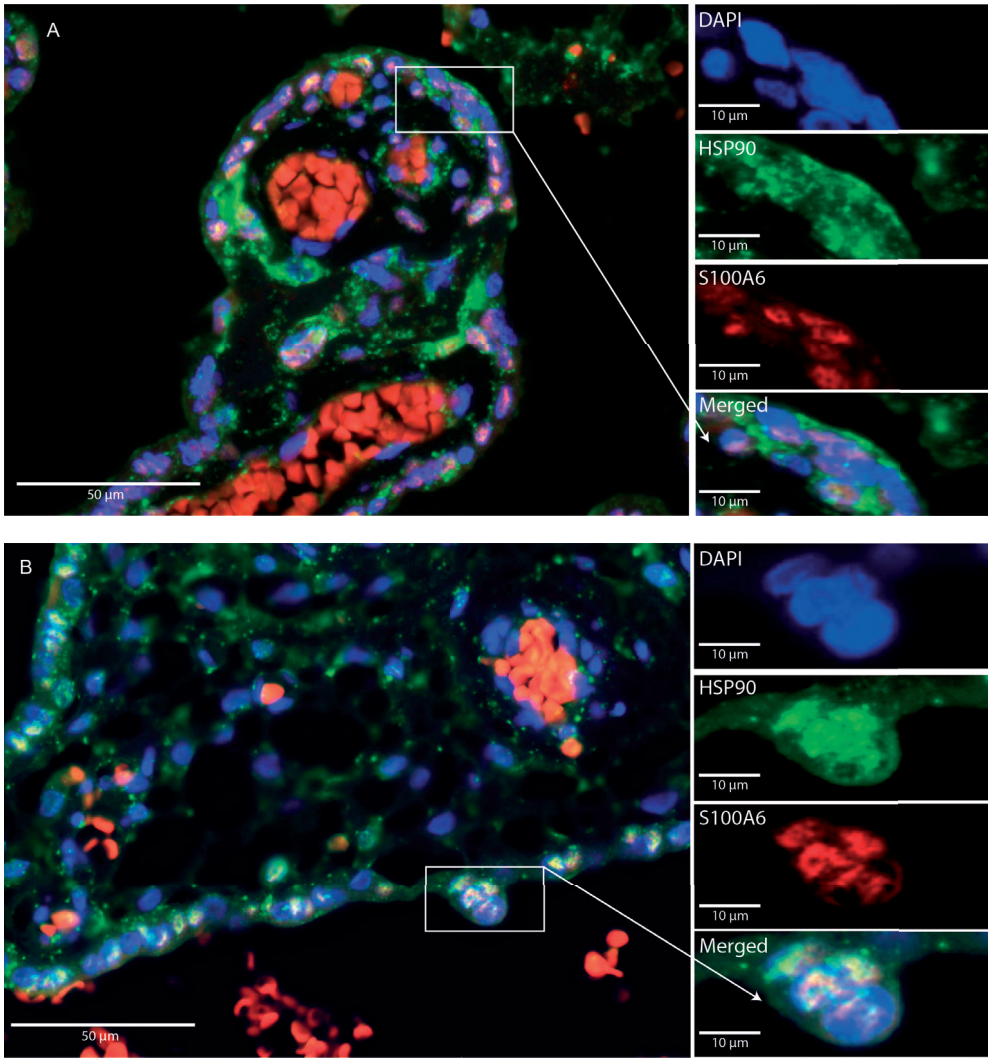

Figure 2. Example of double immunofluorescence staining. It shows trophoblast staining for both proteins *S100A6,* and *HSP90* in a preeclamptic (A) and age-matched preterm delivered control (B) placental tissue at 40x magnification. For *S100A6* (red), both cytoplasm and nucleus (partially) of trophoblast cells were positive, while for *HSP90* (green), only cytoplasm was stained of trophoblast cells. The colocalization of both proteins is indicated with a merged color. Red blood cells showed autofluorescence for *S100A6*. For nuclear counterstain, the slides were stained with DAPI.

The immunofluorescence results showed that often overlap was observed between *S100A6* and *HSP90* in the trophoblast cells. At the stromal part of the chorion villi, no staining or at least no overlap was observed.

Discussion

Serum *S100A6* and *HSP90* levels of matched cases and controls could be measured in a sensitive and high-quality manner. PRM results of *S100A6*, based on endogenous peptide LQDAEIAR, showed a significantly lower serum concentration in the second trimester of pregnancy in women with PE compared to normotensive controls. PRM results of *HSP90*, based on endogenous peptide YIDQEELNK, showed a significantly higher serum concentration in the third trimester of pregnant women with PE compared to normotensive controls, but not in the first and second trimesters.

The finding that a significant decrease was observed of *S100A6* levels in the second trimester of PE patients was remarkable and suggests that *S100A6* is involved in the pathophysiology of PE as was already observed previously in placental tissue (109). In placental tissue, we observed that *S100A6* was higher abundant in patients with PE. However, the expression in serum of this protein may be more complex and different from the expression in placental tissue. So, the idea that elevated levels in tissue would also automatically result in higher levels in serum could be not true because *S100A6* might have a different clearance rate from the blood or have a different degradation process in serum or in the originating tissue. The precise biological or cellular function of *S100A6* remains unclear (123). It is known that *S100A6* plays a role in cellular stress response; there is an up-regulation of *S100A6* in cells which are exposed to oxidative stress. Placental oxidative stress is known to precede the development of PE (124). Placentas from preeclamptic women have reduced antioxidant capacity showing lower levels of antioxidants in blood (124). *S100A6* is a member of the S100 subfamily, which consists of two EF-hand calcium-binding motifs that act as a signal-transducer in intracellular processes (78). Intracellularly, these proteins function as Ca^{2+}-signaling and Ca^{2+}-buffering proteins. Calcium induces a conformational change of the protein structure. By this change, an interaction site of S100 proteins with their target proteins is exposed (125). Extracellularly, the S100 proteins (including *S100A6*) are known to be interacting with the Receptor for Advanced Glycation End products, known as RAGE-receptors (126). These proteins have a cytokine-like function and could, for example, act as chemotactic molecules during inflammation. Recent evidence suggests RAGE play a separate role in inflammatory and vascular autoimmune diseases. RAGE proteins are expressed in several cells in vasculature tissue such as endothelial cells, infiltrating inflammatory cells, cardiomyocytes, and fibroblasts (127). Placental cells from PE patients were found to have increased levels of RAGE proteins (128), suggesting the involvement of *S100A6* protein in the pathophysiology of PE.

Because of the limited power of the study, it was not possible to establish significant differences between early- and late-onset PE per trimester. Most likely, *HSP90* increases also as a consequence of secondary mechanisms (e.g., inflammation) and not necessarily as a cause or as an early event that leads to the clinical onset of PE. *S100A6* and *HSP90*

are both expressed in trophoblast cells, as confirmed by double immunofluorescence staining (Figure 2). *S100A6* is partially located in nuclei and cytoplasm, while *HSP90* was only found in cytoplasm of trophoblast cells, although these proteins have also been found outside cells (129). A similar expression is described in "The Human Protein Atlas" (http://www.proteinatlas.org). *S100A6* interacts with heat shock proteins such as *HSP70*/*HSP90* complexes and may promote endothelial cell-cycle progression by this interaction. *HSP90* is the most abundant heat shock protein in eukaryotic cells. It consists of two isoforms with largely similar functions known as *HSP90*α and *HSP90*β. In this study, we made no distinction between these two protein isoforms. *HSP90* is a chaperone protein that plays a role in the folding, stabilization, and activation of denatured and synthesized proteins that are involved in various cellular processes. *HSP90* plays an important role in stress responses and maintaining cellular homeostasis. *HSP90* proteins interact with other heat shock proteins regulated by *S100A6* (100-102). Recent research showed that *S100A6*-binding protein and Siah-1 interacting protein (CacyBP/SIP) interact directly with *HSP90* (130). There are a few studies about *HSP90* levels in PE. Although not comparable with this study, Hromoadnikova *et al.* found decreased *HSP90* mRNA in whole peripheral blood of mothers with PE. On the other hand, they found a significant up-regulation of *HSP90* in placental tissue in patients with mild PE while there was no difference in severe PE (131).

The immunofluorescence results of *S100A6* and *HSP90* (Figure 2) showed partial colocalization in trophoblast cells. The numbers of placenta tissue analyzed in this study (n=5 in each group) were too small to report information on whether *HSP90* was up-regulated in PE. In case of *S100A6*, we reported previously that *S100A6* was elevated in a larger cohort (n=138) (109).

Heme oxygenase plays a role in the protective mechanism against oxidative and nitrosative stress. Ekambaram *et al.* (132) showed increased levels of *HSP90* in umbilical cord blood RBC (red blood cells) and decreased heme oxygenase-2 in PE. *HSP90* is thought to play a role in this mechanism. Higher hemoglobin concentrations have been associated with inadequate plasma volume expansion, which may be part of the preeclamptic syndrome (133). An alternative explanation for the higher *HSP90* level in PE in the third trimester of pregnancy might be that patients with PE frequently show hemolysis. In order to investigate this, we tested the correlation of *HSP90* levels in the third trimester of pregnancy with haptoglobin and lactate dehydrogenase concentrations, which were available in the PE group. We did not find correlation between *HSP90* and these parameters of hemolysis (data not shown). However, this might have been due to the small size of this group (n=9). By unsupervised hierarchical clustering of the metadata the preeclamptic and control group were completely separated. *S100A6* and *HSP90* contributed to the hierarchical clustering.

Serum levels of *S100A6* and *HSP90* were measured to our knowledge for the first time in a relatively large group of women with PE and normotensive controls, although for an elaborate statistical analysis still low in number. Moreover, measuring these samples cross-sectionally during all trimesters of pregnancy is unique. Although EU activities in that direction to get access to larger numbers of PE and control serum samples are ongoing (the IMPROvED program, http://www.fp7-improved.eu), the uniqueness of collecting these samples hampers the finding of reliable biomarkers for PE. Another limitation of this study is that samples were collected in a tertiary hospital setting in which some patients suffered from other chronic diseases. For example, *S100A6* levels were notably high in patients with diabetes mellitus and gestational diabetes (134). This may be related to the fact that the RAGE receptor plays an important role in diabetes. However, excluding the five patients with this diagnosis from the analysis did not change the results.

In the last decades, many inventories have been made to find good predictive biomarkers for PE. However, still low predictive values with markers have been reached, for both single and multiple protein markers (135). To get more insight into the pathophysiological process during impaired placentation and PE will lead to more targeted ways for searching predictive markers. We showed that *S100A6* and *HSP90* are proteins that need further validation as candidate biomarkers in dedicated large cohort study initiatives for PE as the IMPROvED program mentioned above.

In conclusion, we developed a PRM method to measure concentrations of *S100A6* and *HSP90* that could play a role during the pathophysiological process in PE, in a unique set of maternal serum samples transversally collected in all trimesters of pregnancy from women with PE and age-matched normotensive controls.

Statement of clinical relevance

We compared concentrations of *HSP90*α by SRM and PRM with a commercially available and frequently used immunoassay. SRM and PRM have both the possibility to measure proteins in a multiplexed way in complex samples without the use of antibodies and other types of specific binders. A separation (e.g., SCX fractionation) that can also be performed by automation is necessary to reduce ion suppression and the effect of interfering compounds. It is concluded that notably, PRM that makes use of high-resolution mass spectrometry reaches sensitivity comparable with the immunoassay (ng/mL). For PRM, even a better reproducibility was observed compared to the immunoassay. This opens ways to address in a multiplexed manner complex samples such as serum for quantitative analysis of dozens of proteins in a single run using a relatively small volume of serum (seven microliters as used in present study). The present study addresses a medical need to measure sets of proteins for which no antibodies or partly characterized antibodies are available and if the amount of serum sample is limited, for instance, in population studies.

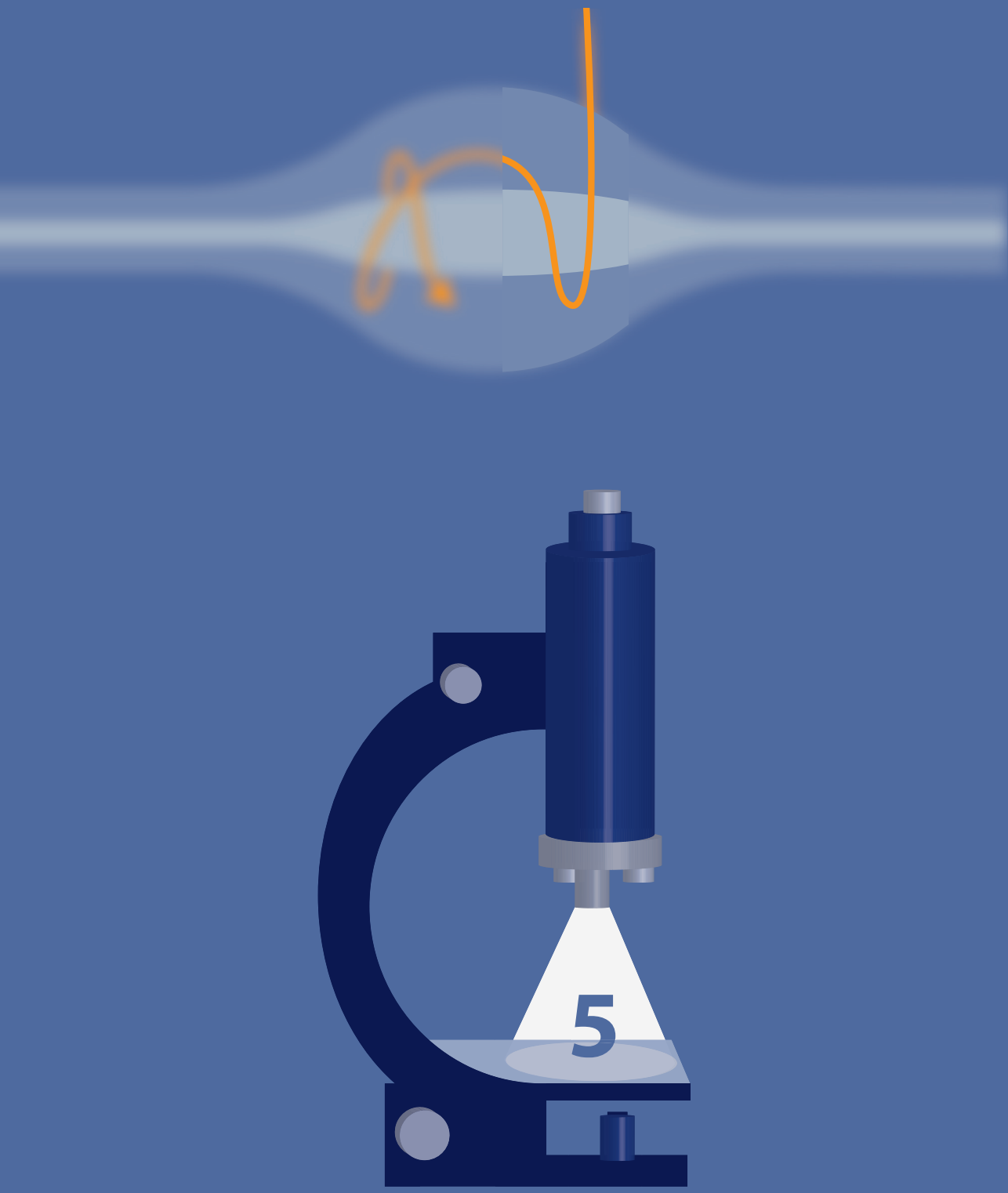
5

Chapter 5

Comparison of targeted mass spectrometry techniques with an immunoassay: a case study for HSP90α

Coşkun Güzel[1], Natalia I. Govorukhina[2], Christoph Stingl[1], Lennard J.M. Dekker[1], Alexander Boichenko[2], Ate G.J. van der Zee[3], Rainer Bischoff[2] and Theo M. Luider[1]

[1] Department of Neurology, Neuro-Oncology, Clinical and Cancer Proteomics Laboratory, Erasmus University Medical Centre, Rotterdam, the Netherlands
[2] Department of Analytical Biochemistry, Centre for Pharmacy, University of Groningen, Antonius Deusinglaan 1, 9713 AV, Groningen, the Netherlands
[3] Department of Gynecology, University Medical Centre Groningen, Hanzeplein 1, 9713 GZ, Groningen, the Netherlands

Proteomics Clin Appl. 2018 Jan;12(1). doi: 10.1002/prca.20170010

Abstract

Purpose

The objective of this study was to better understand factors governing the variability and sensitivity in SRM and PRM, compared to immunoassay.

Experimental design

A 2D-LC-MS/MS-based SRM and PRM assay was developed for quantitative measurements of *HSP90α* in serum. Forty-three control sera were compared by SRM, PRM, and ELISA following the manufacturer's instructions. Serum samples were trypsin-digested and fractionated by SCX chromatography prior to SRM and PRM measurements. Analytical parameters such as linearity, LOD, LOQ, repeatability, and reproducibility of the SRM, PRM, and ELISA were determined.

Results

PRM data obtained by high-resolution mass spectrometry correlated better with ELISA measurements than SRM data measured on a triple quadrupole mass spectrometer. All three methods (SRM, PRM, ELISA) were able to quantify *HSP90α* in serum at the ng/mL level, but the use of PRM on a high-resolution mass spectrometer reduced variation and showed comparable sensitivity to immunoassay.

Conclusions and clinical relevance

Using fractionation, it is possible to measure ng/mL levels of *HSP90α* in a reproducible, selective, and sensitive way using PRM in serum. This opens the possibility to use PRM in a multiplexed way as an attractive alternative for immunoassays without the use of antibodies or comparable binders.

Introduction

Targeted proteomics by SRM on triple quadrupole mass spectrometers is a widely used strategy to quantify multiple proteins in complex body fluids like serum (32-34). While SRM is a highly selective method, interferences in complex biological samples often limit sensitivity in comparison to immunoassays unless appropriate sample preparation is performed (38-40). Co-eluting peptides with a precursor ion mass close to the peptide of interest may result in fragment ions that overlap with the targeted transitions resulting in considerable chemical noise. Such noise limits sensitivity and contributes to diminished accuracy and precision. While SRM has emerged as the most widely used experimental approach to quantify proteins in biological samples by mass spectrometry (35, 36), it is nevertheless challenging to quantify low levels of proteins in biological samples like serum or plasma due to the limited loading capacity of capillary or nano-LC columns and to the often insufficient resolution needed to separate interfering compounds. This is the reason that ligand binding assays (LBAs) and notably enzyme-linked immunosorbent assays (ELISA) are routinely used for protein bioanalysis despite their limitations such as the high development cost for sensitive, well-characterized antibodies, and cross-reactivity with other proteins or interference from other ligands binding to the target protein (4). Advantages of the immunoassay technology are the high sensitivity (detection limits <1 ng/mL) (3) and the ease with which they can be performed in a high-throughput format. While multiplexing is possible with immunoassays, for example, those based on flow cytometry, analytical quality generally suffers (6). PRM using high-resolution mass spectrometry (136) goes beyond SRM in that it covers a wider dynamic concentration range and provides data with higher mass accuracy (ppm- to sub-ppm level) thus reducing interferences caused by co-eluting compounds with similar but not identical mass transitions (43, 136). Moreover, PRM methods for individual peptides are easier to set up, since all transitions are monitored and optimal transitions can be retrieved and combined in a post-analysis way (45). Literature on PRM shows the feasibility of the approach for quantification of proteins in complex biological samples after proteolytic digestion (43, 46, 47). Notably, Domon and coworkers published on the use of PRM in large-scale experiments (137-141). However, reaching the ng/mL level in body fluids without using affinity binders (e.g. immunoglobulins) remains a challenge. This study shows the feasibility to measure low protein levels (ng/mL) in pre-fractionated, trypsin-digested serum in a reproducible manner. As an example, we targeted *HSP90α*, a protein that is up-regulated in various cancers and is thus pursued as a target for early diagnosis, prognosis and anticancer therapy (52, 142, 143). It plays a crucial role in protein folding and assists in removal of misfolded proteins. In this study, we compared the concentration of *HSP90α* in 43 sera from healthy subjects measured by SRM, by PRM and by a commercially available ELISA with respect to comparability, repeatability and sensitivity.

Materials and methods

Samples

Forty-three serum samples were obtained from the Department of Gynecology (UMCG). All newly referred women are routinely asked to give written informed consent for collection and storage of pretreatment and follow-up serum samples in a serum bank for future research. Relevant data and follow-up results are retrieved and transferred to an anonymous, password-protected database. Identity is protected by study-specific, unique codes, and true identity is only known to two dedicated data managers. According to Dutch regulations, these precautions mean that no further institutional review board approval is needed (http://www.federa.org). The serum samples used for this study were from women referred to the UMCG for an abnormal cytological analysis but who did not show any signs of developing cervical cancer upon follow up examination. Glass tubes (Becton Dickinson, #367953), with a separation gel and micronized silica to accelerate clotting, were used for blood collection. Serum was prepared by letting freshly collected blood coagulate at room temperature at least for 2 hours (till 8 hours), followed by centrifugation at room temperature for 10 min at 3000 rpm. Serum samples were stored at −80°C in aliquots until analysis.

Prefractionation by SCX chromatography

Forty-three serum samples from healthy subjects (Table S1, Supporting Information) were analyzed, and a sample of pooled serum from a separate set of healthy volunteers containing approximately 100 ng/mL *HSP90*α was used as quality control (QC1). Seven μL from each serum sample was diluted 47-times in 0.01% RapiGest SF (Waters, Milford, MA) in 50 mM ammonium bicarbonate pH 7.8, reduced using 15 mM DTT, alkylated with 15 mM iodoacetamide (IA) and subsequently digested by adding 30 μL trypsin (100 μg/mL 3 mM Tris-HCl pH 8.8) (Gold, Mass Spectrometry Grade, Promega, Madison, WI) at 37°C overnight. The enzymatic reaction was stopped by adding 50% FA in water to reach a final concentration of 0.5-1.0% FA. Digested sera were spiked with 40 fmol of two SIL (stable isotope-labeled) proteotypic peptides YIDQEELNK ($^{13}C_6{}^{15}N_2$) and DQVANSAFVER ($^{13}C_6{}^{15}N_4$) (Thermo Fisher Scientific, Bremen, Germany; purity of >97% as stated by the manufacturer (Ultimate-grade)). Subsequently, the digested samples were desalted using a macroporous reversed-phase mRP-C18 column (Agilent, Palo Alto, California, USA; 4.6 mm × 50 mm) at a flow rate of 750 μL/min according to Boichenko *et al.* (144) and off-line fractionated on a Luna 5 μm, 150 × 2 mm SCX column (Phenomenex, Torrance, CA) under the following conditions: buffer A (14 mM KH_2PO_4, 24 mM H_3PO_4, pH 2.5, adjusted with 37% (w/w) HCl) in 25% (v/v) acetonitrile (HPLC grade; Biosolve, Valkenswaard, the Netherlands) in Milli-Q water; buffer B (buffer A containing 350 mM KCl); linear gradient from 100% buffer A to 40% buffer B in 40 min, followed by a wash with 100% buffer B until 45 min at a flow rate of 200 μL/min and equilibration of the column in buffer A for 17 min. All chemicals used for SCX fractionation were purchased from Sigma-Aldrich (St Louis, MO). Fifty μL fractions

(180 fractions in total for each serum sample) were collected in 384-well plates (VWR, Amsterdam, the Netherlands) and sealed with an adhesive aluminum foil (VWR, Amsterdam, the Netherlands). Fractions were dried down in SpeedVac concentrator (RVT4104, Scientific Savant, San Jose, CA) and subsequently stored at - 20°C until further analysis. Samples were reconstituted in 0.1% FA prior SRM and PRM measurements. Figure 1 shows a general flowchart of how the study was performed.

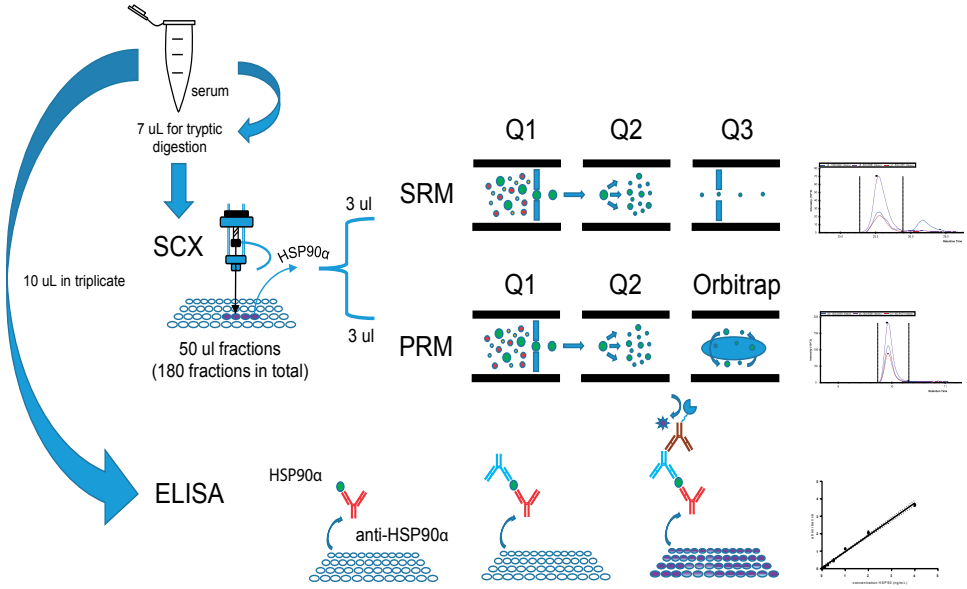

Figure 1. Flowchart of experimental design.

SRM

SRM for quantitative measurements of *HSP90α* in the 43 SCX-fractionated serum digests was performed targeting the two proteotypic peptides YIDQEELNK and DQVANSAFVER. The peptides were selected after analyzing a tryptic digest of recombinant *HSP90α* (Genway Biotech Inc, San Diego, CA) by LC-MS/MS, since they generated the most intense fragment ions. The shotgun mass spectrometry proteomics data have been deposited to the ProteomeXchange Consortium via the PRIDE (119) partner repository with the dataset identifier PXD007601 and 10.6019/PXD007601. Peptides containing potential missed cleavage sites, methionine, cysteine, or ragged ends KK, KR, and RR were excluded. An online BLAST analysis (Program: NCBI BLASTP 2.2.29, database: UniProtKB database, January 3, 2014) showed that YIDQEELNK could be used to quantify *HSP90α* (P07900) and *HSP90β*

(P08238) while DQVANSAFVER is specific for *HSP90*α only (85.8% sequence homology between *HSP90*α and *HSP90*β). The possibility of detection of *HSP90*β is fairly small, since this protein is present at much lower levels in serum levels (~1-2 ng/mL) (117, 118) than *HSP90*α. SCX-fractionated peptides were separated using a nanoACQUITY LC system equipped with a reversed-phase analytical BEH300 C18, 300 Å, 1.7 μm, 75 $\mu\text{m} \times 200$ mm column. Samples were desalted at a flow rate of 8 $\mu\text{L/min}$ with a C18 trap column, 5 μm, 100 Å, 180 $\mu\text{m} \times 20$ mm for 5 min using 0.1% formic acid (FA) in water prior separation. Separation was performed on the above mentioned analytical column at a flow rate of 300 nL/min with 0.1% aqueous FA (mobile phase A) and 0.1% FA/ACN (mobile phase B) as solvents with a linear gradient from 1.5% B at 0 min to 40% B at 30 min. The column was washed with 80% B for 4.9 min and equilibrated with 1.5% B for 24.9 min. All LC solvents were UHPLC grade and purchased at Biosolve (Valkenswaard, the Netherlands). The nanoACQUITY LC system was connected to a Xevo TQ-S (Waters Corp., Milford, MA) triple quadrupole mass spectrometer in positive electrospray ionization mode. SRM signals were recorded for all samples in a single measurement for the doubly-charged peptide precursor ions YIDQEELNK (*m/z* 580.29 for the $^{13}C_6{}^{15}N_2$ labeled peptide) and DQVANSAFVER (*m/z* 623.31 for the $^{13}C_6{}^{15}N_4$ labeled peptide). The following parameters were set using a nanoflow Z-spray ion source: capillary voltage 3000 V, nebulizer gas (nitrogen) 0.15 bar, collision gas flow 0.15 mL/min (argon), source temperature 70°C, LM/HM (low mass/high mass) quad 1 resolution 3.0/15.20, LM/HM quad 2 resolution 2.90/14.80, ion energy 0.9, and cycle time was set to automatic operation. The selected transitions for YIDQEELNK and DQVANSAFVER are shown in Table 1.

Table 1. Selected transitions for YIDQEELNK (y5, y6, and y7) and DQVANSAFVER (y7, y8, and y9) with their corresponding fragment masses that were used to perform quantitative LC-MS/MS assays in the SRM and PRM mode. Both CV and weighted CV (see text for discussion) were calculated from 43 SCX-fractionated serum samples. Significantly, more variation (weighted CV) was observed for endogenous DQVANSAFVER than for YIDQEELNK when measured by SRM. PRM measurements did not show such significant differences. The SIL peptides showed a similar effect, although to a lesser extent because on average five times more SIL peptide was applied than the measured endogenous peptide (one outlier by PRM (sample no. 2, see Supporting Information Figure S3) was observed and this sample was removed from CV analysis only).

Peptide	y5	y6	y7
YIDQEELNK (m/z **576.28, +2**)	**632.33**	**760.38**	**875.41**
CV%/weighted CV%	SRM: 31.8/2.5	SRM: 47.7/2.6	SRM: 3.9/3.4
	PRM: 13.3/0.7	PRM: 9.9/0.7	PRM: 1.1/1.0
YIDQEELNK (SIL) (m/z **580.29, +2**)	**640.34**	**768.40**	**883.43**
CV%/weighted CV%	SRM: 21.4/1.3	SRM: 26.2/1.0	SRM: 2.3/2.1
	PRM: 5.4/0.3	PRM: 6.7/0.4	PRM: 0.6/0.5
Peptide	y7	y8	y9
DQVANSAFVER (m/z **618.30, +2**)	**822.41**	**893.45**	**992.52**
CV%/weighted CV%	SRM: 26.9/5.4	SRM: 15.0/8.0	SRM: 22.3/6.0
	PRM: 3.8/0.9	PRM: 2.5/1.2	PRM: 2.9/0.8
DQVANSAFVER (SIL) (m/z **623.31, +2**)	**832.42**	**903.46**	**1002.52**
CV%/weighted CV%	SRM: 10.5/2.2	SRM: 5.8/3.1	SRM: 6.0/1.4
	PRM: 1.9/0.4	PRM: 1.2/0.6	PRM: 1.6/0.4

The indicated collision energy varied from 15-18 V and 17-19 V depending on the fragment ion, respectively. The SRM signals were integrated using Skyline software (version 3.5.0.9321) tool (61) and *HSP90*α concentration was calculated by using the peak area ratio of endogenous and SIL peptide.

The two peptides were found in six (on average) SCX fractions. These six fractions were pooled to obtain a QC2 sample. A serial dilution of five SIL peptide concentrations (calibrants) between 0 ng/mL – 30 ng/mL (i.e. 0, 0.3, 1.2, 3.0, 6.0, 30.0 ng/mL) was prepared in the QC2 sample and in its pure condition (dissolved in just 0.1% aqueous FA). Three microliters of each concentration were injected onto the nano-LC MS. Subsequently, regression analysis was performed by plotting the concentration versus total peak area (of all related y-transitions) of each SIL peptide. The proteomics data (.raw and .mzML files) and the transition list (.csv

file) were deposited in the Peptide Atlas SRM Experiment Library (PASSEL) assigned with identifier PASS01047 (http://www.peptideatlas.org/PASS/PASS01047).

To determine the variability (in CV%) of the transitions (endogenous and SIL) of YIDQEELNK and DQVANSAFVER for all 43 sera measured, the percent contribution of each transition was calculated by the ratio of its peak area to the total peak area from all transitions for each serum sample. Considering that the intensities of the observed transitions differ considerably, we also calculated weighted CV. The weighted CV (in weighted%) for each transition was calculated by multiplying the CV% with the averaged peak area ratio transition/total transition of the 43 samples. Additionally, the statistical significance (unpaired *t*-test) was determined of the weighted CVs between YIDQEELNK and DQVANSAFVER (endogenous and SIL) for both SRM and PRM.

PRM

The identical 43 SCX-fractionated serum digests and same serial dilutions, as described in the previous section were measured by PRM based on a single measurement and analyzed in Skyline. These measurements were carried out on a nano-LC system (Ultimate 3000 RSLCnano, Thermo Fisher Scientific, Germering, Germany) online coupled to an Orbitrap Fusion mass spectrometer (Thermo Fisher Scientific, San Jose, CA, US). Samples were loaded onto a trap column (PepMap C18, 300 µm ID × 5 mm length, 5 µm particle size, 100 Å pore size; Thermo Fisher Scientific), washed and desalted for 5 min using 0.1% TFA/water as loading solvent. Next, the trap column was switched in-line with the analytical column (PepMap C18, 75 µm ID × 250 mm, 2 µm particle and 100 Å pore size, Thermo Fisher Scientific). Peptides were eluted with the following binary gradient starting with 12% solvent B for 4 min and then from 12% to 25% solvent B in 14.7 min, where solvent A consisted of 0.1% FA in water, and solvent B consisted of 80% acetonitrile and 0.08% FA in water. The column flow rate was set to 250 nL/min, and the oven temperature to 40°C. All LC solvents were from identical UHPLC grade, as mentioned above in the previous section. For electrospray ionization, nano ESI emitters (New Objective, Woburn, MA) were used, and a spray voltage of 1.8 kV was applied. For PRM of the doubly charged precursor ions of YIDQEELNK and DQVANSAVER (endogenous and SIL), we used the targeted MS/MS mode set up as follows: isolation width of 1.4 Da, HCD fragmentation at a normalized collision energy of 24%, ion injection time of 502 ms (by setting the AGC target to 500,000 ions), Orbitrap resolution of 240,000. Selection of precursor ions was time scheduled (0 - 5.8 min for YIDQEELNK; 5.8 - 20 min for DQVANSAFVER), and each duty cycle consisted of two targeted MS/MS scans (endogenous and SIL form of a peptide) yielding a scan rate of approximately 0.9 Hz. Fluoranthene (202.0777 Da) was infused as lock mass (Easy IC option active). The mass spectrometry proteomics data have been deposited to the ProteomeXchange Consortium via the PRIDE (119) partner repository with the dataset identifier PXD006618 and 10.6019/PXD006618.

The variabilities (CV and weighted CV) of each fragment ion was calculated as described above for SRM. To investigate the effect of MS/MS resolution independently from different instrumental parameters, we set up a PRM method where MS/MS detection was conducted in the linear ion trap (resolution approximately 0.35 Da FWHM) of the Orbitrap Fusion MS. The value of a high-resolution mass spectrometer (PRM) in contrast to a triple-quad instrument (SRM) was demonstrated by comparing the presence of co-eluting peaks and MS2 spectra with identical samples (four SCX fractions) measured in PRM and by PRM at quadrupole ion trap resolution (IT-PRM) of the Orbitrap instrument under identical conditions. The IT-PRM method was set up in such a manner that MS/MS spectra were acquired in the ion trap (normal scan rate, AGC target of 100,000 ions, and maximum injection time of 500 ms). All other parameters were identical to the common PRM method described above. To exclude that differences between SRM and PRM are an effect of different experimental set-up (such as type of column, gradient, run time) four fractions of three different SCX-fractionated serum digests with relative high co-eluting peaks which were observed by SRM were also measured by IT-PRM. To gain insight in the effects of co-elution, peak ratios (between peak areas) were calculated between transitions of the endogenous peptides YIDQEELNK and DQVANSAFVER at the apex, half-height and one-quarter-height on the right side of the mass spectral peak and corresponding SIL peptides in pure condition (0.1% aqueous FA). The weighted CVs were calculated as described above for each transition at each peak height and evaluated. It was assumed that intensities and ratios were similar if interferences were not present.

Data analysis (LOD/LOQ, repeatability, reproducibility, stability)
Linearity, LOD, and LOQ of the *HSP90α*-derived peptides were calculated based on the slope (S) and the residual standard deviation of the slope (σ) from linear regression analysis according to ICH guidelines (http://www.ich.org) for single measurements. The LOD was defined as $3.3 \times \sigma/S$ and the LOQ as $10 \times \sigma/S$. Correlations were plotted to determine the relationship between both endogenous HSP90 peptides and linear regression coefficients were calculated.

To evaluate the repeatability, three technical replicates (three SRM or PRM measurements of an SCX-fractionated QC1 sample) were measured over a short time period (<4 days; kept at 4°C) and CVs in percentages calculated. Additionally, for stability testing, the SCX-fractionated QC1 sample was repeatedly measured over a longer period with long-term intervals (ranging from 4 days to 6 months) and was kept at 4°C during storage) by SRM and PRM. CVs of *HSP90α* concentrations were calculated for both YIDQEELNK and DQVANSAFVER. To determine the matrix effect on the two SIL peptides a regression analysis was performed of pure (dissolved in 0.1% aqueous FA) and matrix-spiked (spiked into background of SCX fractions) samples over a range of 0 ng/mL – 30 ng/mL (described

above in the section: "SRM") measured by SRM and PRM. From these calibration curves, the slopes were compared between both matrix-spiked and pure SIL peptides. We calculated the ratio (expressed in percentages) of the mean peak areas of calibrants related to matrix-spiked and pure SIL peptides. Statistical differences were calculated, and a probability lower than 0.05 was considered to be significant.

ELISA-based quantification

*HSP90*α was quantified in the identical set of 43 sera, including the QC1 sample with a commercial ELISA (Enzo Life Science, ADI-EKS-895). This assay has been described in several publications (145-148). Briefly, 100 µL of diluted serum (1:10 in Sample Diluent buffer) was incubated for 1 hour at room temperature in the microtiter plate pre-coated with anti-*HSP90*α antibody. Subsequently, a 400× diluted *HSP90*α monoclonal antibody conjugated to HRP (horseradish peroxidase) in HRP diluent was added followed by stabilized TMB (tetramethylbenzidine) substrate solution. The reaction was stopped by adding 100 µL of acidic stop solution provided by the manufacturer. The *HSP90*α standard (part no. 80-1564, Enzo Life Science, ADI-EKS-895) with 7 dilutions (i.e. 0.0625, 0.125, 0.250, 0.500, 1.000, 2.000, 4.000 ng/mL including a zero standard) was used for calibration. The absorbance for individual samples and the serial dilutions (two microtiter plates in total) were measured on a Multiscan Ascent microtiter plate reader (Thermo Electron, Marietta, Ohio, USA) at 450 nm. To determine the repeatability, each serum sample was measured in triplicate on the microtiter plate to calculate intra-microtiter plate variation (mean CV%). Four samples were measured on different ELISA plates to calculate inter-microtiter plate variation. Both LOD and LOQ were determined by linear regression analysis in analogy to the SRM and PRM measurements. *HSP90*α levels obtained in SRM and PRM mode were compared to ELISA measurements by correlation plots. Bland-Altman plots for the ELISA to SRM/PRM method comparison were constructed showing 95% limits of agreement. Methods were considered to be in agreement if the chosen mean bias interval was within ± 5%. The significance of these method comparisons was determined by the Welch *t*-test.

Comparability SIL peptides and immunoassay standard

To determine the comparability of the SRM, PRM based on the SIL peptides and the immunoassay recombinant *HSP90*α standard (1 µg/mL; calibration standard provided with the ELISA kit), an amount of four ng of the HSP90 SIL peptides was mixed with two ng of the immunoassay standard and reduced (5.1 mM DTT), alkylated (15.1 mM IA) and trypsin (50 ng) digested at 37°C overnight. The sample which corresponded to 56.7 pg on column (three µL of injection volume) was measured in triplicate by SRM and PRM as described before. Subsequently the ratios between the endogenous peptides of the *HSP90*α standard and SIL peptides were used to determine the *HSP90*α concentration. Additionally, to assess the purity of the protein standard, a data-dependent acquisition was used. For nano-LC separation (also three µL of the corresponding sample), a linear gradient from 4% to 38%

solvent B in 90 minutes was used and followed by a shotgun method with Orbitrap MS1 acquisition from *m/z* 400 – 1600 at 120,000 resolution (AGC = 40,000 ions) followed by ion trap CID MS/MS spectra (30% normalized collision energy, AGC = 10,000 ions, and maximum injection time of 40 ms) for at most 3 seconds ('top-speed' type DDA method). Peptides were identified and assigned to proteins by exporting features, for which MS/MS spectra were recorded, using the ProteoWizard software (version 3.0.9248; http://proteowizard.sourceforge.net). Resulting mgf file was submitted to Mascot (version 2.3.02, Matrix Science, London, UK) and applied to the human database (UniProtKB/Swiss-Prot, version 151112, 20194 entries) for protein identifications. The following parameters were used: fragment ion mass tolerance of 0.50 Da, parent ion mass tolerance of 10 ppm, maximum number of missed cleavages of two. In the Mascot search engine oxidation of methionine was specified as a variable modification while carbamidomethylation of cysteine was set as a fixed modification. Scaffold software (version 4.7.5, Proteome Software Inc., Portland, OR) was used to compute protein grouping, peptide probabilities and protein probabilities (149). Peptides identified with Mascot ions sore >25 were considered to be true identifications. The mass spectrometry proteomics data have been deposited to the ProteomeXchange Consortium via the PRIDE (119) partner repository with the dataset identifier PXD006615 and 10.6019/PXD006615.

LOD/LOQ comparison of PRM with ELISA

LOD/LOQ obtained by *HSP90*α ELISA were compared with PRM only (not measured by SRM due to too low sensitivity). For this purpose, serial dilutions of SIL peptides were prepared in the pooled fraction of the SCX-fractionated QC1 sample (as described above in the section: "ELISA-based quantification") containing comparable concentrations of the *HSP90*α calibrants used for ELISA. The LOD and LOQ were calculated using regression analysis as described above in the section: "Data analysis".

Results

We combined fractionation of peptides by SCX chromatography of trypsin-digested serum with LC-MS in the SRM or the PRM mode to quantify *HSP90α* and compared the results with a commercially available *HSP90α* ELISA.

Linearity, LOD, LOQ of SRM, PRM and ELISA by linear regression analysis

An overview of the calculated LODs and LOQs for both SRM and PRM assays (concentration range 0 – 30 ng/mL), and for the ELISA, for which a linear regression analysis was performed as recommended by the manufacturer (concentration range 0 - 4 ng/mL), is shown in Table 2.

Table 2. Calculated LOD and LOQ levels in ng/mL for *HSP90α* in the pooled fraction of the SCX-fractionated QC1 sample based on SIL peptides YIDQEELNK and DQVANSAFVER for SRM, PRM and comparable *HSP90α* ELISA measurements.

SRM

Peptide	LOD (ng/mL)	LOQ (ng/mL)
YIDQEELNK	5.6	17.4
DQVANSAFVER	6.7	20.4

PRM

Peptide	LOD (ng/mL)	LOQ (ng/mL)
YIDQEELNK	1.0 (0.5)*a*	2.9 (1.6)*a*
DQVANSAFVER	1.3 (0.5)*a*	3.8 (1.5)*a*

ELISA

Cat No. ADI-EKS-895, Enzo Life Science	LOD (ng/mL)	LOQ (ng/mL)
HSP90α specific mouse monoclonal antibody	0.4	1.2

a) Calculated if the same standard dilutions were used as described by the manufacturer of the ELISA.

In addition, from an independently prepared serial dilution (comparable to the ELISA range from 0 - 4 ng/mL, according to the manufacturer) measured by PRM, an R^2 of 0.986 and 0.989 was obtained for YIDQEELNK between ELISA and DQVANSAFVER between ELISA, respectively. In the PRM measurements and from regression analysis, the LOD for both YIDQEELNK and DQVANSAFVER was found to be 0.5 ng/mL. An LOQ of 1.6 ng/mL and 1.5 ng/mL was calculated for YIDQEELNK and DQVANSAFVER, respectively. These values are significantly lower than those listed in Table 2 and are on a par with those obtained by ELISA. It can be seen from Table 2 that in the SRM mode, the LOD and LOQ values for both peptides are considerably larger (by a factor of about 6) than in the PRM mode, attesting to the superiority of the PRM method. Calibration curves for the two *HSP90α* SIL peptides spiked into the pooled fraction of the SCX-fractionated QC1 sample as well as for pure standards based on five serial dilutions (i.e., 0, 0.3, 1.2, 3.0, 6.0, 30.0 ng/mL) are shown in Figure S1. High correlations between results of matrix-spiked and pure conditions were obtained in PRM (>0.990). To determine effects due to matrix, the mean ratios were calculated between the peak areas for the matrix-spiked and pure conditions of all calibrants (0.3 - 30 ng/mL) based on the calibration curves as seen in Figure S1. SRM gave mean ratios of 252.3% and 295.9% for YIDQEELNK and DQVANSAFVER, respectively. Similar ratios were obtained for PRM for YIDQEELNK and DQVANSAFVER with 217.3% and 241.4%, respectively. Thus, peptides spiked into matrix consistently gave a stronger response compared to the pure peptide dissolved in 0.1% aqueous FA, especially at low ng/mL concentrations. This may be due to less adsorption as a result of other (sacrificial) matrix peptides which bind to

the surface of the vial, as also observed for oligonucleotides (150). Linearity was better for peptides spiked into matrix compared to those spiked into 0.1% aqueous FA for SRM and PRM measurements.

Comparison of the repeatability and stability of SRM, PRM and ELISA assay

The repeatability of PRM was significantly better than for SRM for both peptides YIDQEELNK (CV of 1.1% for PRM versus 8.4% for SRM) and DQVANSAFVER (CV of 1.8% for PRM versus 11.8% for SRM, see Table S2, Supporting Information). Repeatability for PRM was also superior compared to the commercial ELISA assay (intra-microtiter plate CV of 4.2%; inter-microtiter plate mean CV of 7.5%, see Table S2).

The stability experiments showed CVs of 15.6% for YIDQEELNK and 17.7% for DQVANSAFVER from repeated measurements by SRM and 4.5% and 8.9% for PRM, respectively.

Quantification of HSP90α by SRM, PRM, and ELISA in serum

Table S1 shows serum *HSP90α* levels measured based on the proteotypic peptides YIDQEELNK relating to the α and β isoforms and DQVANSAFVER relating to the α isoform, by SRM and PRM in comparison to ELISA. Both SRM and PRM assays had adequate sensitivity to quantify *HSP90α* in all trypsin-digested, SCX-fractionated serum samples. The mean concentration of *HSP90α* across all sera measured by SRM was 73.4 ± 32.8 ng/mL based on the YIDQEELNK peptide, while the DQVANSAFVER peptide gave a significantly (unpaired *t*-test, p=0.001) higher concentration of 108.4 ± 60.7 ng/mL, due to a higher variance (see Figure 2A; more examples are shown in Figure S2 in Supporting Information).

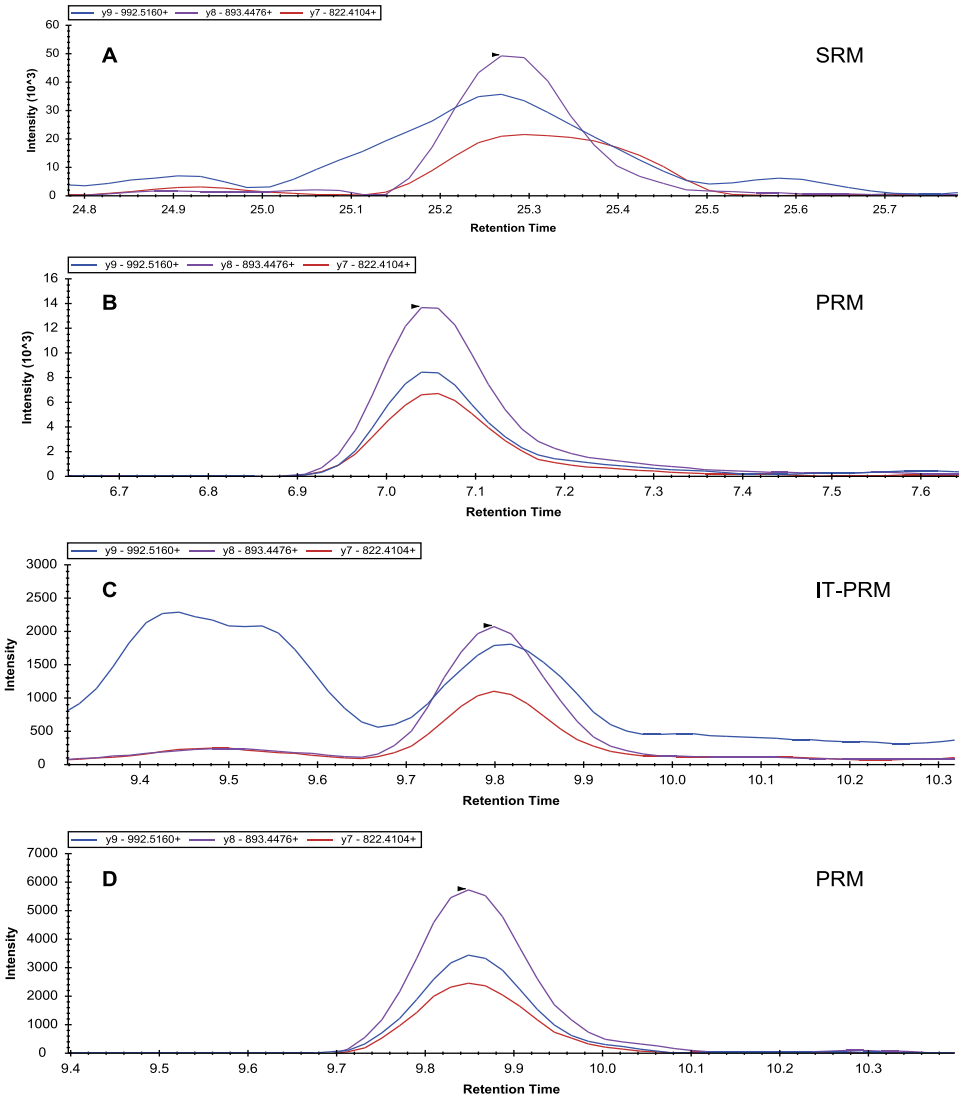

Figure 2. SRM, PRM, and IT-PRM chromatograms of an identical SCX-fractionated serum sample (sample no. 28, see Supporting Information Table S1) as observed in Skyline. An example of co-eluting peaks by means of misaligned transitions (y7, y8, and y9) for DQVANSAFVER was observed in SRM (A) and IT-PRM (C). For comparison, the identical sample was measured by PRM simultaneously with SRM and IT-PRM measurements (B and D, respectively). More examples of these probable interfering co-eluting peaks are shown in Supporting Information Figure S2 and S7.

The mean concentration of *HSP90*α in the same set of samples based on PRM measurements of the peptides YIDQEELNK and DQVANSAFVER was 118.8 ± 66.7 ng/mL and 128.1 ng/mL ± 72.7 ng/mL, respectively, and these concentrations were not different (unpaired *t*-test,

p=0.539). Possible interference of co-eluting compounds was not observed in PRM due to the higher mass resolution (see Figure 2B or 1D and Figure S2). The CVs for the most intensive DQVANSAFVER-related transition y8 were 15.0% and 5.8% in SRM and 2.5% and 1.2% in PRM for the endogenous and the SIL peptides, respectively (Table 1; Figure 3).

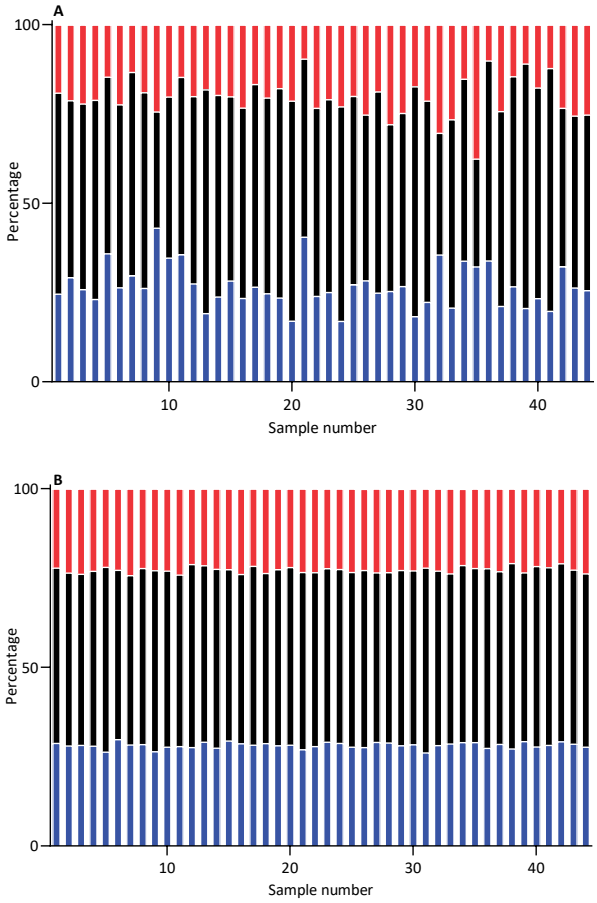

Figure 3. Representation of the variability in the transitions of the *HSP90α* proteotypic peptide DQVANSAFVER measured by SRM (A) and PRM (B). Bars represent normalized peak areas (% of total) of the transitions y7 (red), y8 (black), and y9 (blue) in 43 SCX-fractionated serum samples from healthy subjects. Sample number 44 corresponds to 1 fmol of the pure (0.1% aqueous FA) SIL peptide. See Supporting Information Figure S3 for the corresponding results for YIDQEELNK.

Comparison of the weighted CVs for the y-ions of YIDQEELNK with y-ions of DQVANSAFVER showed that these CVs were significantly different for SRM but not for PRM, indicating interference in the SRM assay. For both SRM and PRM the SIL peptides showed better

weighted CVs compared to the endogenous peptides, but the concentration of the SIL peptides was higher (on average five times).

The correlation between *HSP90α* concentrations based on SRM measurements of YIDQEELNK and DQVANSAFVER was poor with an R^2 of 0.642 (Figure S4 (A); Table S3, Supporting Information) and significantly worse compared to PRM (R^2 = 0.894). Correlations above 0.7 were considered as good (151). To compare the SRM and PRM measurements with an established assay, the same serum samples were measured with a commercially available *HSP90α* ELISA as illustrated in Figure S5, giving an average concentration of 113.7 ± 60.1 ng/mL. This was in excellent agreement (unpaired *t*-test, p=0.465) with the PRM measurements for both peptides (average 123.9 ± 69.6 ng/mL). Comparison of PRM with ELISA showed an R^2 of 0.878 and 0.811 for YIDQEELNK and DQVANSAFVER, respectively (Figure S4 (E-F); Table S3, Supporting Information). Correlation was not significantly different for YIDQEELNK (p=0.709) and DQVANSAFVER (p=0.295), as determined by the Welch *t*-test. Correlation of SRM and ELISA data reached R^2 values of 0.764 and 0.652 for YIDQEELNK and DQVANSAFVER peptides, respectively (Figure S4 (C-D); Table S3, Supporting Information). Measured concentrations of *HSP90α* were significantly different for the SRM assay based on YIDQEELNK ($p<0.001$) and the ELISA results but not for SRM based on DQVANSAFVER (p=0.686) although significantly more variation was observed for DQVANSAFVER than for YIDQEELNK (Table 1 and Figures 2 and S3). Comparison of the measured concentrations by SRM and PRM with the ELISA in a Bland-Altman plot with a +/- 95% confidence interval showed a bias of -41.0% for the YIDQEELNK endogenous peptide measured in SRM (Figure S6, Supporting Information), while PRM had a bias of 3.9%. The bias for DQVANSAFVER by SRM was -5.7% and 11.1% by PRM, respectively. The kind and degree of interference of unknown components can vary from sample to sample and this causes SRM signals to display a much larger spread than PRM signals because these unknown components have less chance to be included in the PRM experiments, see Figure 3.

Comparability of SIL proteotypic peptides with HSP90α as calibration standard

One major difference between MS-based methods and the ELISA assay is that the first uses stable isotope-labeled, synthetic, proteotypic peptides as standards while the latter uses *HSP90α* protein. In order to link these two principles of assay calibration, we mixed 4 ng of our SIL peptides with 2 ng of the ELISA standard as described in the section: "Materials and methods" and measured the *HSP90α* concentration by SRM and PRM, respectively. In this way, the final concentration of the ELISA standard is 1.0 $\mu g/mL$. SRM and PRM measurements based on YIDQEELNK gave 1.4 µg/mL *HSP90α* and 1.1 µg/mL *HSP90α*, respectively. Both SRM and PRM measurements based on DQVANSAFVER gave a significantly lower concentration of 0.36 µg/mL *HSP90α*. To gain a better insight into this unexpected discrepancy, we evaluated the purity of the *HSP90α* ELISA standard by shotgun proteomics using a data-dependent acquisition (DDA) approach. A database search resulted

in 32 (Table S4, Supporting Information) identified proteins of which the top five hits (based on the number of exclusive unique peptide counts) were related to high-abundant proteins (e.g., serum albumin, various types of keratin I and II) while *HSP90α* was ranked halfway of the list. The results showed further that identification of *HSP90α* was based on only 2% sequence coverage related to one peptide that did not correspond to the two selected proteotypic peptides used for this study. The protein complexity of the ELISA standard used in the ELISA could well explain the discrepancy observed above between ELISA and mass spectrometry-based techniques (SRM and PRM). Thus, these results show that while the *HSP90α* ELISA standard can be ideal for immunoassays, it is not very easy to use in mass spectrometry-based analyses because the *HSP90α* ELISA standard contains other proteins.

High-resolution PRM and PRM at quadrupole mass resolution (IT-PRM)

To rule out the possibility that the discrepancy observed between SRM and PRM is due to instrument effects, we measured four fractions of three different SCX-fractionated serum digests (sample no. 9, 28, 32, Table S1) by SRM, by IT-PRM (PRM at quadrupole ion trap resolution) and by PRM (high-resolution) (Figure 2 and Figure S7 (Supporting Information)). Co-eluting peaks seen in SRM were also observed in IT-PRM, while in PRM no such observation was observed for identical samples applying the appropriate resolution settings during data analysis. The variation of transitions related to endogenous and the SIL peptides YIDQEELNK and DQVANSAFVER measured by IT-PRM and PRM at three points (apex, half-height, and one-quarter-height) of the peak is illustrated in Figure S8 (Supporting Information). For PRM, the intensities of each transition extracted from the three measured points of the endogenous peptides showed little aberration (weighted CV of ~3% for both YIDQEELNK and DQVANSAFVER, Table S5, Supporting Information), while variation for IT-PRM was considerably larger (highest weighted CV of 33.1% (y7-ion) for YIDQEELNK; highest weighted CV of 9.9% (y9-ion) for DQVANSAFVER, Table S5; see for more details Figure S9, Supporting Information). Transitions for pure SIL peptides showed almost identical intensities at the three measurement points by IT-PRM and PRM. These results show that the poorer performance of SRM in comparison to PRM is due to the lower resolution of ion analysis rather than to instrumental parameters.

Discussion

We developed a quantitative 2D-LC-MS/MS assay using SRM and PRM technology to measure *HSP90α* concentrations relating to two proteotypic peptides YIDQEELNK and DQVANSAFVER. The DQVANSAFVER is *HSP90α* specific, while the peptide YIDQEELNK relates to both *HSP90α* and β isoforms. However, it is very likely that only the α isoform was measured due to the presence of a very low contribution in serum of the β isoform (~1-2 ng/ml), as known from literature (117, 118). Both YIDQEELNK and DQVANSAFVER peptides could have post-translational modifications like phosphorylation considering the presence of serine and tyrosine in their sequence. It is very unlikely that these peptides

are phosphorylated according to literature (http://www.uniprot.org). However, some references (http://www.phosphosite.org) (152-154) indicate that the phosphorylation site of S505 can be phosphorylated in a few cell lines. By phosphoproteomics of cervical tissue and serum from a healthy volunteer, we could not detect such phosphorylation using TiO_2-based phosphopeptide enrichment for both peptides YIDQEELNK and DQVANSAFVER. Therefore, we assume that the contribution of phosphorylation is negligible.

To achieve sufficient sensitivity to detect *HSP90*α peptides, trypsin-digested sera were fractionated by SCX chromatography. Both HSP90 peptides were highly stable in SCX-fractionated serum and thus very suitable for this comparison. Comparison of the data of high-resolution mass spectrometry in PRM mode compared to SRM showed significantly better performance for PRM with respect to linearity, repeatability, sensitivity, and the almost complete removal in PRM of components which co-elute in SRM. For PRM, this resulted in a better LOD and LOQ compared to SRM and an almost identical LOD/LOQ ratio compared to ELISA. PRM results for both endogenous YIDQEELNK and DQVANSAFVER gave comparable levels to ELISA measurements ($p=0.709$ and 0.295, respectively) and correlated better for both peptides with ELISA data (R^2 = 0.878 and 0.811, respectively) than levels obtained by SRM (R^2 =0.764 and 0.652, respectively) (Figure S4). SRM results based on YIDQEELNK differed significantly ($p<0.001$) from the results of a commercial *HSP90*α ELISA, while those from the other peptide DQVANSAFVER showed no significant difference ($p=0.686$). This was unexpected because intense co-eluting peaks were observed for DQVANSAFVER but not for YIDQEELNK in SRM mode. From this, it can be concluded that co-eluting peaks do not correlate linearly with the observed differences. PRM showed almost no detectable co-eluting peaks (Figure 3), as was observed in SRM. Altogether PRM for YIDQEELNK- and DQVANSAFVER-derived fragment ions compared to SRM fragment ions resulted in much better weighted CVs, as shown in Table 1. Significantly more variation (weighted CV) was observed for endogenous DQVANSAFVER than for YIDQEELNK when measured by SRM, while PRM measurements did not show significant differences. The SIL peptides showed a similar effect, but to a lesser extent because on average five times more SIL peptide was used than the measured endogenous peptide. It is the variability of interfering (unidentified) components which causes the SRM signals to display a much larger spread than PRM signals, as also exemplified in Figure 3.

PRM is a technique that monitors all product ions within a certain scan range, meaning that fragment ion intensities are available for all observed fragments in PRM in contrast to SRM. For this reason, beyond the preselected ions (y5, y6, y7, y8, and y9 for both HSP90 peptides) more transitions can be evaluated. Selecting other transitions than used in this study did not affect the results; for comparison reasons, only the transitions used for SRM were analyzed. To rule out that discrepancies between SRM and PRM that were caused by a variation in experimental conditions (for instance, chromatography), four SCX fractions were measured

by IT-PRM (to resemble a triple quadrupole instrument as close as possible) and PRM on identical sample material in the same device. It is expected that the distribution of the transition intensities should align with each other if no interfering of co-eluting peaks (as demonstrated for the pure SIL peptides) were present. The deviation of the ideal situation became larger for low intense mass transitions related to both endogenous peptides observed by PRM measurements, while in IT-PRM mode significantly more deviation for all transitions (low and high intense) was noted compared to the pure peptide. This emphasized that SRM and IT-PRM are more susceptible to variation than PRM due to the lower mass resolution of the fragment ion spectra. Differences achieved by PRM were, therefore not due to different sample handling, ion-generation or chromatography, but due to the application of high-resolution mass spectrometry that reduced the number of co-eluting peaks that potentially generate interference. By the application of high-resolution mass spectrometry, a much better selection of the peptide of interest and its transitions can be made than in a triple quadrupole and possible interferences of neighboring co-eluting peaks can be avoided resulting in better sensitivity and repeatability. Overall, PRM resulted in better analytical performance for the YIDQEELNK and DQVANSAFVER peptides (both endogenous and SIL) compared to SRM.

The accurate determination of the amount of molecules is different for immunoassay and PRM. In immunoassay, mostly a recombinant protein is used that can be accurately measured by a protein assay. In these determinations, it is assumed that a recombinant protein mimics the protein present in a tissue or a biofluid. In SRM and PRM SIL peptides are synthesized, purified and accurate composition of amino acids is determined assuming resemblance with the peptide which is part of the protein of interest. Therefore, variations in the correct concentration of standards can be expected in these techniques. Bland-Altman plots (Figure S6) were calculated to determine whether the SRM and PRM were in agreement with ELISA results. From this, it was concluded that the YIDQEELNK peptide measured by PRM (and no peptides for SRM) was similar to ELISA measurements based on chosen criteria (within ± 5% bias interval level). For the peptide DQVANSAFVER measured by PRM, it was not expected that it would fall outside the criteria of 5% (i.e., 11.1%) since it reached in general good results in all conditions as described before in terms of repeatability, low LOD/LOQ, no co-eluting peaks, good correlation with ELISA. However, as was discussed above (see Table 1), the peptide DQVANSAFVER was found to generally perform slightly less than YIDQEELNK.

Comparability experiments in which the *HSP90α* level of the ELISA standard was determined by SRM and PRM measurements revealed that the discrepancy might be explained by the presence of many other proteins than *HSP90α* in this *HSP90α* standard. Likely the presence of these extra proteins could influence the SRM and PRM measurements if no fractionation is performed.

We demonstrated the high reproducible, robustness and sensitive PRM assay to determine *HSP90*α concentrations in SCX-fractionated sera at relative low ng/mL level. The sensitivity by PRM was in agreement as determined by ELISA data and showed better repeatability. By PRM and SRM, the quality of samples can easily be assessed by an aberrant transition distribution (Figure 3) whereas ELISA results caused by aberrations in the assay are much more difficult to detect.

If fractionation of biological samples is technically feasible, PRM can be used as an attractive alternative for immunoassay to quantify highly-reproducible proteins at the ng/mL scale in complex protein mixtures, including sera without the use of antibodies or comparable binders.

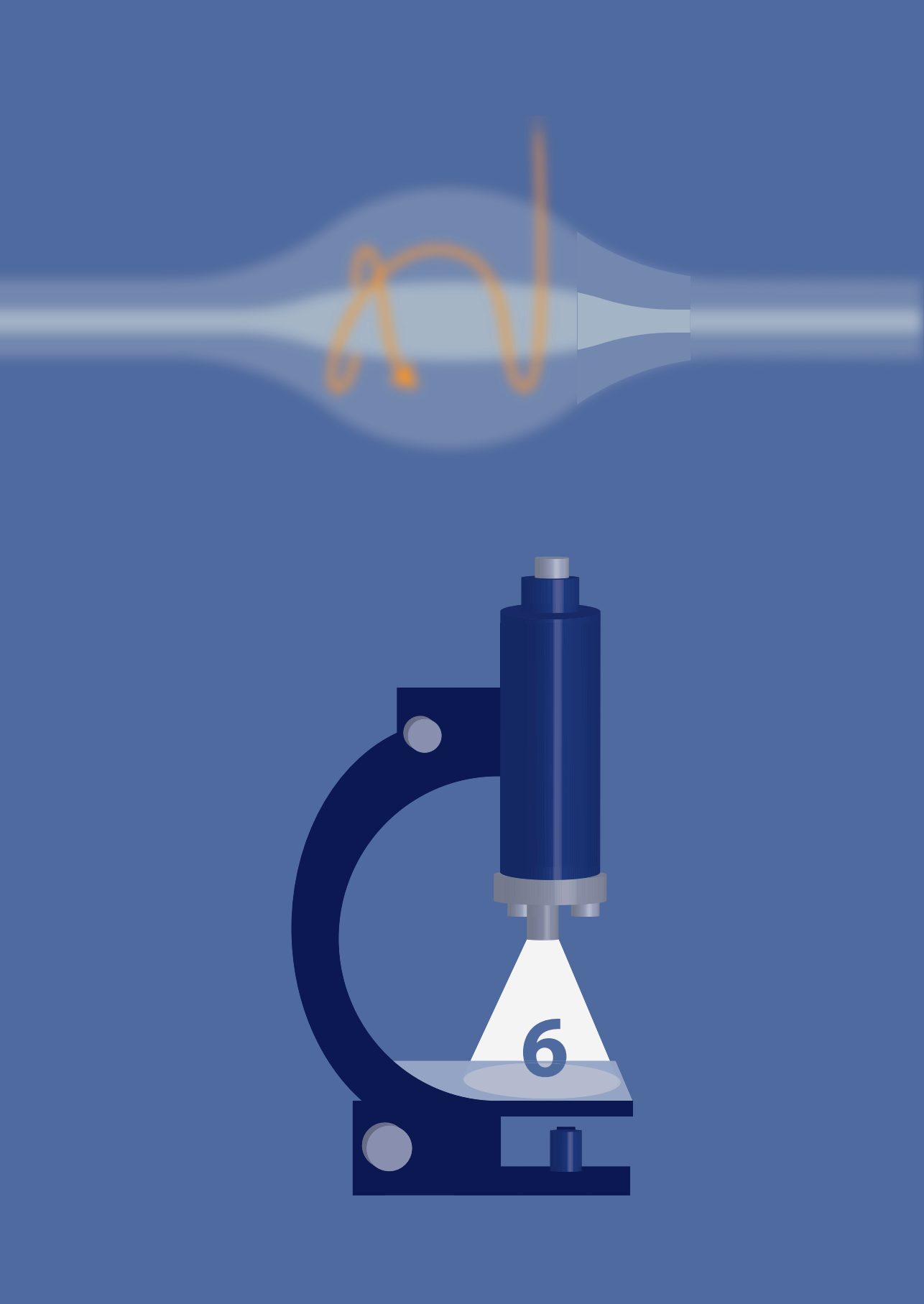
6

Chapter 6
Proteomic alterations in early stage cervical cancer

Coşkun Güzel[1], Natalia I. Govorukhina[2], G. Bea A. Wisman[3], Christoph Stingl[1], Lennard J.M. Dekker[1], Harry G. Klip[3,†], Harry Hollema[4], Victor Guryev[2], Peter L. Horvatovich[2], Ate G.J. van der Zee[3], Rainer P.H. Bischoff[2] and Theo M. Luider[1]

[1] Laboratory of Neuro-Oncology/Clinical & Cancer Proteomics, Department of Neurology, Erasmus University Medical Center Rotterdam, Wytemaweg 80, 3015 CN, Rotterdam, the Netherlands

[2] Department of Analytical Biochemistry, Centre for Pharmacy, University of Groningen, Antonius Deusinglaan 1, 9713 AV, Groningen, the Netherlands

[3] Department of Gynecologic Oncology, Cancer Research Center Groningen, University of Groningen, University Medical Center Groningen, Hanzeplein 1, 9713 GZ, Groningen, the Netherlands

[4] Department of Pathology, University Medical Center Groningen, University of Groningen, Hanzepein 1, 9713 GZ, Groningen, the Netherlands

[†]In memory of

Oncotarget. 2018 Apr 6;9(26):18128-18147. doi: 10.18632/oncotarget.24773

Abstract

Laser capture microdissection (LCM) allows the capture of cell types or well-defined structures in tissue. We compared in a semi-quantitative way the proteomes from an equivalent of 8,000 tumor cells from patients with squamous cell cervical cancer (SCC, n=22) with healthy epithelial and stromal cells obtained from normal cervical tissue (n=13). Proteins were enzymatically digested into peptides which were measured by high-resolution mass spectrometry and analyzed by "all-or-nothing" analysis, Bonferroni, and Benjamini-Hochberg correction for multiple testing. By comparing LCM cell type preparations, 31 proteins were exclusively found in early stage cervical cancer (n=11) when compared with healthy epithelium and stroma, based on criteria that address specificity in a restrictive "all-or-nothing" way. By Bonferroni correction for multiple testing, 30 proteins were significantly up-regulated between early stage cervical cancer and healthy control, including six members of the MCM protein family. MCM proteins are involved in DNA repair and expected to be participating in the early stage of cancer. After a less stringent Benjamini-Hochberg correction for multiple testing, we found that the abundances of 319 proteins were significantly different between early stage cervical cancer and healthy controls. Four proteins were confirmed in digests of whole tissue lysates by Parallel Reaction Monitoring (PRM). Ingenuity Pathway Analysis using correction for multiple testing by permutation resulted in two networks that were differentially regulated in early stage cervical cancer compared with healthy tissue. From these networks, we learned that specific tumor mechanisms become effective during the early stage of cervical cancer.

Introduction

Cervical cancer is one of the most common cancers in women worldwide (155-157). It is more prevalent in developing countries, where 83% of cases occur and where squamous cell cervical cancer (SCC) accounts for 15% of newly diagnosed cancers in women. In developed countries, it accounts for 3.6% of all new cancer cases (158). It was shown that 99% of cervical cancers are linked to infection with "high-risk" strains of human papillomavirus (HPV) (159, 160). HPV type 16 and 18 together are responsible for 70% of cervical cancers (161). HPV infections are associated with the development of high-grade cervical intraepithelial neoplasia (CIN2/3), which may eventually lead to SCC (162). It seems that the HPV E7 gene, which disrupts Rb function is devoid of genetic variants in precancer and cancer cases and strict conservation of 98 amino acids is critical for HPV16 carcinogenesis (163). To gain a deeper insight into the relation between genomic alterations and the development of cervical cancer, Ojesina *et al.* (164, 165) performed exome and whole genome sequencing. They showed relationships between recurrent somatic mutations, copy-number alterations, changes in transcript levels and gene alterations as a consequence of HPV integration, and the development of cervical cancer. Whole-genome sequencing showed that HPV integration disrupts HPV genes as well as probably nearby host genes. These disruptions can lead to specific mechanisms in cervical cancer. Linking genomics to proteomics data has recently led to new insights into these mechanisms in cancer development (166, 167). Laser capture microdissection (LCM) is a technique that allows the capture of different cell types or well-defined structures in tissue for subsequent genomics and proteomics analyses (168, 169). Notably, tissue from cancer patients has been analyzed by proteomics following this LCM technique (35, 170-174). Although this approach is very challenging due to the minimal amount of tissue material available for analysis, it was shown previously that a few hundred proteins could be identified from about 12,000 isolated cells from cervical cytological specimen (175). We compared by semi-quantitative analyses the protein abundances of 4,488 proteins based on one peptide using approximately 8,000 cells obtained from LCM-derived cervical cancer tissue with healthy cervical epithelium or stroma from women with a normal cervix. Parallel Reaction Monitoring (PRM) was applied to confirm selected differential proteins found by the shotgun proteomics approach. Data were subjected to Ingenuity Pathway Analysis (IPA) linking published genomics data to proteomics data generated in this study. From the networks acquired, we learned that specific tumor mechanisms become effective during the early stage of cervical cancer.

Results

The study included patients with squamous cell cervical cancer (SCC, n=22) and controls collected from patients who have undergone a hysterectomy for non-malignant reasons (n=13) (see Table 1).

Table 1. Overview of all squamous cervical cancer patients and healthy controls from which tissue was obtained.

Sample number	Age	FIGO stage
Early stage cervical cancer I/II		
1218	50	Ib2
1230	44	IIb
1239	43	Ib1
1291	34	Ib2
1298	80	Ib2
2110	77	IIb
2146	46	Ib2
2163	39	Ib1
2180	74	IIb
2246	73	Ib1
2252	44	Ib2
Late stage cervical cancer III/IV		
1225	58	IIIb
1348	71	IIIa
1685	26	IIIb
1966	75	IVb
1981	68	IIIb
1998	72	IIIb
2008	84	IIIa
2087	49	IIIb
2247	76	IIIb
2265	83	IVb
2297	52	IVa
Healthy cervical epithelium		Type
1247	43	hypermenorrhea /meno-/metrorrhagia
1262	51	prolapse
1315	36	prolapse
1477	41	uterine leiomyoma
1516	39	dysmenorrhea
1525	41	hypermenorrhea /meno-/metrorrhagia
1542	46	prolapse
1826	45	uterine leiomyoma

Sample number	Age	FIGO stage
1849	51	hypermenorrhea /meno-/metrorrhagia
1936	41	hypermenorrhea /meno-/metrorrhagia
1948	60	prolapse
2000	41	uterine leiomyoma
2001	49	uterine leiomyoma

Protein profiling by high-resolution mass spectrometry

By shotgun proteomics, the technical reproducibility of a tissue lysate digest in triplicate showed an overlap of identified proteins of 65%. The methodological overlap for three independently prepared identical LCM samples (performing digestion and microdissection) was 76%. Analysis of eleven early stage and eleven late stage SCC, thirteen healthy epithelium and healthy stroma samples by nano-LC-MS/MS resulted in a total of 2,989 identified proteins with a minimum number of two peptides, an FDR rate of 0.4% and an FDR rate of 0.04% for peptides based on 262,136 MS/MS spectra. On average 1,700 proteins per sample (1,296 – 2,189) were identified. Interestingly, levels of members of the Minichromosome Maintenance (MCM) family (*MCM2*, *MCM3*, *MCM4*, *MCM5*, *MCM6*, *MCM7*) (176, 177) were found to be highly significantly increased in cervical cancer tissue from early and late stage patients as compared to healthy tissue. A volcano plot illustrates the difference in abundance of proteins in the comparison of both early stage and late stage cervical cancer with the healthy epithelium (Figure 1A and 1B).

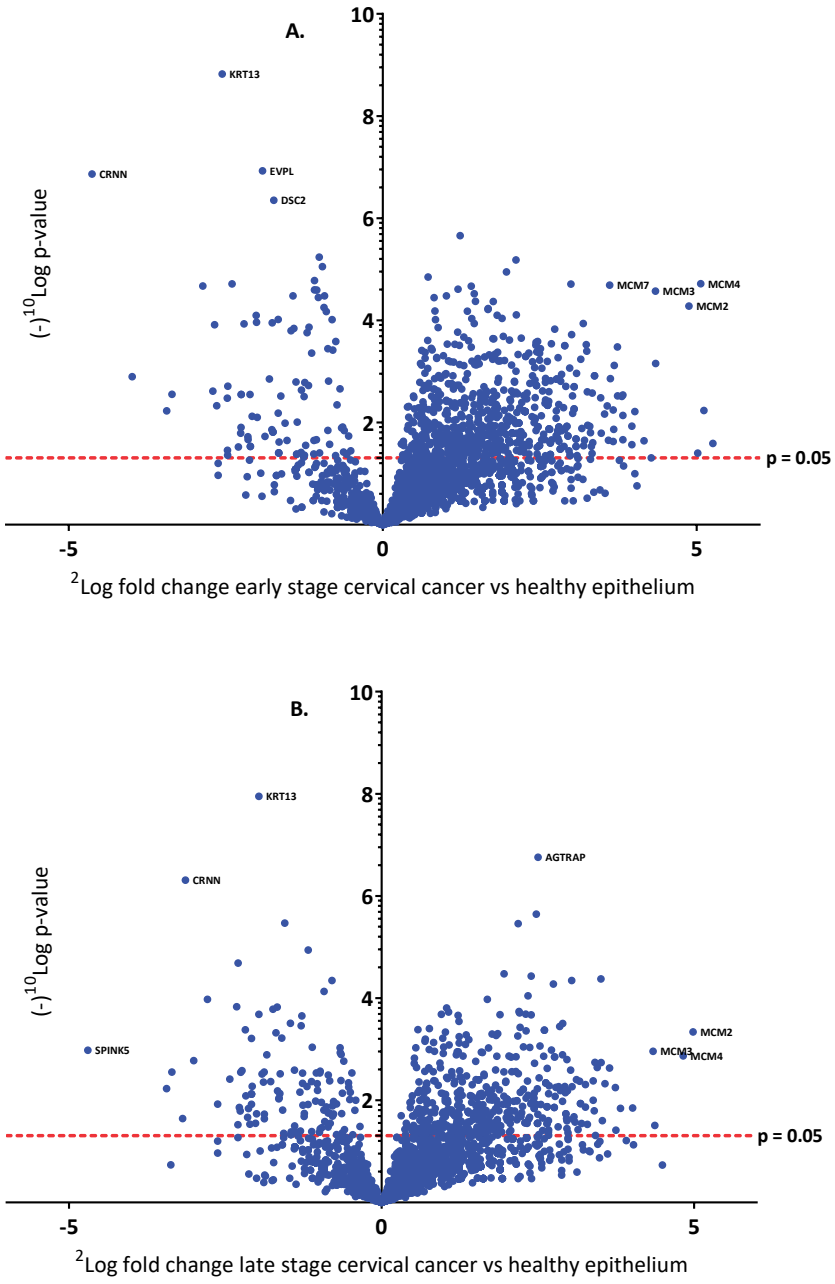

Figure 1. Differentially expressed proteins between early stage (A) and late stage (B) cervical cancer compared to healthy epithelium illustrated by a volcano plot. The x-axis represents the ^{2}log fold-change and y-axis the (-)^{10}log p-value. Examples of proteins that are differentially expressed with high significance are indicated with their names.

Data were analyzed by three analysis approaches to find proteins which were highly discriminative ("all-or-nothing" method, Bonferroni and a third less restrictive method Benjamini-Hochberg). In the most stringent "all-or-nothing" analysis, we searched for proteins being present in the early stage cervical cancer group (it was allowed that these proteins are presented in late stage cervical cancer as well) and not in healthy epithelium or stroma. This approach showed that 31 proteins ($p<0.05$) were discriminative between early stage cervical cancer and healthy epithelium (Table 2A). With this analysis, only *MCM4* of the MCM2-7 family was observed in early and late stage cervical cancer and not detectable in healthy epithelium and stroma cells. On the other hand, three proteins, *ENDOU*, *MT-ND4* and *RDH12* were exclusively present in healthy epithelium (in at least six out of thirteen samples). For stroma, six proteins *TNXB*, *COL21A1*, *OLFML1*, *FMOD*, *HSPB6* and *ABI3BP* were found (in at least six out of thirteen samples). After correction for multiple testing using the Bonferroni analysis ($p=9.88 \times 10^{-6}$), 30 proteins (Table 2B) were significantly different in the comparison of early stage cervical cancer tissue and healthy epithelium, while thirteen proteins (Table S1, Supplemental data) were significantly different between late stage cervical cancer tissue and healthy epithelium. Using the Benjamini-Hochberg correction (FDR = 5%) for multiple testing as the less stringent method, the abundances of 319 proteins (Table S2, Supplemental data) were found to be significantly different between early stage cervical cancer and healthy epithelium. Comparison of late stage cervical cancer with healthy epithelium resulted in 140 proteins (Table S3, Supplemental data) having significantly different levels.

Table 2. List of significant different proteins between early stage cervical cancer and healthy epithelium based on "all-or-nothing principle" (A; n=31) and after Bonferroni analysis (B; n=30). Zero counts were converted to 0.125 to enable log calculations. Table S1 shows a complete list of proteins assigned to late stage cervical cancer analyzed by Bonferroni analysis (here indicated with an asterisk (*)) and individual comparison of early and late stage cervical cancer with healthy epithelium using Benjamini-Hochberg as shown in Table S2 and S3, respectively.

A. "All-or-nothing" analysis			
Protein name	Gene name	p-value	2log fold-change
DNA replication licensing factor MCM4	MCM4	1.92E-05	5.1
Protein S100-P	S100P	3.13E-04	2.9
DNA polymerase delta catalytic subunit	POLD1	3.13E-04	2.9
DnaJ homolog subfamily C member 13	DNAJC13	1.21E-03	3.4
Replication factor C subunit 2	RFC2	1.21E-03	3.4
Inactive tyrosine-protein kinase 7	PTK7	1.42E-03	2.8
Synembryn-A	RIC8A	1.42E-03	2.8
Cytospin-B	SPECC1	1.88E-03	2.4
U6 snRNA-associated Sm-like protein LSm2	LSM2	1.88E-03	2.4
ADP-dependent glucokinase	ADPGK	1.88E-03	2.4
Eyes absent homolog 3	EYA3	1.96E-03	2.9
Polypeptide N-acetylgalactosaminyltransferase 2	GALNT2	1.99E-03	3.0
PEST proteolytic signal-containing nuclear protein	PCNP	1.99E-03	3.0
HLA class II histocompatibility antigen, DRB1-16 beta chain	HLA-DRB1	2.00E-03	4.2
E3 ubiquitin-protein ligase DTX3L	DTX3L	3.00E-03	3.7
Importin subunit alpha-2	KPNA2	3.08E-03	3.8
CTP synthase 1	CTPS1	4.58E-03	2.6
Prolyl 3-hydroxylase 1	LEPRE1	4.58E-03	2.6
Peptidyl-tRNA hydrolase 2, mitochondrial	PTRH2	4.58E-03	2.6
15 kDa selenoprotein	SEP15	4.58E-03	2.6
Intercellular adhesion molecule 1	ICAM1	4.75E-03	3.6
Acyl-coenzyme A thioesterase 9, mitochondrial	ACOT9	5.42E-03	3.0
Poly [ADP-ribose] polymerase 9	PARP9	5.66E-03	3.7
Nuclear pore membrane glycoprotein 210	NUP210	6.09E-03	4.0
Carcinoembryonic antigen-related cell adhesion molecule 5	CEACAM5	7.27E-03	3.8
Structural maintenance of chromosomes flexible hinge domain-containing protein 1	SMCHD1	1.19E-02	2.9
DBIRD complex subunit ZNF326	ZNF326	1.19E-02	2.9
E3 ubiquitin-protein ligase BRE1A	RNF20	1.43E-02	2.8
Mitochondrial Rho GTPase 2	RHOT2	1.43E-02	2.8
Sterile alpha motif domain-containing protein 9	SAMD9	2.17E-02	3.8
Myeloperoxidase	MPO	3.96E-02	5.0

B. Bonferroni correction for multiple testing Protein name			
Keratin, type I cytoskeletal 13 *	KRT13	1.50E-09	-2.6
Envoplakin	EVPL	1.18E-07	-1.9
Cornulin *	CRNN	1.37E-07	-4.6
Desmocollin-2 *	DSC2	4.47E-07	-1.7
Acidic leucine-rich nuclear phosphoprotein 32 family member A	ANP32A	1.57E-06	1.4
DNA topoisomerase 1	TOP1	6.56E-06	2.1
Protein disulfide-isomerase TMX3	TMX3	1.13E-05	2.0
Protein disulfide-isomerase A3	PDIA3	1.42E-05	0.7
DNA replication licensing factor MCM4	MCM4	1.92E-05	5.1
DNA replication licensing factor MCM6 *	MCM6	1.95E-05	3.0
DNA replication licensing factor MCM7 *	MCM7	2.04E-05	3.6
Desmoglein-1	DSG1	2.12E-05	-2.9
Ribosome-binding protein 1	RRBP1	2.15E-05	1.4
Exportin-2	CSE1L	2.45E-05	1.2
DNA replication licensing factor MCM3	MCM3	2.68E-05	4.3
Heterogeneous nuclear ribonucleoproteins A2/B1	HNRNPA2B1	3.31E-05	1.0
Keratin, type II cytoskeletal 5	KRT5	3.55E-05	-1.0
78 kDa glucose-regulated protein	HSPA5	3.60E-05	0.8
Calreticulin	CALR	4.23E-05	1.5
Nucleoprotein TPR	TPR	4.28E-05	1.8
DNA replication licensing factor MCM2	MCM2	5.24E-05	4.9
Endoplasmic reticulum resident protein 29 *	ERP29	7.93E-05	1.8
Nuclear pore complex protein Nup155	NUP155	9.16E-05	1.9
Phospholipase A-2-activating protein	PLAA	1.15E-04	3.2
Flap endonuclease 1 *	FEN1	1.49E-04	2.7
Tryptophan--tRNA ligase, cytoplasmic	WARS	1.90E-04	3.0
Pre-mRNA-processing factor 6	PRPF6	2.99E-04	3.2
Protein S100-P	S100P	3.13E-04	2.9
DNA polymerase delta catalytic subunit	POLD1	3.13E-04	2.9
Serpin H1	SERPINH1	3.30E-04	3.7

The IPA software tool was used to find networks in which the identified differentially abundant proteins might be involved. Fourteen out of the 30 proteins that were significant for early stage cervical cancer after Bonferroni analysis were classified to the cell cycle control network ("DNA Replication, Recombination, and Repair"), which comprised a total of 35 proteins (Figure 2) and had a network score of 30.

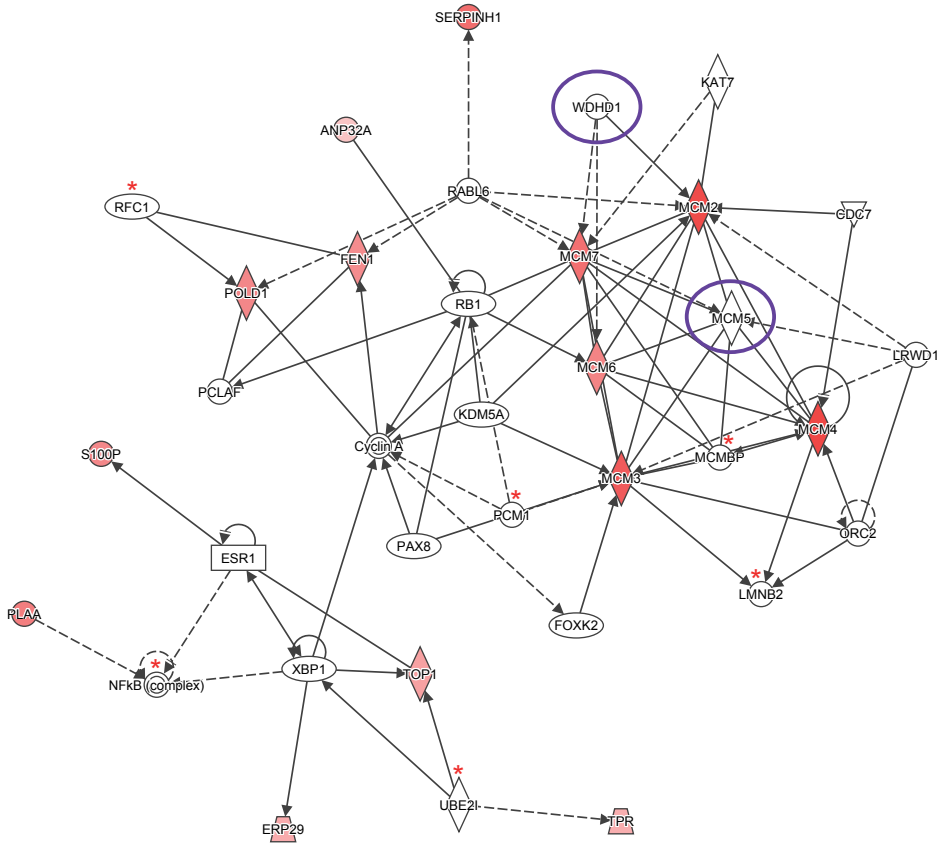

Figure 2. Ingenuity Pathway Analysis (IPA) of the 30 significantly up- and down-regulated proteins (after Bonferroni analysis) for early stage cervical cancer versus healthy controls. Pathway analysis indicated that the network "DNA Replication, Recombination, and Repair", containing fourteen out of the 30 significant proteins, is up-regulated. The network itself consists of 35 proteins. The up-regulated proteins in early stage cervical cancer are marked red, while those that were down-regulated were not identified in this pathway. The intensity of the color relates to fold-change. Proteins indicated with a red asterisk were found by LCM, although not differential. Benjamini-Hochberg analysis of the same data resulted in two more proteins (encircled in purple) belonging to this network (*MCM5* and *WDHD1*). The symbols shown in the network are explained at http://www.qiagenbioinformatics.com/products/ingenuity-pathway-analysis.

This score was above the upper 95% confidence level of the mean threshold (i.e., upper 95% Cl mean of 27.2) that was calculated by permutation from randomly taken 30 proteins of UniProt database. Six proteins from the network (*LMNB2*, *MCMBP*, *NF-κB complex*, *PCM1*, *RFC1*, *UBE2I*) were identified but not differential by the LCM approach with at least one peptide. Two proteins belonging to this network (*MCM5* and *WDHD1*) were found by Benjamini-Hochberg analysis of the same data.

The "all-or-nothing" analysis and Bonferroni analysis between late stage cervical cancer and healthy epithelium had scores below the upper 95% confidence level of the mean threshold (i.e., 22<28.9 and 8<11.8, respectively) and for this reason the created networks were not further investigated. On the other hand, for the Benjamini-Hochberg analysis, two networks (i.e., "DNA Replication, Recombination, and Repair" and "Cardiac Arrhythmia, Cardiovascular Disease, Organismal Injury and Abnormalities"; see Figure 3 and Figure 4, respectively) were found with an identical score that passed the threshold (i.e., 43>41.4). For the other group, comparing late stage cervical cancer with healthy epithelium one network (also related to "DNA Replication, Recombination, and Repair"; see Figure 5) identified by the Benjamini-Hochberg analysis exceeded the threshold score of 40.8 (i.e., 48>40.8).

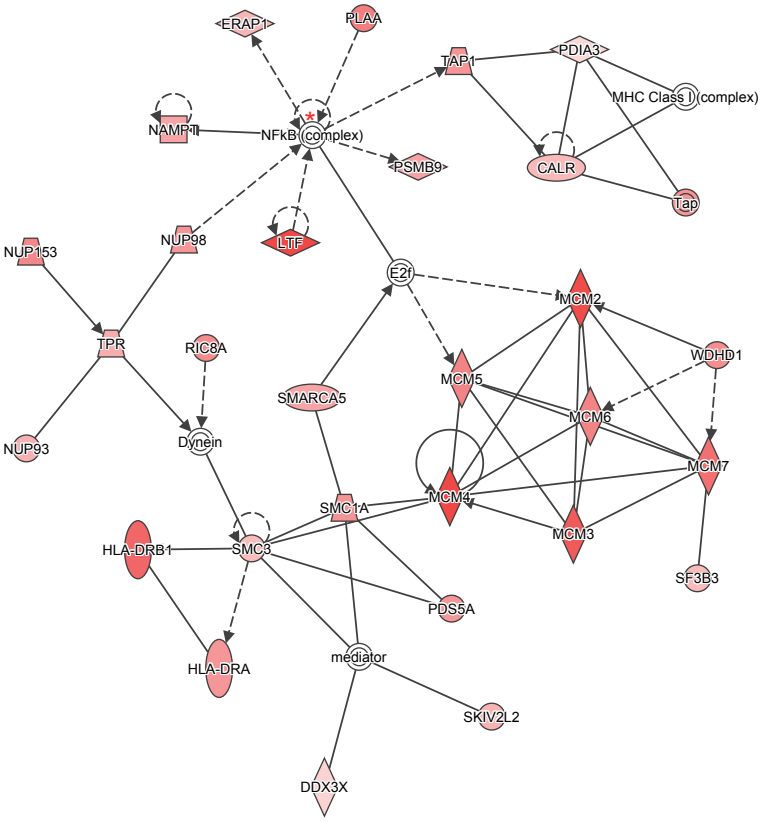

Figure 3. The 319 significant proteins (up- and down-regulated) that were found by Benjamini-Hochberg analysis for early stage cervical cancer were applied to the IPA analysis tool. The pathway analysis resulted in two networks with identical scores that passed the threshold. The network indicated below matched to "DNA Replication, Recombination, and Repair" containing 29 out of the 319 significant proteins. The network itself consists of 35 proteins. The up-regulated proteins in early stage cervical cancer are marked red, while those that were down-regulated were not identified in this pathway. The intensity of the color relates to fold-change. The NF-κB complex protein indicated with a red asterisk was identified once (99% protein- and 95% peptide probability with at least one peptide) by LCM, although not differential. The second network that passed the permutation background score is represented in Figure 4. The symbols shown in the network are explained at http://www.qiagenbioinformatics.com/products/ingenuity-pathway-analysis.

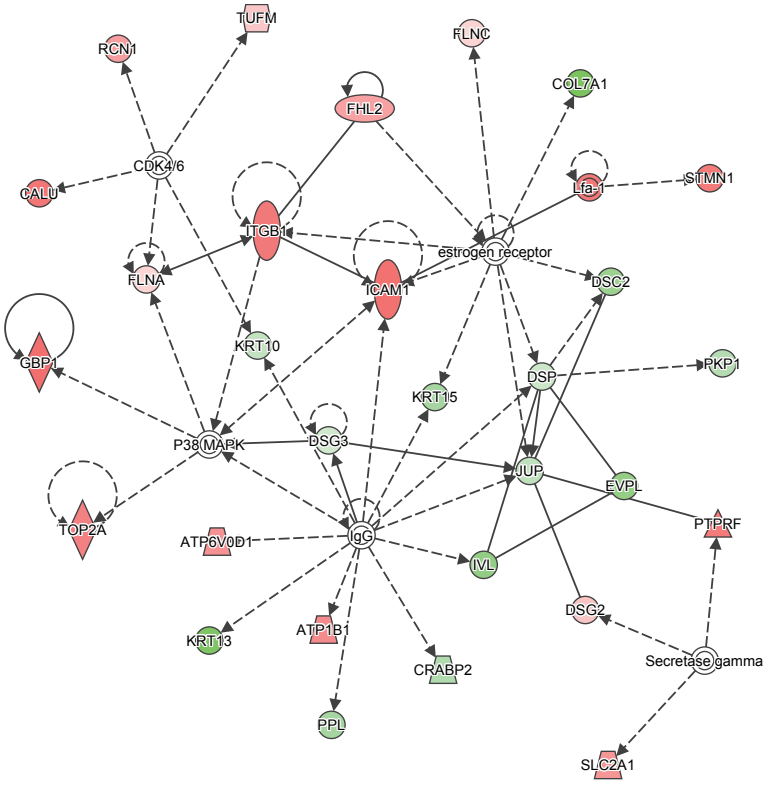

Figure 4. The second network with an identical score as shown in the previous network (Figure 3). The 319 significant proteins (up- and down-regulated) that were found by Benjamini-Hochberg analysis for early stage cervical cancer were applied to the IPA analysis tool. The pathway analysis resulted in the finding of the network "Cardiac Arrythmia, Cardiovascular Disease, Organismal Injury and Abnormalities" containing 29 out of the 319 significant proteins. The network itself consists of 35 proteins. The up-regulated proteins in early stage cervical cancer are marked red and those up-regulated in healthy epithelial cells are marked green. The intensity of the color (red or green) relates to fold-change. Interestingly, almost 50% (13 out of 29) of proteins identified were down-regulated. The symbols shown in the network are explained at http://www.qiagenbioinformatics.com/products/ingenuity-pathway-analysis.

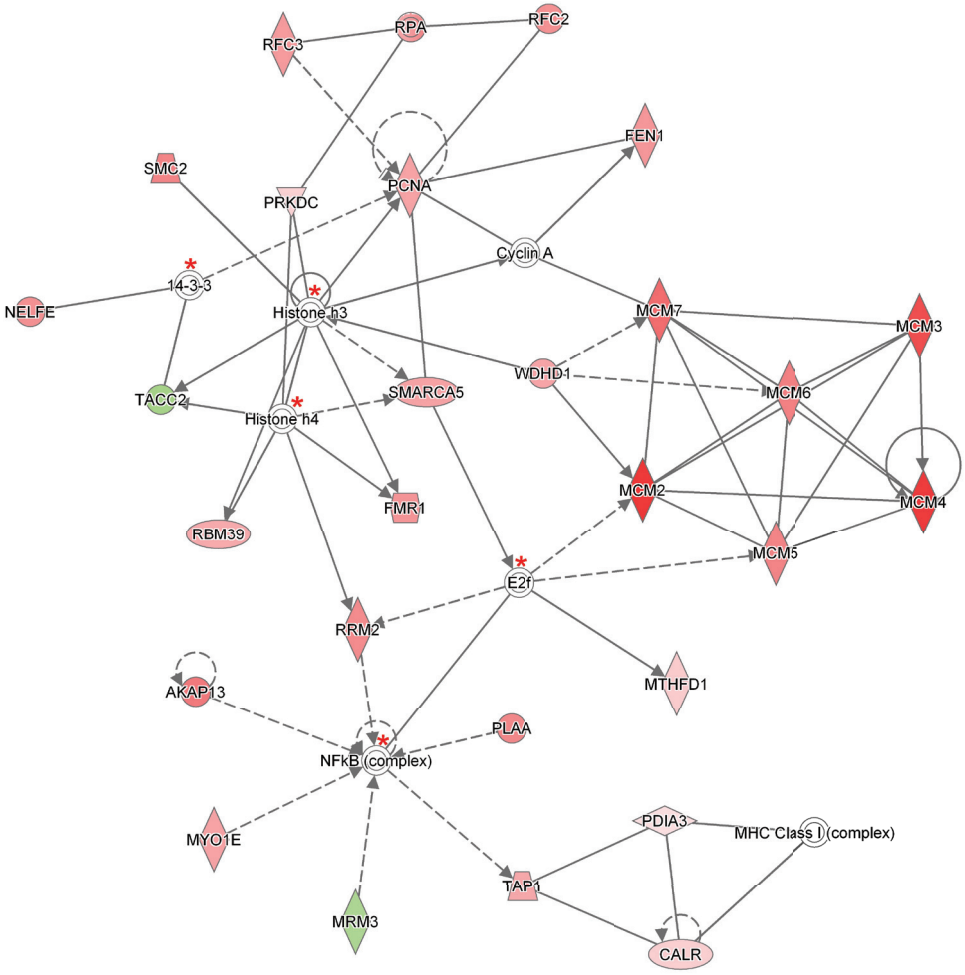

Figure 5. The 140 significantly proteins (up- and down-regulated) that were found by Benjamini-Hochberg analysis for late stage cervical cancer were applied to the IPA analysis tool. The pathway analysis resulted in the finding of the network "DNA Replication, Recombination, and Repair" containing 27 out of the 140 significant proteins. The network itself consists of 35 proteins. The up-regulated proteins in late stage cervical cancer are marked red and two proteins which were up-regulated in healthy epithelial cells are indicated with a green color. The intensity of the color (red or green) relates to fold-change. Proteins (n=5) indicated with a red asterisk have been identified minimal once (99% protein- and 95% peptide probability with at least one peptide) by LCM, although not differential. The symbols shown in the network are explained at http://www.qiagenbioinformatics.com/products/ingenuity-pathway-analysis.

Proteins indicated in the "DNA Replication, Recombination, and Repair" network identified by IPA (i.e., Figure 2, Bonferroni analysis; Figures 3 and 5, Benjamini-Hochberg analysis) showed an overlap close to 30% of all network proteins mentioned. The other network

("Cardiac Arrhythmia, Cardiovascular Disease, Organismal Injury and Abnormalities", Figure 4) consisted of almost 50% of down-regulated proteins that did not show any overlap with the first network mentioned (Figure 3). An overview of the different analyses achieved by comparison of individual early and late stage cervical cancer with healthy epithelium is displayed in Table 3.

Table 3. Overview of different types of analyses between early stage cervical cancer (EC) with healthy epithelium (H) and late stage cervical cancer (LC) with healthy epithelium. After applying the significant differential proteins analyzed by three analyses, i.e. "all-or-nothing", Bonferroni and Benjamini-Hochberg to IPA, the network scores were matched with a threshold score determined by permutation. This score was obtained after a permutation test (n=10) according to the number of proteins identified by the three analyses and defined as the upper 95% CL of mean value. Network scores above this value were selected for discussion.

Type of analysis	EC versus H			Threshold score by permutation (n=10) related to EC versus H	Number of networks found above threshold score related to EC versus H	LC versus H			Threshold score by permutation (n=10) related to LC versus H	Number of networks found above threshold score related to LC versus H
	Number of differential proteins		IPA score***			Number of differential proteins		IPA score***		
"all-or-nothing"	31		22	28.9 (18.1 - 28.9) *	0	-		-	-**	-**
Bonferroni	30		30	27.2 (17.8 - 27.2) *	1	13		8	11.8 (3.2 - 11.8) *	0
Benjamini-Hochberg	319		43	41.4 (37.1 – 41.1) *	2	140		48	40.8 (28.0 - 40.8) *	1

** The lower and upper 95% CI of mean. ** Not applied for LC vs H analyzed by the "all-or-nothing" analysis. *** IPA scores were calculated by IPA using right-tailed Fisher's Exact test.*

Hierarchical clustering of the differentially abundant fourteen proteins found in the "DNA, Replication, Recombination and Repair Network" by IPA analysis of the Bonferroni analysis resulted in clusters of proteins showing similarities between the early and late stage cervical cancer, while for the healthy epithelium group this was significantly different (Figure 6).

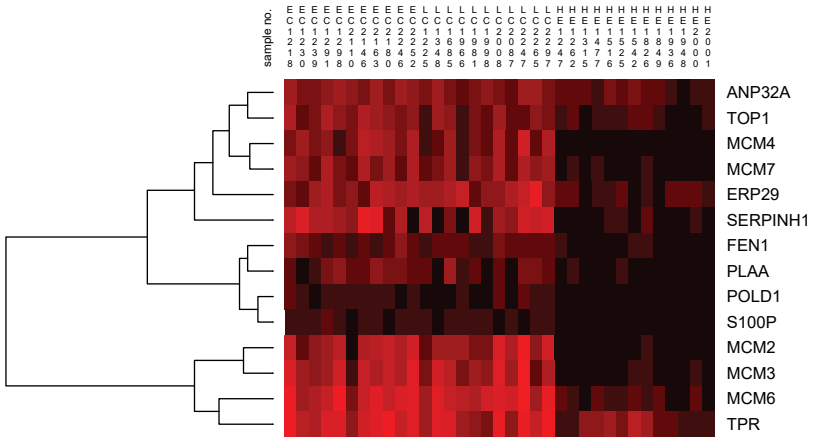

Figure 6. Hierarchical clustering of fourteen proteins found by the IPA tool related to early stage cervical cancer (EC), late stage cervical cancer (LC) and healthy epithelium (HE) visualizes the heterogeneity among individual samples. For the early and late stage cervical cancer group, clustering of MCM proteins was readily observed and showed high similarity between samples. Interestingly, the *MCM2*, *MCM3*, *MCM6* and *MCM4*, *MCM7* clustered in two different clusters. For the healthy epithelium group, the result was different compared to early and late stage cervical cancer group in which only *MCM6* from the MCM2-7 family clustered separately. The abundance levels of proteins were indicated with red (high) and black (low). Sample numbers correspond to those shown in Table 1.

Protein profiles in early stage cervical cancer tissue by LCM with HeLa, U87 and HEK293 cell lines

From the 31 proteins (Table 2A) that were exclusively found by the "all-or-nothing" analysis in early stage cervical cancer and that all meet an extra criterion: ^{2}log fold-change >1, 30 were up-regulated in late stage cervical cancer tissue, 24 in the HeLa cell line, eleven in U87 and nine in HEK293 cells. From the 30 significantly different proteins selected after using Bonferroni analysis (Table 2B), according to identical criterion as mentioned above, 22 were up-regulated in both early stage cervical cancer and in the HeLa cell line and nineteen in late stage cervical cancer tissue. Fifteen out of the 30 significantly different proteins were up-regulated in the U87 cell line, while fourteen proteins were up-regulated in HEK293 cells. From the 319 significantly different proteins selected after using Benjamini-Hochberg correction (Table S2) using identical criterion, 249 were up-regulated in early stage cervical cancer, 210 in the late stage cervical cancer, 244 in the HeLa cell line, 163 in the U87 cell line and 109 were up-regulated in the HEK293 cell line.

Three out of the 35 proteins (Figure 2) that were related to the network "DNA Replication, Recombination, and Repair" were significantly up-regulated (^{2}log fold-change >1) in both early and late stage cervical cancer and in the HeLa cell line compared to healthy epithelium (*NF-κB complex*, *PLAA*, *POLD1*, *S100P* and *WDHD1*), but were absent in the other two cell lines (U87 and HEK293). In Figure 7, the presence or absence of the differential proteins found by Bonferroni analysis only related to this network observed in early and late stage cervical cancer is illustrated.

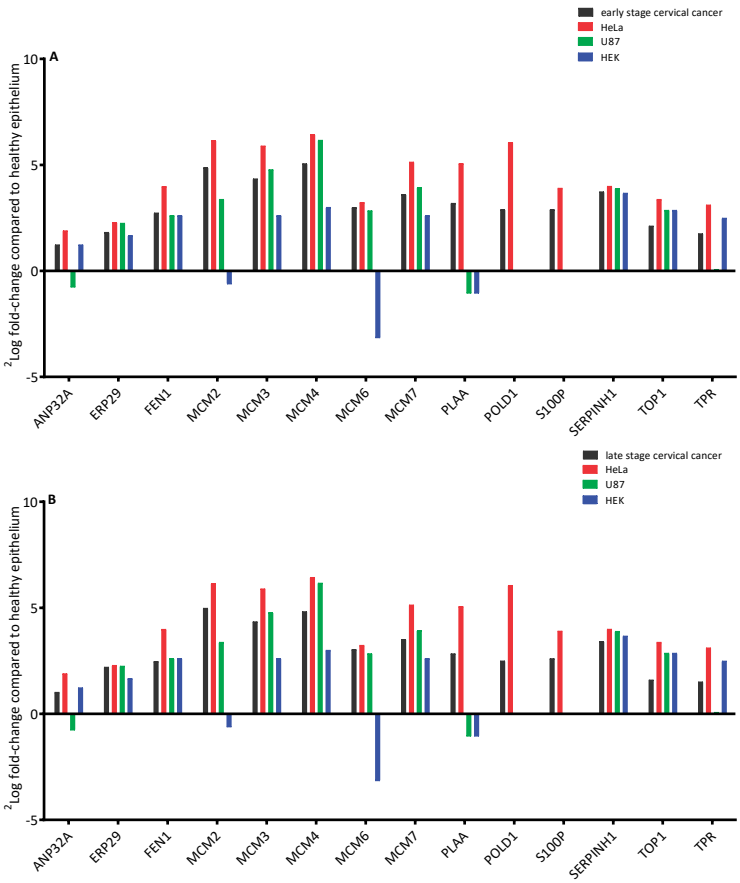

Figure 7. Laser microdissected healthy epithelial cells were compared in a semi-quantitative way with early (A) and late (B) stage cervical cancer, a cervical cancer derived cell line (HeLa) and two cell lines that were derived from brain tumor (U87) and normal embryonal kidney tissue (HEK). Most of the fourteen differential proteins which were from the network behave similar between healthy epithelium and various tumor types, except for a few. The proteins *PLAA*, *POLD1* and *S100P* were only observed in cervical cancer and HeLa digests when comparing to healthy epithelium (zero counts were converted into 0.125 to allow logarithm calculation). It was shown that MCM proteins in cervical cancer could have a 32-fold increase (^{2}log fold-change of 5, e.g., *MCM4*) in abundance compared to healthy epithelium.

Furthermore, comparison of results derived from all proteins identified with LCM-derived tumor cells from early and late stage cervical cancer and HeLa cell line (following criterion: ^{2}log fold-change relative to healthy epithelium ≥2.5), with non-cervical U87 and HEK293 cell lines showed nineteen highly significantly up-regulated proteins. Following the same criterion, fourteen proteins were found to be exclusively discriminative for the LCM dissected tumor cells only (Table 4).

Table 4. Up- or down-regulated of all identified proteins calculated by ^{2}log fold-changes (all compared to healthy epithelium) for LCM-derived cervical cancer cells and for HeLa cell line compared to other cell lines U87 and HEK293**.** Panel A represents nineteen up-regulated proteins found in the early and late stage cervical cancer of LCM-derived cells and HeLa only. Panel B shows fourteen significant proteins exclusively found by LCM. For both panels, the following criterion was used: ^{2}log fold-change ≥2.5, zero counts were converted to 0.125 to enable log calculations. Proteins indicated with (superscripts) ^{A}, ^{B} and ^{BH} were found by the "all-or-nothing", Bonferroni and Benjamini-Hochberg correction for multiple testing, respectively.

A.	Gene name	EC (LCM)	LC (LCM)	HeLa	U87	HEK293
A-kinase anchor protein 13	AKAP13	3.1	3.2	4.3	0.0	0.0
Antigen peptide transporter 2	TAP2	2.8	2.8	3.0	-0.6	-0.6
DBIRD complex subunit ZNF326 $^{A, BH}$	ZNF326	2.9	3.2	5.0	0.0	0.0
E3 ubiquitin-protein ligase UBR4 ^{BH}	UBR4	2.8	3.0	6.5	0.0	0.0
G patch domain and KOW motifs-containing protein	GPKOW	2.7	2.7	5.2	0.0	0.0
Intercellular adhesion molecule 1 $^{A, BH}$	ICAM1	3.6	3.6	4.4	0.0	0.0
Leucine-rich repeat-containing protein 16A	LRRC16A	2.7	2.6	4.0	0.0	0.0
Melanoma-associated antigen D2	MAGED2	2.8	2.5	4.4	0.0	0.0
Periostin	POSTN	3.2	2.6	2.6	-1.4	-1.4
Phospholipase A-2-activating protein $^{B, BH}$	PLAA	3.2	2.8	5.1	-1.1	-1.1
Protein RCC2 ^{BH}	RCC2	2.8	2.7	3.8	-2.1	-2.1
Protein S100-P $^{A, B, BH}$	S100P	2.9	2.6	3.9	0.0	0.0
Receptor-type tyrosine-protein phosphatase F ^{BH}	PTPRF	3.3	3.0	2.7	-2.3	-2.3
RNA-binding protein 10 ^{BH}	RBM10	3.0	2.5	4.2	-0.6	-0.6
Shootin-1	KIAA1598	2.6	2.6	4.5	-0.6	-0.6
Sterile alpha motif domain-containing protein 9 ^{A}	SAMD9	3.8	3.9	2.8	0.0	0.0
Thrombospondin-1	THBS1	3.5	3.1	6.1	0.0	0.0
Ubiquitin-like protein ISG15	ISG15	2.5	3.4	3.4	0.0	0.0
Zinc finger RNA-binding protein ^{BH}	ZFR	2.7	3.7	5.8	0.0	0.0

B.	Gene name	EC (LCM)	LC (LCM)	HeLa	U87	HEK293
Calcium-activated chloride channel regulator 4	CLCA4	2.8	3.3	0.0	0.0	0.0
Carcinoembryonic antigen-related cell adhesion molecule 5 [A, BH]	CEACAM5	3.8	2.8	0.0	0.0	0.0
Cathelicidin antimicrobial peptide	CAMP	3.8	2.7	0.0	0.0	0.0
Collagen alpha-1(XII) chain	COL12A1	4.0	3.5	-2.1	-2.1	-2.1
Dimethylaniline monooxygenase [N-oxide-forming] 3	FMO3	3.5	2.6	0.0	0.0	0.0
E3 ubiquitin-protein ligase DTX3L [A, BH]	DTX3L	3.7	3.2	0.0	0.0	0.0
Epithelial cell adhesion molecule	EPCAM	3.2	3.2	0.0	0.0	0.0
Fibulin-2	FBLN2	3.1	3.0	0.0	0.0	0.0
HLA class II histocompatibility antigen, DRB1-16 beta chain [A, BH]	HLA-DRB1	3.7	3.3	-0.6	-0.6	-0.6
HLA class II histocompatibility antigen, DRB1-7 beta chain	HLA-DRB1	3.8	3.0	0.0	0.0	0.0
Myeloperoxidase [A]	MPO	5.0	3.6	0.0	0.0	0.0
Poly [ADP-ribose] polymerase 9 [A, BH]	PARP9	3.7	2.6	0.0	0.0	0.0
Stimulator of interferon genes protein	TMEM173	3.0	2.8	0.0	0.0	0.0
Transgelin	TAGLN	3.5	2.9	-1.7	-1.7	-1.7

EC: early stage cervical cancer
LC: late stage cervical cancer

Quantification of MCM3, CEACAM5, S100P and ICAM1 in whole tissue lysates by PRM

The concentrations of four proteins, *MCM3*, *CEACAM5*, *S100P* and *ICAM1*, that were highly significant in cervical cancer tissue found by the shotgun approach of each sample are represented in Supplemental Excel data file 1. The PRM data have been deposited to the ProteomeXchange Consortium via the PRIDE (119) partner repository with the dataset identifier PXD008723 and 10.6019/PXD008723. An example of the calculated concentrations of the four targeted proteins by PRM is illustrated in Figure 8. Linearity, LOD (limit of detection), LOQ (limit of quantification) and reproducibility of serial dilutions of SIL peptide standards are represented in Supplemental Excel data 2.

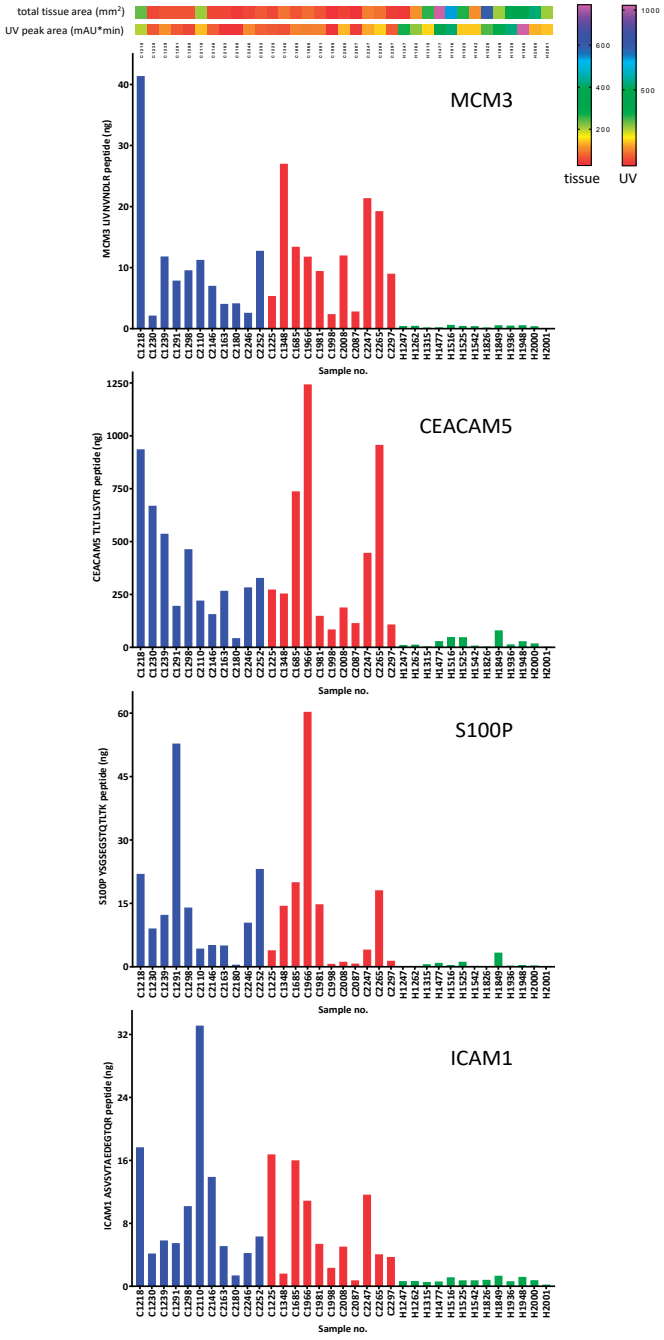

Figure 8. Example of targeted mass spectrometry by PRM. Total amount (in nanograms) of the proteins *MCM3*, *CEACAM5*, *S100P* and *ICAM1* were determined in digests of whole tissue lysates. Total tissue areas (mm^2) and UV peak areas (mAU*min) were applied on top of the figure to estimate the amount of tissue used. Blue, red and green bars correspond to early stage cancer, late stage cancer and healthy samples, respectively.

Comparison of protein profiles with transcriptome data

All proteins of the "all-or-nothing" and Bonferroni analyses (n=55, which were common and exclusively found for both analyses, see Table 2A and 2B, respectively) were observed as relative high gene expression levels extracted from transcriptome data (Ojesina *et al*. (164)). Most of these overlapping proteins were found as highly differential in early stage cervical cancer when compared to the average gene expression level in the Ojesina *et al.* transcriptome data. This is illustrated in the Supplemental data, Figure S1 ("all-or-nothing" analysis) and Figure S2A (Bonferroni analysis). In these heat maps, it is shown that only four out of the 55 selected genes have low abundance, i.e., *MPO* (Figure S1), *CRNN*, *DSG1*, and *PDIA3* (Figure S2A); *CRNN* and *DSG* in agreement with our proteomics study. The other 51 out of 55 genes were expressed at relatively high level, around ^{2}log (FPKM) of 5. In general, many genes had undetectable transcript expressions, with ^{2}log (FPKM) below -5 and those which were expressed had low values, i.e., ^{2}log (FPKM) of 3 and 4. To prove that genes were differentially expressed on protein level among highly expressed genes on RNA level, an analysis of gene expression of a background gene list was performed. This set was based on a selection of genes, corresponding to the list of the total identified proteins from LCM-derived samples (where 3,847 out of 4,138 genes from single peptide identification with removal of decoys were found in the transcriptome sequencing data) showed that about 10% of the proteins were expressed at a very low level, see Figure S2B, Supplemental data. With this taken in account, for the early stage cervical cancer analysis using Bonferroni (Table 2B) and for both early (Table S2) and late stage cervical cancer analysis (Table S3) using Benjamini-Hochberg the genes were significantly higher expressed (compared to background set, Wilcoxon rank-sum test, $p<0.01$) on transcriptome level. The early stage cervical cancer using the "all-or-nothing" analysis (Table 2A) and the late stage cervical cancer using the Bonferroni analysis (Table S1) did not exhibit a significantly elevated RNA expression ($p=0.427$ and $p=0.395$, respectively). Heat maps, which were created for proteins analyzed by Benjamini-Hochberg for the comparison of individual early and late stage cervical cancer with healthy epithelium are represented in the Supplemental data, Figure S3 and S4, respectively.

Furthermore, mutated or expressed genes as listed by Ojesina *et al*. were compared for presence or absence in the total number of 2,989 proteins (identified with at least one peptide) identified by our LCM approach. The comparisons are compiled in Table S4 (Supplemental data), resulting in five overlapping proteins (*CBFB*, *CEACAM5*, *MAPK1*, *PARN* and *TP63*). For this panel, only *CEACAM5* was significantly different in abundance ($p=0.007$) between early stage cervical cancer and healthy epithelium found by LCM and mass spectrometry.

Discussion

The combination of laser capture microdissection and high-resolution mass spectrometry in tissue sections from squamous cell cervical cancer patients showed increased levels of proteins in tumor tissue versus healthy epithelium and stroma. Most striking was the increase in the members of the MCM family (up to 32-fold increase in abundance) and associated proteins. MCM proteins are molecular motors that unwind duplex DNA and power fork progression during DNA replication. This process starts with the initiation of DNA replication occurring during S phase when two copies of each chromosome are present. *Cdc6* and *Cdt1* are then recruited by the origins recognition complex (ORC) and they, in turn, recruit the MCM complex to the ORC, forming the pre-RC and licensing the DNA for replication (178-180). Because of its critical role during DNA replication, deregulation of MCM function contributes to human carcinogenesis (181). Previous studies have shown that MCM proteins are highly expressed in various malignant human cancers and cells at an early stage of malignant transformation (182, 183). Members of the MCM family have also been described as diagnostic cancer markers because they are not expressed in quiescent somatic cells that have been arrested in the G_0 phase of the cell cycle. We and others hypothesize that up-regulation of MCM proteins is critical for tumor progression and that MCM proteins might serve as viable targets for anticancer therapy as well as molecular markers for diagnosis.

As mentioned above, we used three analysis techniques that were restrictive in finding differential proteins. In addition, we used an extra threshold by a permutation approach in the protein network finding. Using these restrictive analyses, we believe to be confident in finding the most discriminative proteins and networks of these proteins. Apparently, the differences between cervical cancer cells and healthy epithelial cells were that large that we were able to find relatively high number of proteins that fulfill these restrictions.

Our IPA analysis indicated that the biological interactions of the 30 proteins identified by Bonferroni related to cervical cancer correlated to the network “DNA Replication, Recombination, and Repair”. The same network was assigned to analyses determined by Benjamini-Hochberg. Remarkably, another network “Cardiac Arrhythmia, Cardiovascular Disease, Organismal Injury and Abnormalities” that was found with the proteins from the Benjamini-Hochberg analysis was filled with a high number of down-regulated proteins. Most probably cervical specific proteins are lost in early cancer cells during the tumor oncogenesis. For diagnostic purposes, elevation of a protein marker could be more applicable than down-regulated proteins.

We found nineteen proteins (Table 4) that were up-regulated in cervical cancer (early and late stage) tissue and HeLa when compared to healthy epithelium from controls obtained by LCM. Some of these proteins might be cervical cancer-related since they were not up-

regulated in cells from other non-cervical HEK and U87 cell cultures but only in the HeLa cell line. Nevertheless, more cervical cancer cell lines ought to be investigated to confirm this. One of these proteins is *CEACAM5*, a protein with HPV integration sites that was also found by *Ojesina et al.* (164) to be highly expressed (Figure S1). CEACAM5 is related to cell-adhesion molecules and belongs to the carcinoembryonic antigen (CEA) gene family. It is strongly expressed in epithelial cells and known as a tumor marker for early detection of recurrent disease due to its expression in several adenocarcinomas (e.g., colon, lung, breast, ovarian) (184). However, there is no literature related to cervical cancer.

The coding mutation in *ERBB2* described by Ojesina *et al.* (164) as being specific for cervical cancer could not be detected by our LCM approach. *MAPK1*, also described *as being* specific for cervical cancer was detected. However, the abundance level did not change in cervical cancer compared to healthy epithelial or stromal cells according to our analysis. *S100P* was found to be up-regulated in cervical cancer tissue from early and late stage patients as well as in HeLa cells. It was not found in healthy epithelium, stroma, U87 and HEK293 cells, although it is overexpressed in several other cancers (185). *S100P* is a member of the S100 protein family that is characterized by its calcium-binding properties due to structural motifs containing 2 EF-hand domains. *S100P* was first isolated from human placenta and has a crucial role in several biological functions; however, its exact function in cervical cancer remains unclear (185, 186). Quantitative proteomics by PRM was used to confirm the observation of four proteins. It was shown that full agreement was obtained on digests of whole tissue lysates. As sensitivity is in PRM much better than in shotgun proteomics, an almost all-or-nothing difference was observed between the cancer and healthy samples. The difference for *MCM3* was detectable for all samples with roughly two to three orders of magnitude.

National population-based cervical cancer screening programs have reduced the incidence of cervical cancer significantly in the western world (187). However, in both the technical aspects and performance of different screening test, there is room for improvement. The most widely used cervical cancer screening test is cytology-based testing. Primary screening for cervical cancer is currently changing in many countries including the Netherlands. HrHPV testing is becoming the preferred primary screening test over cytology. By hrHPV testing, the sensitivity for detecting premalignant lesions is much higher (23, 188, 189). Because of this increased sensitivity, more CIN2+ lesions will be detected and less carcinomas will be missed. A disadvantage of the hrHPV test for primary screening is the lower specificity of this test, resulting from detection of women with transient HPV infection who will not develop (premalignant) cervical cancer. To prevent unnecessary referral to the gynecologist and associated high costs, there is a need for risk stratification by triage testing of hrHPV positive women and the four selected proteins for PRM might help in that respect.

Simple, more specific biomarkers for cervical cancer and its precancerous stages are required that can be used on, e.g., liquid-based cytology (LBC) samples. These samples used for routine screening in a precancerous stage could be used for targeting differentially expressed proteins in a multiplexed manner (e.g. >50 proteins). LBC samples can be related much more directly to cervical tissue because they are less complex compared to e.g., sera where the extreme range of different serum proteins puts limits on the detection of proteins in the ng/mL range without the use of antibody or other new affinity enrichment steps.

In conclusion, we have shown that LCM proteomics with high-resolution mass spectrometry is a viable approach to detect differences in individual protein levels in tissues of early stage squamous cell cervical cancer patients compared to healthy control tissues. For four proteins, we were able to confirm in a quantitative way these rather large differences in protein levels. In addition, we have found two significant differential networks. A down-regulated network that probably shows the loss of cervical specific proteins in cancer cells and a highly-up-regulated network that relates to a cancer mechanism that involves proliferation and progression in cervical cancer. These networks can be used as sources for diagnostics and will add to understanding the early processes in cervical cancer.

Materials and methods

Sample procurement

All patients referred to the outpatient clinic of the University Medical Center Groningen (UMCG) with squamous cervical cancer were routinely asked to participate in our ongoing 'Methylation study' which has been approved by the Institutional Review Board (IRB) of the UMCG. Cervical tissue and clinicopathologic data were prospectively collected and stored in our tissue bank. Within our 'Methylation study', tissue samples and clinicopathologic data that were collected from normal cervical tissues, were also collected from patients who planned to undergo a hysterectomy for non-malignant reasons. All cervical tissues that were used for the healthy control group were judged as histopathological normal. For determination of the percentage of tumor in the cancer specimen, 4 µm sections were cut and haematoxylin & eosin (HE) stained. Only specimens with more than 70% tumor were used. For LCM, we selected frozen tissue of 22 SCC patients and from thirteen controls (Table 1). The median age of the cervical cancer patients was 55 years (IQR 44-75) and for the patients with normal cervices 43 years (IQR 41-50). The stage of SCC patients was: 3 (14%) FIGO stage IB1, 5 (23%) FIGO stage IB2, 3 (14%) FIGO stage IIB, 2 (9%) FIGO stage IIIA, 6 (27%) FIGO stage IIIB and 3 (14%) FIGO stage IV. FIGO stages I-II and III-IV were defined as early stage and late stage cervical cancer, respectively. All tissues were primary tumors and patients did not receive neoadjuvant therapy.

LCM

Areas for LCM were selected on HE-stained cryosections. Cryosections of 10 µm were prepared from each of the eleven early and eleven late stage cervical cancer, and the thirteen healthy cervical tissue samples. The sections were mounted on polyethylene naphthalate (PEN)-covered glass slides (Carl Zeiss, Zwijndrecht, the Netherlands). An area corresponding to approximately 8,000 cells was microdissected. We calculated the number of cells by assuming an average volume of 10 x 10 x 10 µm for one cell. The tissue pieces were collected in 20 µL 0.1% Rapigest SF detergent (Waters, Milford, MA, USA) and reduced using 4.7 mM dithiothreitol at 60°C for 30 minutes followed by alkylation using 16.9 mM iodoacetamide in the dark at room temperature for 30 minutes. Subsequently, the tissue pieces were enzymatically digested by adding 2 µL trypsin (Mass Spectrometry grade, 100 µg/mL in 3 mM Tris-HCl, pH 8.8) at 37°C overnight.

Protein identification by nano-LC-MS/MS

Online nano-LC-ESI-MS/MS using an application of a shotgun proteomics workflow was used for identification of tryptic peptides. A digested peptide mixture equivalent to 8,000 cells was separated on an Ultimate 3000 HPLC system (Thermo Fisher Scientific, Germering, Germany) and subsequently online measured in an Orbitrap Fusion mass spectrometer (Thermo Fisher Scientific, San Jose, CA, USA) in the data-dependent acquisition mode. Samples were loaded on to a trap column (PepMap C18, 300 µm ID, 5 mm length, 5 µm particle size, 100 Å pore size; Thermo Fisher Scientific), washed and desalted for 8 minutes using 0.1% trifluoroacetic acid as loading solvent at a flow rate of 20 µL/min. The trap column was switched in-line with the analytical column (PepMap C18, 75 µm ID x 500 mm, 2 µm particle size and 100 Å pore size, Thermo Fisher Scientific) and peptides were eluted with a 90-minute acetonitrile gradient ranging from 3% to 30% (and formic acid concentration from 0.1% to 0.08%, respectively). All LC solvents were purchased at Biosolve (Valkenswaard, the Netherlands). Column flow rate was set to 250 nL/min, and eluting peptides were measured at 214 nm in a 3 nL nano flow cell (Thermo Fisher Scientific), online coupled to the mass spectrometer. For electrospray ionization nano ESI emitters (New Objective, Woburn, MA, USA) were used and a spray voltage of 1.7 kV was applied. For MS detection, a data-dependent acquisition method was used with a survey scan from 350–1650 Th at 120,000 resolution (AGC target 400,000) and consecutively isolated and fragmented by collisional induced dissociation (CID) at 35% normalized collision energy (AGC target 10,000) of the most abundant precursors in the linear ion trap until a duty cycle time of 3 seconds was reached ('Top Speed' method). Precursor masses that were selected once for MS/MS were excluded from further fragmentation for the next 60 seconds.

Proteins from the LCM-derived samples were assigned by exporting features, for which MS/MS spectra were recorded, using the ProteoWizard software (version 3.0.9248; http://proteowizard.sourceforge.net). Resulting mgf files were submitted to Mascot (version

2.3.01, Matrix Science, London, UK) and applied to the human database (UniProtKB/Swiss-Prot, version 2013_07, human taxonomy, 20,265 entries) for protein identifications assuming trypsin digestion and applying the following parameters: fragment ion mass tolerance of 0.50 Da, parent ion mass tolerance of 10 ppm, maximum number of missed cleavages of two. Oxidation of methionine was specified in Mascot as a variable modification, while carbamidomethylation of cysteine was set as a fixed modification. Scaffold (version 4.7.2, Proteome Software Inc., Portland, OR) was used to summarize and filter the MS/MS-based peptide data from all Mascot searches. The number of proteins was derived from the peptide data according to the following criteria. Peptide identifications needed to have more than 95% probability as specified by the Peptide Prophet algorithm. Protein identifications had to have more than 99% probability and contain at least one peptide identified.

Data analysis

Technical and methodological reproducibility was determined by performing the measurements in triplicate and doing the entire experiment (microdissection and tryptic digestion) also in triplicate. For technical reproducibility, a tryptic digested tissue lysate was used, while for methodological reproducibility an LCM-derived sample was taken and measured. A diagram illustrating the experimental design is shown in Figure 9.

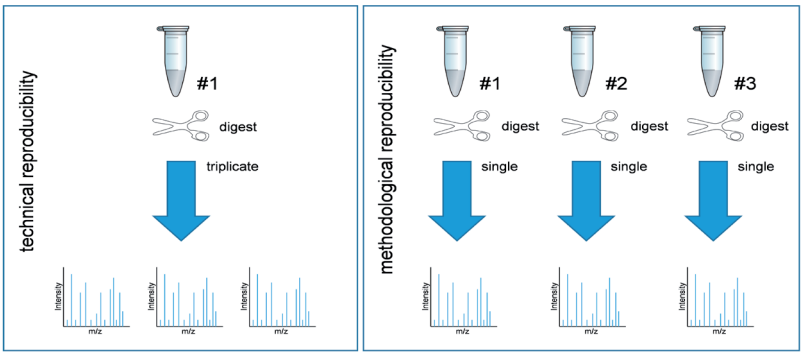

Figure 9. Experimental design of technical and methodological reproducibility.

For both reproducibility types, the total number of overlapping identified proteins was analyzed by Scaffold and eventually the percentage was used as a readout. For both reproducibility types, an overlap greater than 50% was indicated as acceptable (190, 191).
A volcano plot was created to determine changes in protein abundances indicated as ^{2}log fold-changes between individual early and late stage cervical cancer with the healthy epithelium group ($p<0.05$). The ^{2}log fold-changes were calculated based on comparison of the individual early and late stage cervical cancer with healthy epithelium according to spectral

counts (zero counts were converted to 0.125 to enable log calculations). Three different analysis methods were chosen for comparison of the early stage cervical cancer with the healthy epithelium and late stage cervical cancer group with the healthy epithelium group. Two stringent analyses were used, i.e., an analysis based on an "all-or-nothing" criteria and second a Bonferroni analysis to correct for multiple testing, and third a less stringent correction for multiple testing i.e. Benjamini-Hochberg. The "all-or-nothing" analysis was deemed discriminative when 1) a protein was not identified in healthy epithelium and stroma and when 2) a protein was at least identified in seven out of the eleven early stage cervical cancer subjects. In addition, the identified proteins from early stage cervical cancer were allowed to be present in late stage cervical cancer. We have chosen for these three analyses to classify in a restrictive way (Bonferroni) and a more relaxed analysis (Benjamini-Hochberg), and the "all-or-nothing" analysis that offers more possibilities to handle missing values in mass spectrometry. The differentially abundant proteins found by these three analysis methods have been introduced into pathway analysis using the IPA software (192). Data were entered into the IPA tool to assign the differentially expressed proteins to different network interactions according to their respective significance levels to fit in that network. A permutation test was performed to determine a threshold score by selection of random 31 (comparable numbers with those analyzed by the "all-or-nothing" criteria), 30 and 13 proteins (comparable numbers with those analyzed by Bonferroni analysis between individual early and late stage cervical cancer with healthy epithelium, respectively), 319 and 140 proteins (comparable numbers with those analyzed by Benjamini-Hochberg between individual early and late stage cervical cancer with healthy epithelium, respectively) that were extracted from the UniProt database (uniprot_sprot_HUMAN_v151112; 20194 entries). The test was repeated ten times and from the networks with highest score (as calculated by IPA using right-tailed Fisher's Exact test) the mean value of the ten repeats was calculated and subsequently the lower- and upper 95% confidence level (Cl) of the mean were calculated. Network scores which exceeded the 95% Cl of the mean threshold (assumed as background) were taken into account as confidential differential.

To determine the heterogeneity among patients, a hierarchical clustering analysis was performed of fourteen differential IPA classified proteins that belonged to Bonferroni analysis when comparing early stage cervical cancer with healthy epithelium. The IPA classified proteins were clustered individually in samples from the groups early and late stage cervical cancer and healthy epithelium. For hierarchical clustering analysis PermutMatrix 1.9.3. was used (http://www.atgc-montpellier.fr/permutmatrix) selecting the Euclidean distance for dissimilarity, Wards' method, as a clustering method and Bipolarization seriation (120, 121).

Confirmation by PRM mass spectrometry
Identical numbers of the tissue samples (Table 1) were measured by PRM to quantify *MCM3*, *CEACAM5*, *S100P* and *ICAM1* in digests of whole tissue lysates using stable isotope-labeled (SIL) peptides purchased from Pepscan BV (Lelystad, the Netherlands).

A subset of nine peptides was selected to be quantified by PRM (Table S5). Collected tissue pieces were compiled in 200 µL 0.1% Rapigest SF detergent, sonicated for 3 minutes using a horn sonifier bath (Ultrasonic Disruptor Sonifier II, Branson Ultrasonics, Danbury, CT, USA) at 85% amplitude and heated for 5 minutes at 99°C for protein denaturation. Subsequently, 50 out of the 200 µL tissue lysates were each spiked with 10 fmol of the SIL peptides prior to enzymatic digestion. Samples were subsequently digested by adding 2 µg trypsin at 37°C overnight. One microliter of each sample was measured by PRM, performed on an Orbitrap Fusion instrument according to our previous work (193). Analytical parameters such as linearity, LOD and LOQ were determined. For reproducibility, CVs were calculated for each serial dilution (0, 0.625, 1.25, 2,5, 5, 10 and 20 fmol/uL) using triplicate measurements.

Comparison of protein profiles in LCM-derived early stage cervical cancer tissue with HeLa, U87 and HEK293 cell lines
The identified proteins from the "all-or-nothing", Bonferroni and Benjamini-Hochberg analysis (comparison of the early stage cervical cancer tissue with healthy epithelium group only) were compared with proteins identified in the cervical cancer-derived HeLa cell line and two other cell lines that are unrelated to cervical cancer (U87; primary glioblastoma and HEK293; Human Embryonic Kidney cell line) by calculating ^{2}log fold-changes related to LCM-derived healthy cervical epithelium. Proteins were filtered with the following criterion for each individual group: ^{2}log fold-change relative to healthy epithelium >1. For HeLa, a standard protein digest (catalog no. 88328, Thermo Scientific, Landsmeer, the Netherlands) was used. From U87 and HEK293 cell lines 10^{6} cells of each cell type were digested according to a protocol as recommended by Thermo Scientific (catalog no. 90110). For all three cell lines one µg of each digest was analyzed by nano-LC-Orbitrap MS/MS. The IPA classified proteins were compared with their abundances in the two cervical cancer groups (early and late stage) and in the various cell lines. Scaffold perSPECtives viewer (version 2.1.0, Proteome Software Inc., Portland, OR) was used for visualization of proteins found in cervical-derived tissue by using LCM simultaneously with results obtained from these three cell lines.

Comparison to existing genomic data
Proteomic data were compared to transcriptome data published by Ojesina et al. (164). Transformed 2log expression values were extracted from the transcriptome sequencing data of tumor samples consisting of squamous cell carcinoma and adenocarcinoma (Supplemental Table 12 in Ojesina *et al.*). These genomic data contained no expression data information about healthy tissue as indicated by Ojesina *et al.* and therefore no comparisons could be

made to the healthy controls in our study. Heat maps were created of the proteins from the three analyses performed in this study (Table 2A, 2B; Table S1, S2, S3, *Supplemental data)*. Genes were selected only from the genomic analysis that overlapped with genes identified with the proteomic approach (set of 4,138 proteins with the removal of decoys). For this selection of genes, an average expression level (across all samples) was defined. Using Wilcoxon rank-sum test, the average mRNA expression levels of genes identified as differentially expressed in proteome analysis (represented in heat maps) was evaluated if this was different from the average mRNA expression products of other genes that were identified on protein level (significance level $p<0.01$).

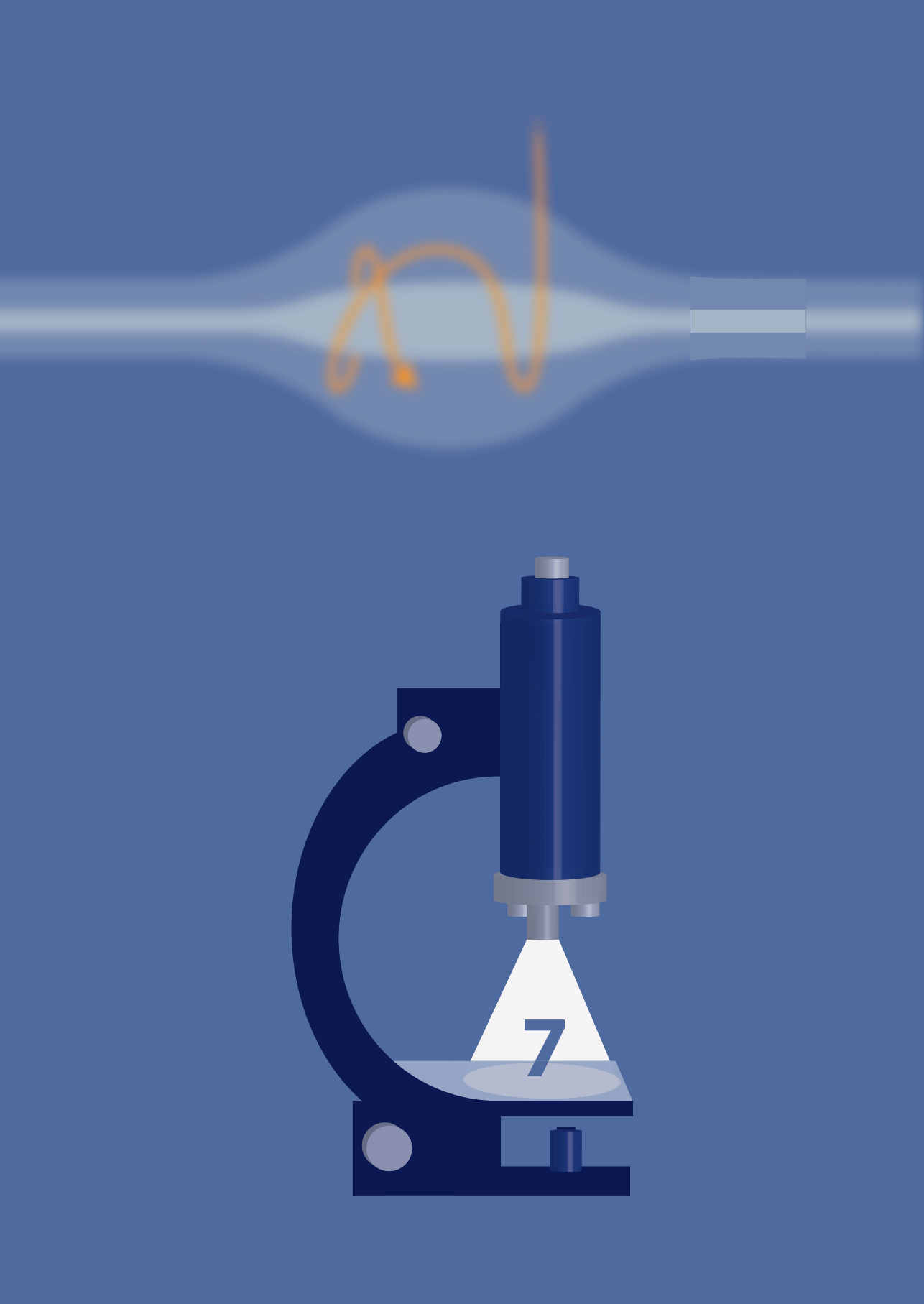
7

Chapter 7
General discussion

In recent years biomarker discovery has been widely performed in biological samples (i.e., serum or plasma, other body fluids, and tissue) (194-196). One major issue in biomarker discovery is the presence of highly abundant proteins, such as albumin in blood and plasma. These high-abundant proteins 'hide' other proteins and naturally occurring peptides that are present at relatively low concentrations (197, 198). Biomarker searches in blood and plasma are notoriously difficult because proteins of interest can be very low in abundance. Therefore, we have chosen to study affected tissue to identify molecules that may be directly related to the disease or even causing or driving it. We preferred for laser capture microdissection technique to isolate affected trophoblast in preeclampsia (**Chapter 2**) and cervical cancer tissue (**Chapter 6**), respectively. In the tissue samples we tried to identify as many proteins as possible by applying a shotgun proteomic approach. We have found proteins that were significantly elevated in the affected tissues compared to normal or healthy related tissues. Subsequently, we analyzed whether these proteins were elevated in serum (for preeclampsia) and cervical scraping (for cervical cancer).

7.1 Preeclampsia

Preeclampsia is a very complex and heterogeneous pregnancy disorder that affects mother and child. The medical need is to detect cases at an early stage of the disease and to monitor women at risk who need intervention or prevention (such as changes in lifestyle, dietary, admission to antioxidants, and medicals). Unfortunately, most studied biomarkers for preeclampsia are only able to detect preeclampsia in a later stage (second and third trimester) (199). Recently, more and more studies (200, 201) predict preeclampsia by different molecular abundance in an early stage (first trimester) of the disease. Most ideally, potential biomarker candidates ought to have both high specificity and sensitivity. Wu *et al.*, 2015 reviewed single laboratory biomarkers used in different study cohorts. The authors concluded that most of the biomarkers analyzed are not useful in clinical practice due to too low sensitivity and specificity. A combination of the markers is most promising, although the results are, for sure, not yet suitable for population screening of pregnant women (AUC<0.90) or even patients at risk.

We previously identified in a discovery phase that calcyclin (*S100A6*) was differently expressed in preeclampsia after comparing trophoblast cells from early-onset preeclamptic placenta with preterm control trophoblast cells (26), followed by validation using immunohistochemistry as described in **Chapter 3**. Extracellularly, *S100A6* is known to be interacting with RAGE-receptors (Receptor for Advanced Glycation End products), as discussed in **Chapter 4**. Various pathophysiological processes are linked to preeclampsia, such as endothelial dysfunction, oxidative stress, angiogenic, inflammatory factor imbalance and activation of the receptor for RAGE. Binding of *S100A6* to the extracellular domain of RAGE is Ca^{2+}dependent and activates a conformational change of the EF-hand, a motif found

in S100 proteins (123). In previous studies, increased protein levels of RAGE were observed in preeclamptic placentas compared to controls, suggesting a possible involvement of *S100A6* protein as a target protein for RAGE in the pathophysiology of PE. It was discussed in **Chapter 4** that *S100A6* may interact with the TPR domains of the HOP (HSP70/HSP90)-organizing protein in a Ca^{2+}-dependent manner and that the subsequent dissociation from Hop-HSP70 and Hop-HSP90 complex blocks binding to other partner proteins (113). The *HSP90* molecular chaperone family is a homodimeric molecular chaperone expressed in the cytoplasm of almost all organisms, and under normal conditions, HSP90 accounts for 1-2% of cellular proteins. In unstressed situations, it is relatively highly expressed in cells, while in stressful conditions, it can even be up-regulated with a ten-fold increase.

We simultaneously measured both proteins *S100A6* and *HSP90* in serum from preeclamptic women and normotensive controls. Confirmation of both proteins in placental tissue showing partial colocalization suggests that they may be involved in the pathophysiological process of preeclampsia. Elevated levels of proteins in tissue do not have to cause increased levels in serum. Based on our research, the increased *S100A6* levels in placenta of preeclamptic patients resulted in a significant decrease of serum *S100A6* levels in preeclampsia. We hypothesize that *S100A6* might have an altered clearance rate from blood or a change in the degradation process in the affected tissue.

The most important limitation of preeclampsia studies is the small number of cases on which findings are based. Therefore, large cohort or population studies are needed, such as the recently finished IMPROvED (Improved Pregnancy Outcomes by Early Detection) study, an international research consortium that aims to develop a robust predictive blood test for preeclampsia (11). This study has collected samples of 5,000 women, and this is the first study that enables measurements with high statistical power. From this perspective, application of the large cohort study should be considered to analyze the proteins *S100A6* and *HSP90* with a rapid, highly sensitive and highly specific, and well-designed multiplexed detection method, e.g., multiplex immunoassays or targeted multiplex mass spectrometry.

7.2 Cervical Cancer

We choose cervical cancer as a second example for a proof of principle because the current applied screening test (Figure 5) to diagnose cervical cancer at an early stage of the disease shows low sensitivity ~50% (CIN2+, cytology-based testing) and specificity ~85% (hrHPV testing) (19, 20). Using the laser capture microdissection (LCM) approach, we focused on the tumor cell instead of searching directly in serum for differentially expressed proteins (144). In this study, mass spectrometry-based data have shown that acute-phase protein families were up-regulated in serum from cervical cancer patients. However, it is not certain whether this results in leakage of tumor cell-derived proteins in the bloodstream or into

proteins that are present because of secondary mechanisms that are most often also seen in other cancer types.

It is known that *HSP90* is up-regulated in various human cancer types, including cervical cancer. We found increased levels in affected cancer cells by shotgun analysis. Tumor cells undergoing transformation are more *HSP90*-dependent than normal cells and, therefore, "ask" *HSP90* for assistance to improve the chance to survive (202). Inhibition or reduction of *HSP90* could lead to tumor decrease (202-204). In several studies *HSP90* is described as a promising anticancer target due to its role in cell survival signaling pathways in cancer cells (205-207). Many serine, threonine, and tyrosine phosphorylation sites have been identified in *HSP90* and may be potential of interest for protein kinase inhibitors that can be used for treatment (208, 209). We showed that, by mass spectrometry, *HSP90* could be detected in a reproducible and highly sensitive way (**Chapter 5**).

We described 30 highly-significant differential proteins that were expressed by comparing a set of early stage cervical cancer tissues with healthy cervical tissues (**Chapter 6**). Among these 30 proteins that were found after correction for multiple testing (Bonferroni correction), the MCM (Minichromosome maintenance) protein family (MCM2-7), which is involved in DNA replication recombination, repair and cellular development was strongly up-regulated. Finding high levels of MCM family proteins suggests that the progression of tumor development caused by HPV infection is specific for cervical cancer. We assume that the up-regulation of MCM proteins is critical for tumor progression and might serve as a viable target for anticancer therapy as well as a molecular marker for diagnosis of cervical cancer. MCM proteins were discovered in the early 1980s as a class of enzymes responsible for maintaining the integrity of circular plasmids (minichromosomes) in yeasts (210). Eukaryotic DNA replication requires sequential formation of priming complexes at origins (sites in the genome at which replication begins) known as licensing, progression through cellular checkpoints utilized to limit replication to one from each origin of replication per cell division cycle, and activation of the multiprotein complex that powers the replication fork. During DNA replication the MCM2-7 complex is loaded onto origins of DNA during late M and early G1 phases, eventually forming the pre-replicative complex (pre-RC). In this way, the replication is initiated.

MCM2-7 subunits are phosphorylated by several different kinases, including Mec1, cyclin-dependent kinase (CDK), Dbf4-dependent kinase (DDK) and casein kinase 2 (CK2) (211, 212). Checkpoint kinase 1 (Chk1) phosphorylates MCM3 at Ser-205 and is reduced under replicative stress (213). Such post-translational modification may be related to tumor carcinogenesis, and therefore, could be specific for cervical cancer (214). MCM3 may be a potential prognostic or diagnostic marker for cervical cancer to be validated in cervical smears or self-sampled material from large population cohorts. MCM3 has the potential to

utilize, together with current screening tests, hrHPV testing, and PAP smear cytology aiming for increasing sensitivity and specificity (Figure 1).

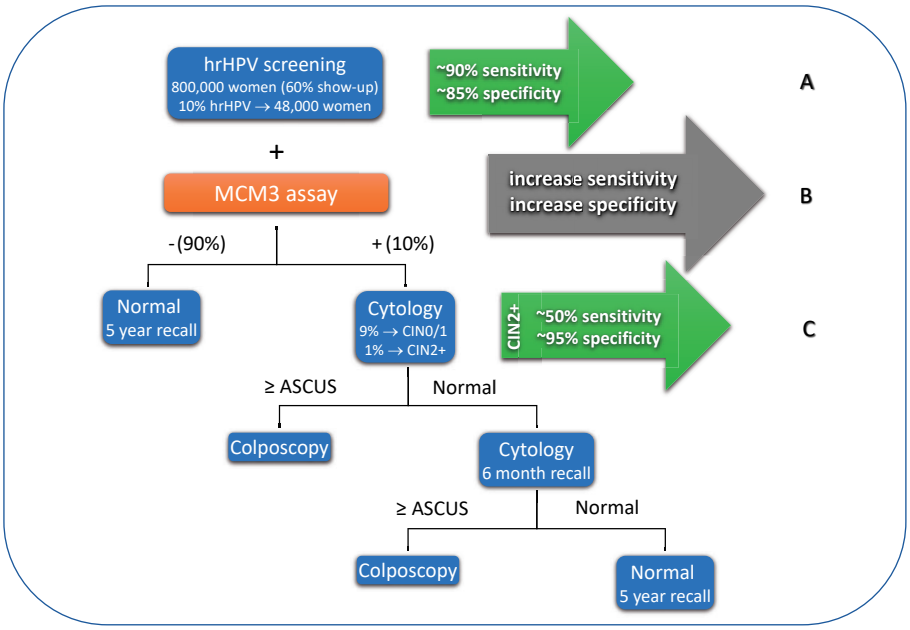

Figure 1. Flow chart of Dutch population-based screening for cervical cancer with the implementation of an extra test MCM3 to the current screening method. A). Indicated sensitivity and specificity that is known for hrHPV testing. B). A potential application of MCM3 assay that can be used in combination with hrHPV testing to increase sensitivity and specificity, that might make drive cytology (C) unnecessary.

A better understanding of how a hrHPV infection develops via precancerous stages into cervical cancer is essential for discovering new pathways, mechanisms, and biomarkers. Novel biomarkers that can determine early precancerous lesions would be a major step towards a low and non-invasive diagnostic test. Classical biomarker identification is used to rely on single technology approaches such as gene expression microarray or proteomic analyses. The current advances in next-generation sequencing and high-sensitive (phospho-) proteomics allow us to combine protein expression, protein phosphorylation status and gene expression data in a single study design. Molecular regulatory models (e.g., obtained by proteogenomic data) with both explanatory and predictive potential might help to identify biomarkers to distinguish between neoplastic lesions and cervical cancer.

Concluding remarks and future perspectives

In this thesis, we described finding potential candidate biomarkers in early-onset preeclamptic placental tissue. Subsequently, we performed validation in a unique set of transversally collected serum samples obtained from women in the first, second and third trimester of pregnancy. The identified calcyclin and its known binding partner *HSP90* may be involved in the pathogenesis of preeclampsia. We suggest validating of the two proteins in a much larger independent cohort across different hospitals. The IMPROvED project, an EU project dedicated to collect serum samples of pregnant women, is a key archive to realize such validation.

For cervical cancer, we were able to find 30 statistically significant different proteins that were compared to healthy controls analyzed by Bonferroni correction for multiple comparisons. Interestingly, the MCM family was highly up-regulated in protein abundance (two to three orders of magnitude) in cervical cancer cells as compared to healthy epithelium. Preliminary data showed that we were able to detect and quantify MCM3 in cervical scraping samples (smears). Validation of MCM proteins in a population-wide screening program as organized by RIVM (National Institute for Public Health and the Environment) must be taken into consideration. We believe that MCM3 can be implemented in the cervical cancer screening program, together with the hrHPV testing to realize higher initial specificity and lower unnecessary referrals for colposcopy.

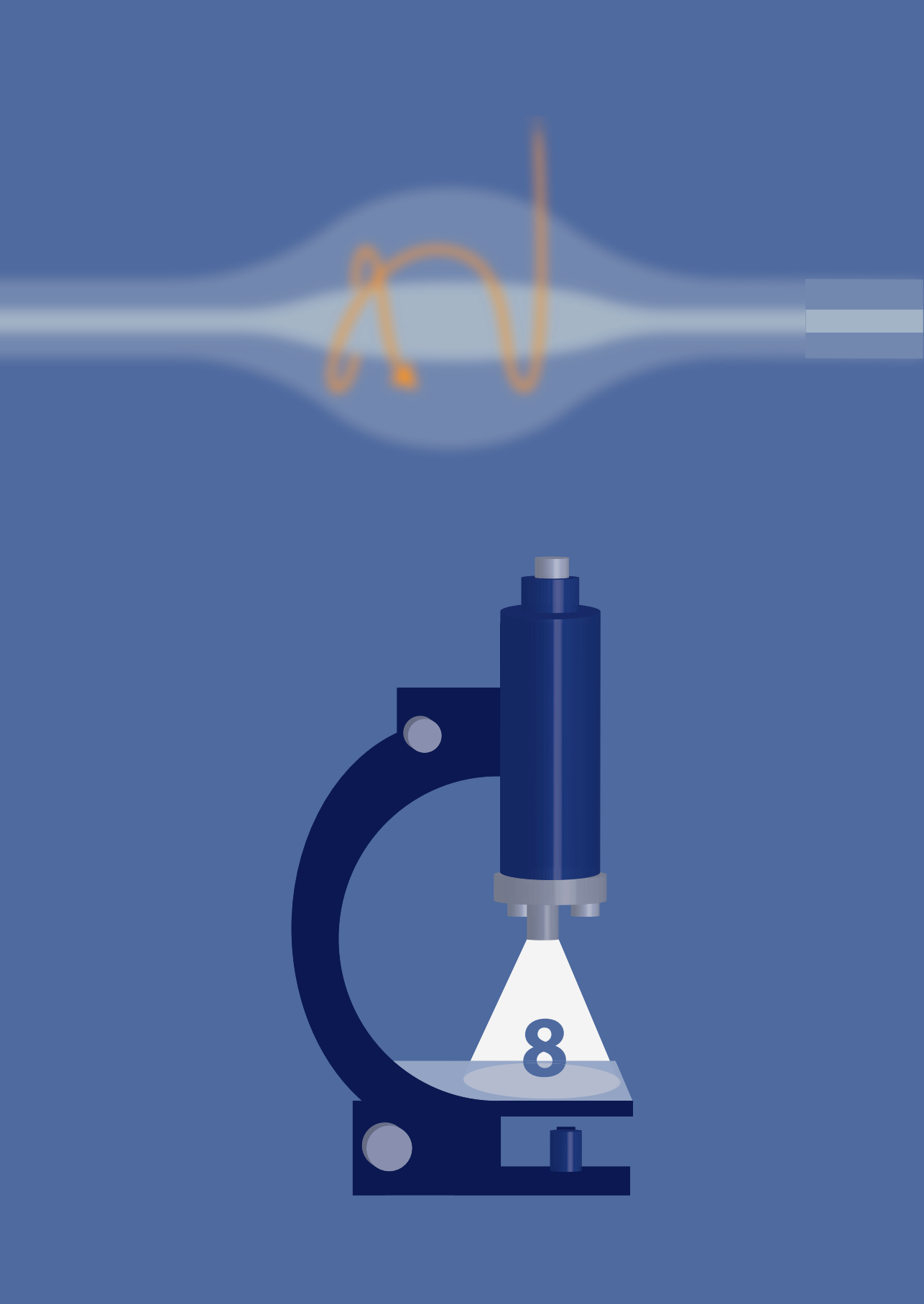
8

Chapter 8
Summary
Samenvatting

Summary

Biomarker research in biofluids is carried out on a large scale and performed, to a lower extent, on tissue level related to the origin of the disease. This thesis describes a method to identify biomarkers in affected tissue. As a proof of principle two diseases were investigated, namely preeclampsia and cervical cancer.

Preeclampsia is a pregnancy-specific syndrome associated with serious perinatal and maternal morbidity and mortality. Endovascular remodeling and invasion of the spiral arteries are impaired, which results in reduced and irregular placental perfusion. The maternal spiral artery remodeling leads to placental oxidative stress, resulting in endoplasmic reticulum-related impaired protein synthesis. We previously found two calcyclin (*S100A6*) peptides significantly higher expressed in preeclampsia measured by MALDI mass spectrometry. This observation was further confirmed through Multiple Reaction Monitoring (MRM), as described in **Chapter 2**. We extended these MRM measurements to Formalin-Fixed Paraffin-Embedded (FFPE) placental material. Laser capture microdissected cells were obtained from controls and preeclamptic FFPE placental material. The number of protein identifications obtained from equal areas of microdissected paired FFPE and frozen placenta tissue was determined by Orbitrap mass spectrometry and compared with each other. Two *S100A6* peptides were detected by MRM and quantified in the microdissected cells from preeclampsia patients and controls. *S100A6* levels were significantly higher in trophoblast cells of preeclampsia patients compared to controls. An overlap of 60% of identified proteins was observed between paired FFPE and frozen tissue. In **Chapter 3**, we described through immunohistochemistry, that preeclamptic trophoblast cells stained heavily with antibodies specific for *S100A6* in contrast to the preterm controls. To extrapolate these findings, we measured *S100A6* and its binding partner heat shock protein 90 (*HSP90*) in serum samples described in **Chapter 4**. A Parallel Reaction Monitoring (PRM) assay was developed for quantitative measurements of *S100A6* and *HSP90* in serum using stable isotope-labeled peptides. Sera from preeclamptic women throughout pregnancy from the first trimester to term were compared with sera of age-matched pregnant controls. To our knowledge, the two proteins *S100A6* and *HSP90* were for the first time studied in all trimesters of pregnancy in patients with preeclampsia and normotensive controls. Both interacting proteins were notably changed in preeclamptic patients as compared to controls; however, without differences in the onset of preeclampsia. *S100A6* was already decreased before the onset of preeclampsia in the second trimester, and *HSP90* was strongly increased in the third trimester. This suggests that these proteins may play a role in the pathogenesis of preeclampsia and ought to be investigated in large cohort studies to determine the clinical value. *S100A6* and *HSP90* are both expressed in trophoblast cells, as confirmed by double immunofluorescence staining. In **Chapter 5**, we described an *HSP90*α SRM and PRM assay that was compared with an *HSP90*α immunoassay. We developed 2D-LC-MS/MS-based SRM and PRM assays to measure *HSP90*α in serum and compared the results with a

commercially available *HSP90*α immunoassay (ELISA). Serum samples were trypsin-digested and fractionated by SCX chromatography prior to SRM and PRM measurements. PRM data obtained by high-resolution mass spectrometry correlated better with ELISA measurements than SRM data measured on a triple quadrupole mass spectrometer. All three methods (SRM, PRM, ELISA) were able to quantify *HSP90*α in serum at the nanograms per ml level, but the use of PRM on a high-resolution mass spectrometer reduced variation. To rule out that the observed differences in SRM and PRM were due to different mass spectrometry systems, the SCX fractions were measured on the same high-resolution instrument (Orbitrap) in the ion trap mode (IT-PRM). These measurements showed that intense co-eluting signals were present in the SRM method, but these interfering peaks were mostly eliminated in the high-resolution PRM mode. Results showed that it is possible to measure nanograms per ml levels of *HSP90*α in a reproducible, selective, and sensitive way using PRM in serum. This opens the possibility to quantify low levels of multiple proteins in complex samples based on a fractionation strategy on tryptic peptides, followed by PRM.

In cervical cancer research (**Chapter 6**), we studied the landscape of proteomes found in cervical tissue through laser capture microdissection (LCM). Cervical cancer is characterized by a well-defined pre-malignant phase, cervical intraepithelial neoplasia (CIN). Identification of high-grade CIN lesions by population-based screening programs and their subsequent treatment has led to a significant reduction of the incidence and mortality of cervical cancer. Cytology-based testing of cervical smears is the most widely used cervical cancer screening method, but is not ideal, as the sensitivity for detection of CIN2 and higher (CIN2+) is 50%. Therefore, more sensitive and specific biomarkers for cervical cancer and its precancerous stages are needed. By comparing early stage, late stage cervical squamous cell cancer tissue with epithelium and stromal cells from healthy subjects, 30 significant differentially expressed proteins were found after correction for multiple testing (Bonferroni correction). Among these 30 proteins, the MCM protein family was strongly up-regulated (up to 32-fold increase). The presence of four proteins (MCM3, CEACAM5, S100P, ICAM1) that were found highly significant in cervical cancer tissue using the LCM approach was confirmed in digests of whole tissue lysates by PRM measurements. We assume that the up-regulation of MCM proteins is critical for tumor progression of cervical cancer. We propose that MCM3 can be implemented together with the hrHPV testing in the current cervical cancer screening program to reach higher initial specificity and to decrease unnecessary referrals for colposcopy.

Samenvatting

Biomarkeronderzoek in lichaamsvloeistoffen wordt op grote schaal uitgevoerd. Dit gebeurt echter in mindere mate op weefselniveau gerelateerd aan de oorsprong van de ziekte. Dit proefschrift beschrijft een methode om biomarkers in aangedane weefsels te identificeren. Om dit te bewerkstelligen werden twee ziektes onderzocht, pre-eclampsie en baarmoederhalskanker.

Pre-eclampsie is een zwangerschapssyndroom geassocieerd met ernstige perinatale en maternale morbiditeit en mortaliteit. Endovasculaire remodellering en invasie van de spiraalvormige slagaders is verstoord, hetgeen resulteert in een verminderde en onregelmatige placenta-perfusie. Dit kan leiden tot oxidatieve stress van de placenta, leidend tot endoplasmatische reticulum stress met verminderde eiwitsynthese. We vonden eerder twee calcycline (*S100A6*) peptiden die significant hoger aanwezig waren bij pre-eclampsie, gemeten door MALDI massaspectrometrie. Deze observatie werd verder bevestigd door middel van Multiple Reaction Monitoring (MRM) massaspectrometrie zoals beschreven in **hoofdstuk 2**. We hebben deze MRM-metingen toegepast op Formaline-Fixed Paraffine-Embedded (FFPE) placenta materiaal. Laser capture micro-gedissecteerde (LCM) cellen werden verkregen uit controle en pre-eclamptische FFPE placenta materiaal. Het aantal eiwitidentificaties verkregen uit gelijke micro-gedissecteerde gebieden van de gepaarde FFPE en bevroren placenta weefsel werden bepaald door Orbitrap massaspectrometrie en vergeleken met elkaar. Twee *S100A6* peptiden werden gedetecteerd en gekwantificeerd door MRM in de micro-gedissecteerde cellen van pre-eclampsie patiënten en controles. De *S100A6* concentraties waren significant hoger in trofoblastcellen van pre-eclampsie patiënten in vergelijking met de controles. Een overlap van 60% van de geïdentificeerde eiwitten werd waargenomen tussen het gepaarde FFPE en bevroren weefsel. In **hoofdstuk 3** beschreven we door middel van immunohistochemie dat pre-eclamptische trofoblastcellen intensiever gekleurd waren met antilichamen specifiek voor *S100A6* in tegenstelling tot de vroeggeboorte controles. Om deze bevindingen te extrapoleren, hebben we *S100A6* en het bindende partnereiwit heat shock protein 90 (*HSP90*) gemeten in serummonsters zoals beschreven in **hoofdstuk 4**. Een Parallel Reaction Monitoring (PRM)-meting werd ontwikkeld voor kwantitatieve metingen van *S100A6* en *HSP90* in serummonsters met behulp van stabiele isotoop gelabelde peptiden. De serummonsters van vrouwen met pre-eclampsie gedurende de hele zwangerschap, van het eerste tot aan het derde trimester van de zwangerschapsduur, werden vergeleken met die van zwangere vrouwen van de op leeftijd afgestemde controles. Voor het eerst werden de twee eiwitten *S100A6* en *HSP90* bestudeerd in alle trimesters van de zwangerschap bij patiënten met pre-eclampsie en normotensieve controles. Beide op elkaar inwerkende eiwitten veranderden met name bij pre-eclampsie patiënten in vergelijking met de controles. *S100A6* was reeds verlaagd vóór het begin van pre-eclampsie in het tweede trimester en *HSP90* sterk verhoogd in het derde trimester. Dit suggereert dat deze eiwitten een rol kunnen spelen in de pathogenese van pre-eclampsie en verder

onderzocht moeten worden in grote cohort studies om de klinische waarde vast te stellen. De *S100A6* en *HSP90* eiwitten werden beide aangetoond in trofoblastcellen, zoals bevestigd door een dubbele immunofluorescentiekleuring. In **hoofdstuk 5** hebben we een *HSP90*α SRM- en PRM-test beschreven die vergeleken werden met een *HSP90*α-immunoassay. We ontwikkelden 2D-LC-MS/MS-gebaseerde SRM- en PRM-methoden om *HSP90*α in serum te meten en te vergelijken met de resultaten van een commercieel beschikbare immunoassay (ELISA). Serummonsters werden eerst behandeld met trypsine en vervolgens gefractioneerd met SCX-chromatografie, voorafgaand aan de SRM- en PRM-metingen. De PRM data verkregen door hoge-resolutie massaspectrometrie correleerden beter met de ELISA-meting, dan de SRM data gemeten op een quadrupool massaspectrometer. Terwijl alle drie methodes (SRM, PRM, ELISA) in staat waren om *HSP90*α in serum op een nanogram per milliliter niveau te kwantificeren, verminderde het gebruik van PRM op een hoge resolutie massaspectrometer de variatie. Om uit te sluiten dat de waargenomen verschillen in SRM en PRM te wijten zijn aan verschillende massaspectrometriesystemen, werden de SCX-fracties gemeten op hetzelfde hoge-resolutie instrument (Orbitrap) in de iontrap modus (IT-PRM); dergelijke metingen toonden aan dat intensieve co-eluerende signalen aanwezig waren in de SRM-methode en deze storende pieken geëlimineerd werden in de hoge-resolutie PRM-modus. De resultaten toonden aan dat het mogelijk is om op een nanogram per milliliter niveau *HSP90*α op een reproduceerbare, selectieve en gevoelige manier te meten met behulp van PRM in serum. Dit opent de mogelijkheid om lage concentraties van meerdere eiwitten in complexe monsters te kwantificeren op basis van een fractioneringsstrategie op tryptische peptiden gevolgd door PRM.

Bij het onderzoek naar baarmoederhalskanker (**hoofdstuk 6**) bestudeerden we het 'eiwitlandschap' gevonden in baarmoederhalsweefsel door middel van LCM. Baarmoederhalskanker wordt gekenmerkt door een gedefinieerde premaligne fase, namelijk cervicale intra-epitheliale neoplasie (CIN). Identificatie van hooggradige CIN-laesies door middel van populatie-gebaseerde screeningprogramma's en de daaropvolgende behandeling heeft geleid tot een significante vermindering van de incidentie en mortaliteit van baarmoederhalskanker. Cytologisch onderzoek van baarmoederhalskanker is de meest gebruikte detectiemethode voor baarmoederhalskanker, maar is niet ideaal, aangezien de gevoeligheid voor de detectie van CIN2 en hoger (CIN2+) slechts 50% is. Er zijn meer gevoelige en specifieke biomarkers nodig voor baarmoederhalskanker en de voorstadia van de ziekte. Door het vergelijken van vroege en late stadia baarmoederhalskanker met epitheel en stroma cellen van gezonde baarmoederhalsweefsel, werden 30 significante eiwitten gevonden na een Bonferroni correctie. Onder deze 30 eiwitten was de MCM-eiwitfamilie sterk verhoogd tot een 32-voudige toename. De vier zeer significante eiwitten MCM3, CEACAM5, S100P, ICAM1, gevonden met behulp van LCM in baarmoederhalskankerweefsel, werden door PRM-metingen bevestigd in hele weefsellysaten. Wij gaan ervan uit dat de up-regulering van MCM-eiwitten van cruciaal belang is voor de progressie van baarmoederhalskanker. We

stellen voor dat MCM3 samen met de hrHPV-test in het huidige screeningsprogramma voor baarmoederhalskanker kan worden geïmplementeerd om een hogere initiële specificiteit te bereiken en onnodige verwijzingen voor colposcopie te verlagen.

References

References

1. Diamandis EP. Cancer biomarkers: can we turn recent failures into success? J Natl Cancer Inst. 2010;102(19):1462-7.
2. Arantes L, De Carvalho AC, Melendez ME, Lopes Carvalho A. Serum, plasma and saliva biomarkers for head and neck cancer. Expert review of molecular diagnostics. 2018;18(1):85-112.
3. Rusling JF, Kumar CV, Gutkind JS, Patel V. Measurement of biomarker proteins for point-of-care early detection and monitoring of cancer. Analyst. 2010;135(10):2496-511.
4. Bults P, van de Merbel NC, Bischoff R. Quantification of biopharmaceuticals and biomarkers in complex biological matrices: a comparison of liquid chromatography coupled to tandem mass spectrometry and ligand binding assays. Expert Rev Proteomics. 2015;12(4):355-74.
5. Bradbury A, Pluckthun A. Reproducibility: Standardize antibodies used in research. Nature. 2015;518(7537):27-9.
6. Tighe PJ, Ryder RR, Todd I, Fairclough LC. ELISA in the multiplex era: potentials and pitfalls. Proteomics Clin Appl. 2015;9(3-4):406-22.
7. Van Gool A, Corrales F, Colovic M, Krstic D, Oliver-Martos B, Martinez-Caceres E, et al. Analytical techniques for multiplex analysis of protein biomarkers. Expert Rev Proteomics. 2020;17(4):257-73.
8. Freedman LP, Cockburn IM, Simcoe TS. The Economics of Reproducibility in Preclinical Research. PLoS Biol. 2015;13(6):e1002165.
9. Paulovich AG, Whiteaker JR, Hoofnagle AN, Wang P. The interface between biomarker discovery and clinical validation: The tar pit of the protein biomarker pipeline. Proteomics Clin Appl. 2008;2(10-11):1386-402.
10. Chen Y, Wang F, Xu F, Yang T. Mass Spectrometry-Based Protein Quantification. Adv Exp Med Biol. 2016;919:255-79.
11. Navaratnam K, Alfirevic Z, Baker PN, Gluud C, Gruttner B, Kublickiene K, et al. A multi-centre phase IIa clinical study of predictive testing for preeclampsia: improved pregnancy outcomes via early detection (IMPROvED). BMC Pregnancy Childbirth. 2013;13:226.
12. Brown MA, Lindheimer MD, de Swiet M, Van Assche A, Moutquin JM. The classification and diagnosis of the hypertensive disorders of pregnancy: statement from the International Society for the Study of Hypertension in Pregnancy (ISSHP). Hypertens Pregnancy. 2001;20(1):IX-XIV.
13. Steegers EA, von Dadelszen P, Duvekot JJ, Pijnenborg R. Pre-eclampsia. Lancet. 2010;376(9741):631-44.
14. Salgado SS, Salgado MKR. Structural changes in pre-eclamptic and eclamptic placentas--an ultrastructural study. J Coll Physicians Surg Pak. 2011;21(8):482-6.
15. Wagner LK. Diagnosis and management of preeclampsia. Am Fam Physician. 2004;70(12):2317-24.
16. Helmo FR, Lopes AMM, Carneiro A, Campos CG, Silva PB, Dos Reis Monteiro MLG, et al. Angiogenic and antiangiogenic factors in preeclampsia. Pathol Res Pract. 2018;214(1):7-14.

17. Bezerra Maia EHMS, Marques Lopes L, Murthi P, da Silva Costa F. Prevention of preeclampsia. J Pregnancy. 2012;2012:435090.
18. Steenbergen RD, Snijders PJ, Heideman DA, Meijer CJ. Clinical implications of (epi)genetic changes in HPV-induced cervical precancerous lesions. Nat Rev Cancer. 2014;14(6):395-405.
19. Boers A, Wang R, van Leeuwen RW, Klip HG, de Bock GH, Hollema H, et al. Discovery of new methylation markers to improve screening for cervical intraepithelial neoplasia grade 2/3. Clin Epigenetics. 2016;8:29.
20. Screening for cervical cancer invitation: Rijksinstituut voor Volksgezondheid en Milieu; 2018 [Available from: https://www.rivm.nl.]
21. Verhoef VM, Bosgraaf RP, van Kemenade FJ, Rozendaal L, Heideman DA, Hesselink AT, et al. Triage by methylation-marker testing versus cytology in women who test HPV-positive on self-collected cervicovaginal specimens (PROHTECT-3): a randomised controlled non-inferiority trial. Lancet Oncol. 2014;15(3):315-22.
22. Boers A, Bosgraaf RP, van Leeuwen RW, Schuuring E, Heideman DA, Massuger LF, et al. DNA methylation analysis in self-sampled brush material as a triage test in hrHPV-positive women. Br J Cancer. 2014;111(6):1095-101.
23. Arbyn M, Ronco G, Anttila A, Meijer CJ, Poljak M, Ogilvie G, et al. Evidence regarding human papillomavirus testing in secondary prevention of cervical cancer. Vaccine. 2012;30 Suppl 5:F88-99.
24. Cuzick J, Arbyn M, Sankaranarayanan R, Tsu V, Ronco G, Mayrand MH, et al. Overview of human papillomavirus-based and other novel options for cervical cancer screening in developed and developing countries. Vaccine. 2008;26 Suppl 10:K29-41.
25. Mustafa RA, Santesso N, Khatib R, Mustafa AA, Wiercioch W, Kehar R, et al. Systematic reviews and meta-analyses of the accuracy of HPV tests, visual inspection with acetic acid, cytology, and colposcopy. Int J Gynaecol Obstet. 2016;132(3):259-65.
26. de Groot CJ, Guzel C, Steegers-Theunissen RP, de Maat M, Derkx P, Roes EM, et al. Specific peptides identified by mass spectrometry in placental tissue from pregnancies complicated by early onset preeclampsia attained by laser capture dissection. Proteomics Clin Appl. 2007;1(3):325-35.
27. de Groot CJ, Steegers-Theunissen RP, Guzel C, Steegers EA, Luider TM. Peptide patterns of laser dissected human trophoblasts analyzed by matrix-assisted laser desorption/ionisation-time of flight mass spectrometry. Proteomics. 2005;5(2):597-607.
28. de Groot CJ, Guzel C, Steegers-Theunissen RP, de Maat M, et al. Specific peptides identified by mass spectrometry in placental tissue from pregnancies complicated by early onset preeclampsia attained by laser capture dissection. PROTEOMICS - Clinical Applications. 2007;1(3):325-35.
29. Espina V, Milia J, Wu G, Cowherd S, Liotta LA. Laser capture microdissection. Methods Mol Biol. 2006;319:213-29.
30. Espina V, Wulfkuhle JD, Calvert VS, VanMeter A, Zhou W, Coukos G, et al. Laser-capture microdissection. Nat Protoc. 2006;1(2):586-603.
31. Espina V, Heiby M, Pierobon M, Liotta LA. Laser capture microdissection technology. Expert review of molecular diagnostics. 2007;7(5):647-57.

32. Bereman MS, MacLean B, Tomazela DM, Liebler DC, MacCoss MJ. The development of selected reaction monitoring methods for targeted proteomics via empirical refinement. Proteomics. 2012;12(8):1134-41.
33. Keshishian H, Addona T, Burgess M, Kuhn E, Carr SA. Quantitative, multiplexed assays for low abundance proteins in plasma by targeted mass spectrometry and stable isotope dilution. Mol Cell Proteomics. 2007;6(12):2212-29.
34. Kim KH, Ahn YH, Ji ES, Lee JY, Kim JY, An HJ, et al. Quantitative analysis of low-abundance serological proteins with peptide affinity-based enrichment and pseudo-multiple reaction monitoring by hybrid quadrupole time-of-flight mass spectrometry. Anal Chim Acta. 2015;882:38-48.
35. Guzel C, Ursem NT, Dekker LJ, Derkx P, Joore J, van Dijk E, et al. Multiple reaction monitoring assay for pre-eclampsia related calcyclin peptides in formalin fixed paraffin embedded placenta. J Proteome Res. 2011;10(7):3274-82.
36. Lange V, Picotti P, Domon B, Aebersold R. Selected reaction monitoring for quantitative proteomics: a tutorial. Mol Syst Biol. 2008;4:222.
37. Vidova V, Spacil Z. A review on mass spectrometry-based quantitative proteomics: Targeted and data independent acquisition. Anal Chim Acta. 2017;964:7-23.
38. Hembrough T, Thyparambil S, Liao WL, Darfler MM, Abdo J, Bengali KM, et al. Selected Reaction Monitoring (SRM) Analysis of Epidermal Growth Factor Receptor (EGFR) in Formalin Fixed Tumor Tissue. Clin Proteomics. 2012;9(1):5.
39. Shi T, Su D, Liu T, Tang K, Camp DG, 2nd, Qian WJ, et al. Advancing the sensitivity of selected reaction monitoring-based targeted quantitative proteomics. Proteomics. 2012;12(8):1074-92.
40. Zhi W, Wang M, She JX. Selected reaction monitoring (SRM) mass spectrometry without isotope labeling can be used for rapid protein quantification. Rapid Commun Mass Spectrom. 2011;25(11):1583-8.
41. Peterson AC, Russell JD, Bailey DJ, Westphall MS, Coon JJ. Parallel reaction monitoring for high resolution and high mass accuracy quantitative, targeted proteomics. Mol Cell Proteomics. 2012;11(11):1475-88.
42. Gallien S, Duriez E, Crone C, Kellmann M, Moehring T, Domon B. Targeted proteomic quantification on quadrupole-orbitrap mass spectrometer. Mol Cell Proteomics. 2012;11(12):1709-23.
43. Kim YJ, Gallien S, El-Khoury V, Goswami P, Sertamo K, Schlesser M, et al. Quantification of SAA1 and SAA2 in lung cancer plasma using the isotype-specific PRM assays. Proteomics. 2015;15(18):3116-25.
44. Guzel C, Govorukhina NI, Stingl C, Dekker LJM, Boichenko A, van der Zee AGJ, et al. Comparison of Targeted Mass Spectrometry Techniques with an Immunoassay: A Case Study for HSP90alpha. Proteomics Clin Appl. 2018;12(1).
45. Ronsein GE, Pamir N, von Haller PD, Kim DS, Oda MN, Jarvik GP, et al. Parallel reaction monitoring (PRM) and selected reaction monitoring (SRM) exhibit comparable linearity, dynamic range and precision for targeted quantitative HDL proteomics. J Proteomics. 2015;113:388-99.
46. Sowers JL, Mirfattah B, Xu P, Tang H, Park IY, Walker C, et al. Quantification of histone modifications by parallel-reaction monitoring: a method validation. Anal Chem. 2015;87(19):10006-14.

47. Yu Q, Liu B, Ruan D, Niu C, Shen J, Ni M, et al. A novel targeted proteomics method for identification and relative quantitation of difference in nitration degree of OGDH between healthy and diabetic mouse. Proteomics. 2014;14(21-22):2417-26.
48. Gallien S, Peterman S, Kiyonami R, Souady J, Duriez E, Schoen A, et al. Highly multiplexed targeted proteomics using precise control of peptide retention time. Proteomics. 2012;12(8):1122-33.
49. Kim YJ, Gallien S, van Oostrum J, Domon B. Targeted proteomics strategy applied to biomarker evaluation. Proteomics Clin Appl. 2013;7(11-12):739-47.
50. Lesur A, Domon B. Advances in high-resolution accurate mass spectrometry application to targeted proteomics. Proteomics. 2015;15(5-6):880-90.
51. Gallien S, Kim SY, Domon B. Large-Scale Targeted Proteomics Using Internal Standard Triggered-Parallel Reaction Monitoring (IS-PRM). Mol Cell Proteomics. 2015;14(6):1630-44.
52. Haque A, Alam Q, Alam MZ, Azhar EI, Sait KH, Anfinan N, et al. Current Understanding of HSP90 as a Novel Therapeutic Target: An Emerging Approach for the Treatment of Cancer. Curr Pharm Des. 2016;22(20):2947-59.
53. Vriend LEM, van den Tempel N, Oei AL, L'Acosta M, Pieterson FJ, Franken NAP, et al. Boosting the effects of hyperthermia-based anticancer treatments by HSP90 inhibition. Oncotarget. 2017;8(57):97490-503.
54. Calderon-Celis F, Encinar JR, Sanz-Medel A. Standardization approaches in absolute quantitative proteomics with mass spectrometry. Mass Spectrom Rev. 2017.
55. Wilffert D, Reis CR, Hermans J, Govorukhina N, Tomar T, de Jong S, et al. Antibody-free LC-MS/MS quantification of rhTRAIL in human and mouse serum. Anal Chem. 2013;85(22):10754-60.
56. Wilffert D, Bischoff R, van de Merbel NC. Antibody-free workflows for protein quantification by LC-MS/MS. Bioanalysis. 2015;7(6):763-79.
57. Guo L, Wang Q, Weng L, Hauser LA, Strawser CJ, Rocha AG, et al. Liquid Chromatography-High Resolution Mass Spectrometry Analysis of Platelet Frataxin as a Protein Biomarker for the Rare Disease Friedreich's Ataxia. Anal Chem. 2018;90(3):2216-23.
58. Guzel C, Govorukhina NI, Wisman GBA, Stingl C, Dekker LJM, Klip HG, et al. Proteomic alterations in early stage cervical cancer. Oncotarget. 2018;9(26):18128-47.
59. Bronsema KJ, Bischoff R, van de Merbel NC. High-sensitivity LC-MS/MS quantification of peptides and proteins in complex biological samples: the impact of enzymatic digestion and internal standard selection on method performance. Anal Chem. 2013;85(20):9528-35.
60. Bronsema KJ, Bischoff R, van de Merbel NC. Internal standards in the quantitative determination of protein biopharmaceuticals using liquid chromatography coupled to mass spectrometry. J Chromatogr B Analyt Technol Biomed Life Sci. 2012;893-894:1-14.
61. MacLean B, Tomazela DM, Shulman N, Chambers M, Finney GL, Frewen B, et al. Skyline: an open source document editor for creating and analyzing targeted proteomics experiments. Bioinformatics. 2010;26(7):966-8.
62. Domanski D, Percy AJ, Yang J, Chambers AG, Hill JS, Freue GV, et al. MRM-based multiplexed quantitation of 67 putative cardiovascular disease biomarkers in human plasma. Proteomics. 2012;12(8):1222-43.

63. Meier F, Beck S, Grassl N, Lubeck M, Park MA, Raether O, et al. Parallel Accumulation-Serial Fragmentation (PASEF): Multiplying Sequencing Speed and Sensitivity by Synchronized Scans in a Trapped Ion Mobility Device. J Proteome Res. 2015;14(12):5378-87.
64. Bruderer R, Bernhardt OM, Gandhi T, Xuan Y, Sondermann J, Schmidt M, et al. Optimization of Experimental Parameters in Data-Independent Mass Spectrometry Significantly Increases Depth and Reproducibility of Results. Mol Cell Proteomics. 2017;16(12):2296-309.
65. Khan KS, Wojdyla D, Say L, Gulmezoglu AM, Van Look PF. WHO analysis of causes of maternal death: a systematic review. Lancet. 2006;367(9516):1066-74.
66. Bulletins--Obstetrics ACoP. ACOG practice bulletin. Diagnosis and management of preeclampsia and eclampsia. Number 33, January 2002. Obstet Gynecol. 2002;99(1):159-67.
67. von Dadelszen P, Magee LA, Roberts JM. Subclassification of preeclampsia. Hypertens Pregnancy. 2003;22(2):143-8.
68. Burton GJ, Jauniaux E. Placental oxidative stress: from miscarriage to preeclampsia. J Soc Gynecol Investig. 2004;11(6):342-52.
69. Jauniaux E, Poston L, Burton GJ. Placental-related diseases of pregnancy: Involvement of oxidative stress and implications in human evolution. Hum Reprod Update. 2006;12(6):747-55.
70. Burton GJ, Yung HW, Cindrova-Davies T, Charnock-Jones DS. Placental endoplasmic reticulum stress and oxidative stress in the pathophysiology of unexplained intrauterine growth restriction and early onset preeclampsia. Placenta. 2009;30 Suppl A:S43-8.
71. Myatt L, Cui X. Oxidative stress in the placenta. Histochem Cell Biol. 2004;122(4):369-82.
72. Wang Y, Walsh SW. Antioxidant activities and mRNA expression of superoxide dismutase, catalase, and glutathione peroxidase in normal and preeclamptic placentas. J Soc Gynecol Investig. 1996;3(4):179-84.
73. Rumbold A, Duley L, Crowther CA, Haslam RR. Antioxidants for preventing pre-eclampsia. Cochrane Database Syst Rev. 2008(1):CD004227.
74. Roberts JM, Cooper DW. Pathogenesis and genetics of pre-eclampsia. Lancet. 2001;357(9249):53-6.
75. Allaire AD, Ballenger KA, Wells SR, McMahon MJ, Lessey BA. Placental apoptosis in preeclampsia. Obstet Gynecol. 2000;96(2):271-6.
76. Redman CW, Sargent IL. Preeclampsia and the systemic inflammatory response. Semin Nephrol. 2004;24(6):565-70.
77. Nedjadi T, Kitteringham N, Campbell F, Jenkins RE, Park BK, Navarro P, et al. S100A6 binds to annexin 2 in pancreatic cancer cells and promotes pancreatic cancer cell motility. Br J Cancer. 2009;101(7):1145-54.
78. Lesniak W, Slomnicki LP, Filipek A. S100A6 - new facts and features. Biochem Biophys Res Commun. 2009;390(4):1087-92.
79. Lesniak W, Szczepanska A, Kuznicki J. Calcyclin (S100A6) expression is stimulated by agents evoking oxidative stress via the antioxidant response element. Biochim Biophys Acta. 2005;1744(1):29-37.

80. Orre LM, Pernemalm M, Lengqvist J, Lewensohn R, Lehtio J. Up-regulation, modification, and translocation of S100A6 induced by exposure to ionizing radiation revealed by proteomics profiling. Mol Cell Proteomics. 2007;6(12):2122-31.
81. Kawamura T, Nomura M, Tojo H, Fujii K, Hamasaki H, Mikami S, et al. Proteomic analysis of laser-microdissected paraffin-embedded tissues: (1) Stage-related protein candidates upon non-metastatic lung adenocarcinoma. J Proteomics. 2010;73(6):1089-99.
82. Nishimura T, Nomura M, Tojo H, Hamasaki H, Fukuda T, Fujii K, et al. Proteomic analysis of laser-microdissected paraffin-embedded tissues: (2) MRM assay for stage-related proteins upon non-metastatic lung adenocarcinoma. J Proteomics. 2010;73(6):1100-10.
83. Hood BL, Darfler MM, Guiel TG, Furusato B, Lucas DA, Ringeisen BR, et al. Proteomic analysis of formalin-fixed prostate cancer tissue. Mol Cell Proteomics. 2005;4(11):1741-53.
84. Prieto DA, Hood BL, Darfler MM, Guiel TG, Lucas DA, Conrads TP, et al. Liquid Tissue: proteomic profiling of formalin-fixed tissues. Biotechniques. 2005;Suppl:32-5.
85. Shi SR, Cote RJ, Taylor CR. Antigen retrieval immunohistochemistry: past, present, and future. J Histochem Cytochem. 1997;45(3):327-43.
86. Bagnato C, Thumar J, Mayya V, Hwang SI, Zebroski H, Claffey KP, et al. Proteomics analysis of human coronary atherosclerotic plaque: a feasibility study of direct tissue proteomics by liquid chromatography and tandem mass spectrometry. Mol Cell Proteomics. 2007;6(6):1088-102.
87. Blonder J, Johann DJ, Veenstra TD, Xiao Z, Emmert-Buck MR, Ziegler RG, et al. Quantitation of steroid hormones in thin fresh frozen tissue sections. Anal Chem. 2008;80(22):8845-52.
88. Van Berkel GJ, Kertesz V, Koeplinger KA, Vavrek M, Kong AN. Liquid microjunction surface sampling probe electrospray mass spectrometry for detection of drugs and metabolites in thin tissue sections. J Mass Spectrom. 2008;43(4):500-8.
89. Tong X, Zhou J, Tan Y. Liquid chromatography/tandem triple-quadrupole mass spectrometry for determination of paclitaxel in rat tissues. Rapid Commun Mass Spectrom. 2006;20(12):1905-12.
90. Bleker OP, Buimer M, van der Post JA, van der Veen F. Ted (G.J.) Kloosterman: on intrauterine growth. The significance of prenatal care. Studies on birth weight, placental weight and placental index. Placenta. 2006;27(11-12):1052-4.
91. Stingl C, van Vilsteren FG, Guzel C, Ten Kate FJ, Visser M, Krishnadath KK, et al. Reproducibility of Protein Identification of Selected Cell Types in Barrett's Esophagus Analyzed by Combining Laser-Capture Microdissection and Mass Spectrometry. J Proteome Res. 2010.
92. Reimel BA, Pan S, May DH, Shaffer SA, Goodlett DR, McIntosh MW, et al. Proteomics on Fixed Tissue Specimens - A Review. Curr Proteomics. 2009;6(1):63-9.
93. Salama I, Malone PS, Mihaimeed F, Jones JL. A review of the S100 proteins in cancer. Eur J Surg Oncol. 2008;34(4):357-64.
94. Schafer BW, Heizmann CW. The S100 family of EF-hand calcium-binding proteins: functions and pathology. Trends Biochem Sci. 1996;21(4):134-40.
95. Sofiadis A, Dinets A, Orre LM, Branca RM, Juhlin CC, Foukakis T, et al. Proteomic Study of Thyroid Tumors Reveals Frequent Up-Regulation of the Ca(2+)-Binding Protein S100A6 in Papillary Thyroid Carcinoma. Thyroid. 2010.

96. Weterman MA, Stoopen GM, van Muijen GN, Kuznicki J, Ruiter DJ, Bloemers HP. Expression of calcyclin in human melanoma cell lines correlates with metastatic behavior in nude mice. Cancer Res. 1992;52(5):1291-6.
97. Gong Y, Alkhalaf B, Murphy LJ, Murphy LC. Differential effects of phorbol esters on proliferation and calcyclin expression in human endometrial carcinoma cells. Cell Growth Differ. 1992;3(11):847-53.
98. Ishii A, Suzuki M, Satomi K, Kobayashi H, Sakashita S, Kano J, et al. Increased cytoplasmic S100A6 expression is associated with pulmonary adenocarcinoma progression. Pathol Int. 2009;59(9):623-30.
99. Guzel C, Ursem NT, Dekker LJ, Derkx P, Joore J, van Dijk E, et al. Multiple reaction monitoring assay for pre-eclampsia related calcyclin peptides in formalin fixed paraffin embedded placenta. J Proteome Res. 2011;10(7):3274-82.
100. Filipek A, Michowski W, Kuznicki J. Involvement of S100A6 (calcyclin) and its binding partners in intracellular signaling pathways. Adv Enzyme Regul. 2008;48:225-39.
101. Slomnicki LP, Nawrot B, Lesniak W. S100A6 binds p53 and affects its activity. Int J Biochem Cell Biol. 2009;41(4):784-90.
102. Spiechowicz M, Zylicz A, Bieganowski P, Kuznicki J, Filipek A. Hsp70 is a new target of Sgt1--an interaction modulated by S100A6. Biochem Biophys Res Commun. 2007;357(4):1148-53.
103. Molvarec A, Tamasi L, Losonczy G, Madach K, Prohaszka Z, Rigo J, Jr. Circulating heat shock protein 70 (HSPA1A) in normal and pathological pregnancies. Cell Stress Chaperones. 2010;15(3):237-47.
104. Chen Y, Voegeli TS, Liu PP, Noble EG, Currie RW. Heat shock paradox and a new role of heat shock proteins and their receptors as anti-inflammation targets. Inflamm Allergy Drug Targets. 2007;6(2):91-100.
105. Anderson UD, Olsson MG, Kristensen KH, Akerstrom B, Hansson SR. Review: Biochemical markers to predict preeclampsia. Placenta. 2012;33 Suppl:S42-7.
106. Roberts JM, Pearson G, Cutler J, Lindheimer M, Pregnancy NWGoRoHD. Summary of the NHLBI Working Group on Research on Hypertension During Pregnancy. Hypertension. 2003;41(3):437-45.
107. Brosens IA, Robertson WB, Dixon HG. The role of the spiral arteries in the pathogenesis of preeclampsia. Obstet Gynecol Annu. 1972;1:177-91.
108. Pijnenborg R, Vercruysse L, Hanssens M. The uterine spiral arteries in human pregnancy: facts and controversies. Placenta. 2006;27(9-10):939-58.
109. Schol PB, Guzel C, Steegers EA, de Krijger RR, Luider TM. Trophoblast calcyclin is elevated in placental tissue from patients with early pre-eclampsia. Pregnancy Hypertens. 2014;4(1):7-10.
110. Wang T, Liang Y, Thakur A, Zhang S, Yang T, Chen T, et al. Diagnostic significance of S100A2 and S100A6 levels in sera of patients with non-small cell lung cancer. Tumour Biol. 2016;37(2):2299-304.
111. Loosen SH, Benz F, Niedeggen J, Schmeding M, Schuller F, Koch A, et al. Serum levels of S100A6 are unaltered in patients with resectable cholangiocarcinoma. Clin Transl Med. 2016;5(1):39.

112. Shimamoto S, Kubota Y, Tokumitsu H, Kobayashi R. S100 proteins regulate the interaction of Hsp90 with Cyclophilin 40 and FKBP52 through their tetratricopeptide repeats. FEBS Lett. 2010;584(6):1119-25.
113. Shimamoto S, Takata M, Tokuda M, Oohira F, Tokumitsu H, Kobayashi R. Interactions of S100A2 and S100A6 with the tetratricopeptide repeat proteins, Hsp90/Hsp70-organizing protein and kinesin light chain. J Biol Chem. 2008;283(42):28246-58.
114. Guzel C, Govorukhina NI, Stingl C, Dekker LJM, Boichenko A, van der Zee AGJ, et al. Comparison of Targeted Mass Spectrometry Techniques With an Immunoassay: A Case Study For HSP90alpha. Proteomics Clin Appl. 2017.
115. Steegers-Theunissen RP, Verheijden-Paulissen JJ, van Uitert EM, Wildhagen MF, Exalto N, Koning AH, et al. Cohort Profile: The Rotterdam Periconceptional Cohort (Predict Study). Int J Epidemiol. 2016;45(2):374-81.
116. van den Berg CB, Duvekot JJ, Guzel C, Hansson SR, de Leeuw TG, Steegers EA, et al. Elevated levels of protein AMBP in cerebrospinal fluid of women with preeclampsia compared to normotensive pregnant women. Proteomics Clin Appl. 2016.
117. Rong B, Zhao C, Liu H, Ming Z, Cai X, Gao W, et al. Erratum: Identification and verification of Hsp90-beta as a potential serum biomarker for lung cancer. Am J Cancer Res. 2016;6(6):1460.
118. Rong B, Cai X, Liu H, Fu T, Gao W, Zhao C, et al. Increased level of Hsp90-beta in bronchoalveolar lavage fluid correlates with lymphatic invasion and advanced stage of lung cancer patients. Am J Transl Res. 2016;8(10):4147-59.
119. Vizcaino JA, Csordas A, del-Toro N, Dianes JA, Griss J, Lavidas I, et al. 2016 update of the PRIDE database and its related tools. Nucleic Acids Res. 2016;44(D1):D447-56.
120. Caraux G, Pinloche S. PermutMatrix: a graphical environment to arrange gene expression profiles in optimal linear order. Bioinformatics. 2005;21(7):1280-1.
121. Meunier B, Dumas E, Piec I, Bechet D, Hebraud M, Hocquette JF. Assessment of hierarchical clustering methodologies for proteomic data mining. J Proteome Res. 2007;6(1):358-66.
122. Tranquilli AL, Brown MA, Zeeman GG, Dekker G, Sibai BM. The definition of severe and early-onset preeclampsia. Statements from the International Society for the Study of Hypertension in Pregnancy (ISSHP). Pregnancy Hypertens. 2013;3(1):44-7.
123. Donato R, Sorci G, Giambanco I. S100A6 protein: functional roles. Cell Mol Life Sci. 2017;74(15):2749-60.
124. Hansson SR, Naav A, Erlandsson L. Oxidative stress in preeclampsia and the role of free fetal hemoglobin. Front Physiol. 2014;5:516.
125. Marenholz I, Heizmann CW, Fritz G. S100 proteins in mouse and man: from evolution to function and pathology (including an update of the nomenclature). Biochem Biophys Res Commun. 2004;322(4):1111-22.
126. Leclerc E, Fritz G, Vetter SW, Heizmann CW. Binding of S100 proteins to RAGE: an update. Biochim Biophys Acta. 2009;1793(6):993-1007.
127. Mahajan N, Dhawan V. Receptor for advanced glycation end products (RAGE) in vascular and inflammatory diseases. Int J Cardiol. 2013;168(3):1788-94.

128. Chekir C, Nakatsuka M, Noguchi S, Konishi H, Kamada Y, Sasaki A, et al. Accumulation of advanced glycation end products in women with preeclampsia: possible involvement of placental oxidative and nitrative stress. Placenta. 2006;27(2-3):225-33.
129. De Maio A, Vazquez D. Extracellular heat shock proteins: a new location, a new function. Shock. 2013;40(4):239-46.
130. Goral A, Bieganowski P, Prus W, Krzemien-Ojak L, Kadziolka B, Fabczak H, et al. Calcyclin Binding Protein/Siah-1 Interacting Protein Is a Hsp90 Binding Chaperone. PLoS One. 2016;11(6):e0156507.
131. Hromadnikova I, Dvorakova L, Kotlabova K, Kestlerova A, Hympanova L, Novotna V, et al. Assessment of placental and maternal stress responses in patients with pregnancy related complications via monitoring of heat shock protein mRNA levels. Mol Biol Rep. 2015;42(3):625-37.
132. Ekambaram P, Jayachandran T, Dhakshinamoorthy L. Differential expression of HSP90alpha and heme oxygenase in cord blood RBC during preeclampsia. Toxicol Mech Methods. 2013;23(2):113-9.
133. Laflamme EM. Maternal hemoglobin concentration and pregnancy outcome: a study of the effects of elevation in el alto, bolivia. Mcgill J Med. 2011;13(1):47.
134. Ramasamy R, Yan SF, Schmidt AM. Receptor for AGE (RAGE): signaling mechanisms in the pathogenesis of diabetes and its complications. Ann N Y Acad Sci. 2011;1243:88-102.
135. Wu P, van den Berg C, Alfirevic Z, O'Brien S, Rothlisberger M, Baker PN, et al. Early Pregnancy Biomarkers in Pre-Eclampsia: A Systematic Review and Meta-Analysis. Int J Mol Sci. 2015;16(9):23035-56.
136. Peterson AC, Russell JD, Bailey DJ, Westphall MS, Coon JJ. Parallel Reaction Monitoring for High Resolution and High Mass Accuracy Quantitative, Targeted Proteomics. Molecular & Cellular Proteomics. 2012;11(11):1475-88.
137. Gallien S, Peterman S, Kiyonami R, Souady J, Duriez E, Schoen A, et al. Highly multiplexed targeted proteomics using precise control of peptide retention time. Proteomics. 2012;12(8):1122-33.
138. Kim YJ, Gallien S, van Oostrum J, Domon B. Targeted proteomics strategy applied to biomarker evaluation. Proteom Clin Appl. 2013;7(11-12):739-47.
139. Lesur A, Domon B. Advances in high-resolution accurate mass spectrometry application to targeted proteomics. Proteomics. 2015;15(5-6):880-90.
140. Gallien S, Kim SY, Domon B. Large-Scale Targeted Proteomics Using Internal Standard Triggered-Parallel Reaction Monitoring (IS-PRM). Molecular & Cellular Proteomics. 2015;14(6):1630-44.
141. Gallien S, Bourmaud A, Kim SY, Domon B. Technical considerations for large-scale parallel reaction monitoring analysis. J Proteomics. 2014;100:147-59.
142. Barrott JJ, Haystead TA. Hsp90, an unlikely ally in the war on cancer. FEBS J. 2013;280(6):1381-96.
143. Ciocca DR, Calderwood SK. Heat shock proteins in cancer: diagnostic, prognostic, predictive, and treatment implications. Cell stress & chaperones. 2005;10(2):86-103.
144. Boichenko AP, Govorukhina N, Klip HG, van der Zee AG, Guzel C, Luider TM, et al. A panel of regulated proteins in serum from patients with cervical intraepithelial neoplasia and cervical cancer. J Proteome Res. 2014;13(11):4995-5007.

145. Shervington L, Patil H, Shervington A. Could the Anti-Chaperone VER155008 Replace Temozolomide for Glioma Treatment. J Cancer. 2015;6(8):786-94.
146. Maehana T, Tanaka T, Kitamura H, Fukuzawa N, Ishida H, Harada H, et al. Heat Shock Protein 90alpha Is a Potential Serological Biomarker of Acute Rejection after Renal Transplantation. PLoS One. 2016;11(9):e0162942.
147. Saito K, Kukita K, Kutomi G, Okuya K, Asanuma H, Tabeya T, et al. Heat shock protein 90 associates with Toll-like receptors 7/9 and mediates self-nucleic acid recognition in SLE. Eur J Immunol. 2015;45(7):2028-41.
148. Ersvaer E, Brenner AK, Vetas K, Reikvam H, Bruserud O. Effects of cytarabine on activation of human T cells - cytarabine has concentration-dependent effects that are modulated both by valproic acid and all-trans retinoic acid. BMC Pharmacol Toxicol. 2015;16:12.
149. Searle BC. Scaffold: a bioinformatic tool for validating MS/MS-based proteomic studies. Proteomics. 2010;10(6):1265-9.
150. Basiri B, Bartlett MG. LC-MS of oligonucleotides: applications in biomedical research. Bioanalysis. 2014;6(11):1525-42.
151. Peng DM, Punn R, Maeda K, Selamet Tierney ES. Diagnosing Neonatal Aortic Coarctation in the Setting of Patent Ductus Arteriosus. Ann Thorac Surg. 2016;101(3):1005-10.
152. Tsai CF, Wang YT, Yen HY, Tsou CC, Ku WC, Lin PY, et al. Large-scale determination of absolute phosphorylation stoichiometries in human cells by motif-targeting quantitative proteomics. Nat Commun. 2015;6:6622.
153. Rigbolt KT, Prokhorova TA, Akimov V, Henningsen J, Johansen PT, Kratchmarova I, et al. System-wide temporal characterization of the proteome and phosphoproteome of human embryonic stem cell differentiation. Sci Signal. 2011;4(164):rs3.
154. Kettenbach AN, Schweppe DK, Faherty BK, Pechenick D, Pletnev AA, Gerber SA. Quantitative phosphoproteomics identifies substrates and functional modules of Aurora and Polo-like kinase activities in mitotic cells. Sci Signal. 2011;4(179):rs5.
155. Global Burden of Disease Cancer C, Fitzmaurice C, Dicker D, Pain A, Hamavid H, Moradi-Lakeh M, et al. The Global Burden of Cancer 2013. JAMA Oncol. 2015;1(4):505-27.
156. Franco EL, Schlecht NF, Saslow D. The epidemiology of cervical cancer. Cancer journal. 2003;9(5):348-59.
157. Soerjomataram I, Lortet-Tieulent J, Parkin DM, Ferlay J, Mathers C, Forman D, et al. Global burden of cancer in 2008: a systematic analysis of disability-adjusted life-years in 12 world regions. Lancet. 2012;380(9856):1840-50.
158. Parkin DM, Bray F, Ferlay J, Pisani P. Global cancer statistics, 2002. CA: a cancer journal for clinicians. 2005;55(2):74-108.
159. Cotton SC, Sharp L, Seth R, Masson LF, Little J, Cruickshank ME, et al. Lifestyle and socio-demographic factors associated with high-risk HPV infection in UK women. Br J Cancer. 2007;97(1):133-9.
160. Monsonego J, Eurogin. HPV infections and cervical cancer prevention. Priorities and new directions. Highlights of EUROGIN 2004 International Expert Meeting, Nice, France, October 21-23, 2004. Gynecol Oncol. 2005;96(3):830-9.

161. Clifford GM, Smith JS, Aguado T, Franceschi S. Comparison of HPV type distribution in high-grade cervical lesions and cervical cancer: a meta-analysis. Br J Cancer. 2003;89(1):101-5.
162. Nguyen HH, Broker TR, Chow LT, Alvarez RD, Vu HL, Andrasi J, et al. Immune responses to human papillomavirus in genital tract of women with cervical cancer. Gynecologic Oncology. 2005;96(2):452-61.
163. Mirabello L, Yeager M, Yu K, Clifford GM, Xiao Y, Zhu B, et al. HPV16 E7 Genetic Conservation Is Critical to Carcinogenesis. Cell. 2017;170(6):1164-74 e6.
164. Ojesina AI, Lichtenstein L, Freeman SS, Pedamallu CS, Imaz-Rosshandler I, Pugh TJ, et al. Landscape of genomic alterations in cervical carcinomas. Nature. 2014;506(7488):371-5.
165. Cancer Genome Atlas Research N, Albert Einstein College of M, Analytical Biological S, Barretos Cancer H, Baylor College of M, Beckman Research Institute of City of H, et al. Integrated genomic and molecular characterization of cervical cancer. Nature. 2017;543(7645):378-84.
166. Zhang H, Liu T, Zhang Z, Payne SH, Zhang B, McDermott JE, et al. Integrated Proteogenomic Characterization of Human High-Grade Serous Ovarian Cancer. Cell. 2016;166(3):755-65.
167. Mertins P, Mani DR, Ruggles KV, Gillette MA, Clauser KR, Wang P, et al. Proteogenomics connects somatic mutations to signalling in breast cancer. Nature. 2016;534(7605):55-62.
168. Datta S, Malhotra L, Dickerson R, Chaffee S, Sen CK, Roy S. Laser capture microdissection: Big data from small samples. Histol Histopathol. 2015:11622.
169. Langenkamp E, Kamps JA, Mrug M, Verpoorte E, Niyaz Y, Horvatovich P, et al. Innovations in studying in vivo cell behavior and pharmacology in complex tissues--microvascular endothelial cells in the spotlight. Cell Tissue Res. 2013;354(3):647-69.
170. Liu NQ, Braakman RB, Stingl C, Luider TM, Martens JW, Foekens JA, et al. Proteomics pipeline for biomarker discovery of laser capture microdissected breast cancer tissue. J Mammary Gland Biol Neoplasia. 2012;17(2):155-64.
171. Okayama A, Miyagi Y, Oshita F, Nishi M, Nakamura Y, Nagashima Y, et al. Proteomic analysis of proteins related to prognosis of lung adenocarcinoma. J Proteome Res. 2014;13(11):4686-94.
172. Liu NQ, Dekker LJ, Stingl C, Guzel C, De Marchi T, Martens JW, et al. Quantitative proteomic analysis of microdissected breast cancer tissues: comparison of label-free and SILAC-based quantification with shotgun, directed, and targeted MS approaches. J Proteome Res. 2013;12(10):4627-41.
173. De Marchi T, Liu NQ, Stingl C, Timmermans MA, Smid M, Look MP, et al. 4-protein signature predicting tamoxifen treatment outcome in recurrent breast cancer. Mol Oncol. 2015.
174. Mu Y, Chen Y, Zhang G, Zhan X, Li Y, Liu T, et al. Identification of stromal differentially expressed proteins in the colon carcinoma by quantitative proteomics. Electrophoresis. 2013;34(11):1679-92.
175. Gu Y, Wu S-L, Meyer JL, Hancock WS, Burg LJ, Linder J, et al. Proteomic Analysis of High-Grade Dysplastic Cervical Cells Obtained from ThinPrep Slides Using Laser Capture Microdissection and Mass Spectrometry. Journal of Proteome Research. 2007;6(11):4256-68.
176. Tsai FL, Vijayraghavan S, Prinz J, MacAlpine HK, MacAlpine DM, Schwacha A. Mcm2-7 Is an Active Player in the DNA Replication Checkpoint Signaling Cascade via Proposed Modulation of Its DNA Gate. Molecular and cellular biology. 2015;35(12):2131-43.

177. Das M, Prasad SB, Yadav SS, Modi A, Singh S, Pradhan S, et al. HPV-type-specific response of cervical cancer cells to cisplatin after silencing replication licensing factor MCM4. Tumour Biol. 2015.
178. Bochman ML, Schwacha A. The Mcm complex: unwinding the mechanism of a replicative helicase. Microbiol Mol Biol Rev. 2009;73(4):652-83.
179. Sanchez-Berrondo J, Mesa P, Ibarra A, Martinez-Jimenez MI, Blanco L, Mendez J, et al. Molecular architecture of a multifunctional MCM complex. Nucleic Acids Res. 2012;40(3):1366-80.
180. Tye BK. MCM proteins in DNA replication. Annu Rev Biochem. 1999;68:649-86.
181. Honeycutt KA, Chen Z, Koster MI, Miers M, Nuchtern J, Hicks J, et al. Deregulated minichromosomal maintenance protein MCM7 contributes to oncogene driven tumorigenesis. Oncogene. 2006;25(29):4027-32.
182. Lei M. The MCM complex: its role in DNA replication and implications for cancer therapy. Curr Cancer Drug Targets. 2005;5(5):365-80.
183. Majid S, Dar AA, Saini S, Chen Y, Shahryari V, Liu J, et al. Regulation of minichromosome maintenance gene family by microRNA-1296 and genistein in prostate cancer. Cancer Res. 2010;70(7):2809-18.
184. Blumenthal RD, Leon E, Hansen HJ, Goldenberg DM. Expression patterns of CEACAM5 and CEACAM6 in primary and metastatic cancers. BMC Cancer. 2007;7:2.
185. Parkkila S, Pan PW, Ward A, Gibadulinova A, Oveckova I, Pastorekova S, et al. The calcium-binding protein S100P in normal and malignant human tissues. BMC Clin Pathol. 2008;8:2.
186. Arumugam T, Logsdon CD. S100P: a novel therapeutic target for cancer. Amino Acids. 2011;41(4):893-9.
187. van der Aa MA, Pukkala E, Coebergh JW, Anttila A, Siesling S. Mass screening programmes and trends in cervical cancer in Finland and the Netherlands. Int J Cancer. 2008;122(8):1854-8.
188. Bulkmans NW, Rozendaal L, Snijders PJ, Voorhorst FJ, Boeke AJ, Zandwijken GR, et al. POBASCAM, a population-based randomized controlled trial for implementation of high-risk HPV testing in cervical screening: design, methods and baseline data of 44,102 women. Int J Cancer. 2004;110(1):94-101.
189. Mayrand MH, Duarte-Franco E, Rodrigues I, Walter SD, Hanley J, Ferenczy A, et al. Human papillomavirus DNA versus Papanicolaou screening tests for cervical cancer. N Engl J Med. 2007;357(16):1579-88.
190. Stingl C, van Vilsteren FG, Guzel C, Ten Kate FJ, Visser M, Krishnadath KK, et al. Reproducibility of protein identification of selected cell types in Barrett's esophagus analyzed by combining laser-capture microdissection and mass spectrometry. J Proteome Res. 2011;10(1):288-98.
191. Tabb DL, Vega-Montoto L, Rudnick PA, Variyath AM, Ham AJ, Bunk DM, et al. Repeatability and reproducibility in proteomic identifications by liquid chromatography-tandem mass spectrometry. J Proteome Res. 2010;9(2):761-76.
192. Kramer A, Green J, Pollard J, Jr., Tugendreich S. Causal analysis approaches in Ingenuity Pathway Analysis. Bioinformatics. 2014;30(4):523-30.

193. Guzel C, Govorukhina NI, Stingl C, Dekker LJM, Boichenko A, van der Zee AGJ, et al. Comparison of Targeted Mass Spectrometry Techniques with an Immunoassay: A Case Study for HSP90alpha. Proteomics Clin Appl. 2017.
194. Boschetti E, D'Amato A, Candiano G, Righetti PG. Protein biomarkers for early detection of diseases: The decisive contribution of combinatorial peptide ligand libraries. J Proteomics. 2018;188:1-14.
195. Geyer PE, Holdt LM, Teupser D, Mann M. Revisiting biomarker discovery by plasma proteomics. Mol Syst Biol. 2017;13(9):942.
196. Chen L, Hu X, Wu H, Jia Y, Liu J, Mu X, et al. Over-expression of S100B protein as a serum marker of brain metastasis in non-small cell lung cancer and its prognostic value. Pathol Res Pract. 2018.
197. Schiess R, Wollscheid B, Aebersold R. Targeted proteomic strategy for clinical biomarker discovery. Mol Oncol. 2009;3(1):33-44.
198. Diamandis EP, van der Merwe DE. Plasma protein profiling by mass spectrometry for cancer diagnosis: opportunities and limitations. Clin Cancer Res. 2005;11(3):963-5.
199. Grill S, Rusterholz C, Zanetti-Dallenbach R, Tercanli S, Holzgreve W, Hahn S, et al. Potential markers of preeclampsia--a review. Reprod Biol Endocrinol. 2009;7:70.
200. Zeisler H, Llurba E, Chantraine FJ, Vatish M, Staff AC, Sennstrom M, et al. The sFlt-1/PlGF Ratio: ruling out pre-eclampsia for up to 4 weeks and the value of retesting. Ultrasound Obstet Gynecol. 2018.
201. Zeisler H, Llurba E, Chantraine F, Vatish M, Staff AC, Sennstrom M, et al. Predictive Value of the sFlt-1:PlGF Ratio in Women with Suspected Preeclampsia. N Engl J Med. 2016;374(1):13-22.
202. Chatterjee S, Bhattacharya S, Socinski MA, Burns TF. HSP90 inhibitors in lung cancer: promise still unfulfilled. Clin Adv Hematol Oncol. 2016;14(5):346-56.
203. Jego G, Hazoume A, Seigneuric R, Garrido C. Targeting heat shock proteins in cancer. Cancer Lett. 2013;332(2):275-85.
204. Chatterjee S, Burns TF. Targeting Heat Shock Proteins in Cancer: A Promising Therapeutic Approach. Int J Mol Sci. 2017;18(9).
205. Mahalingam D, Swords R, Carew JS, Nawrocki ST, Bhalla K, Giles FJ. Targeting HSP90 for cancer therapy. Br J Cancer. 2009;100(10):1523-9.
206. Kumalo HM, Bhakat S, Soliman ME. Heat-shock protein 90 (Hsp90) as anticancer target for drug discovery: an ample computational perspective. Chem Biol Drug Des. 2015;86(5):1131-60.
207. Li QQ, Hao JJ, Zhang Z, Krane LS, Hammerich KH, Sanford T, et al. Proteomic analysis of proteome and histone post-translational modifications in heat shock protein 90 inhibition-mediated bladder cancer therapeutics. Sci Rep. 2017;7(1):201.
208. Miyata Y, Nakamoto H, Neckers L. The therapeutic target Hsp90 and cancer hallmarks. Curr Pharm Des. 2013;19(3):347-65.
209. Mollapour M, Neckers L. Post-translational modifications of Hsp90 and their contributions to chaperone regulation. Biochim Biophys Acta. 2012;1823(3):648-55.
210. Maine GT, Sinha P, Tye BK. Mutants of S. cerevisiae defective in the maintenance of minichromosomes. Genetics. 1984;106(3):365-85.

211. Randell JC, Fan A, Chan C, Francis LI, Heller RC, Galani K, et al. Mec1 is one of multiple kinases that prime the Mcm2-7 helicase for phosphorylation by Cdc7. Mol Cell. 2010;40(3):353-63.
212. Fei L, Xu H. Role of MCM2-7 protein phosphorylation in human cancer cells. Cell Biosci. 2018;8:43.
213. Han X, Mayca Pozo F, Wisotsky JN, Wang B, Jacobberger JW, Zhang Y. Phosphorylation of Minichromosome Maintenance 3 (MCM3) by Checkpoint Kinase 1 (Chk1) Negatively Regulates DNA Replication and Checkpoint Activation. J Biol Chem. 2015;290(19):12370-8.
214. Drissi R, Dubois ML, Douziech M, Boisvert FM. Quantitative Proteomics Reveals Dynamic Interactions of the Minichromosome Maintenance Complex (MCM) in the Cellular Response to Etoposide Induced DNA Damage. Mol Cell Proteomics. 2015;14(7):2002-13.
215. Guzel C, van den Berg CB, Duvekot JJ, Stingl C, van den Bosch TPP, van der Weiden M, et al. Quantification of Calcyclin and Heat Shock Protein 90 in Sera from Women with and without Preeclampsia by Mass Spectrometry. Proteomics Clin Appl. 2018:e1800181.
216. van den Berg CB, Duvekot JJ, Guzel C, Hansson SR, de Leeuw TG, Steegers EA, et al. Elevated levels of protein AMBP in cerebrospinal fluid of women with preeclampsia compared to normotensive pregnant women. Proteomics Clin Appl. 2017;11(1-2).
217. Bliek BJ, Guzel C, de Klein A, Stingl C, Luider TM, Lindemans J, et al. Peptide fingerprinting of folate-responsive proteins in human B lymphoblasts and orofacial clefting. Eur J Clin Invest. 2012;42(7):738-50.
218. Kaletas BK, van der Wiel IM, Stauber J, Lennard JD, Guzel C, Kros JM, et al. Sample preparation issues for tissue imaging by imaging MS. Proteomics. 2009;9(10):2622-33.
219. Dekker LJ, Burgers PC, Guzel C, Luider TM. FTMS and TOF/TOF mass spectrometry in concert: identifying peptides with high reliability using matrix prespotted MALDI target plates. J Chromatogr B Analyt Technol Biomed Life Sci. 2007;847(1):62-4.
220. Bliek JB, de Klein A, Luider TM, Lindemans J, Hulsman L, Guzel C, et al. New approach for the identification of folate-related pathways in human embryogenesis. Cell Mol Biol (Noisy-le-grand). 2004;50(8):939-44.

Appendices

List of publications
Portfolio
About the author

List of publications

This thesis

Güzel C, Stingl C, Klont F, Tans R, Willems E, Bischoff R, van Gool AJ, Luider TM, and the Biomarker Development Center Consortium. Carini et al. (eds.) for a book entitled 'Targeted Proteomics for Absolute Quantification of Protein Biomarkers in Serum and Tissues' in the series Handbook for Biomarkers in Precision Medicine (CRC Press). In press April 2019.

Güzel C, van den Berg CB, Duvekot JJ, Stingl C, van den Bosch TPP, van der Weiden M, Steegers EAP, Steegers-Theunissen RPM, Luider TM. Quantification of Calcyclin and Heat Shock Protein 90 in Sera from Women with and without Preeclampsia by Mass Spectrometry. Proteomics Clin Appl. 2018:e1800181.

Güzel C, Govorukhina NI, Wisman GBA, Stingl C, Dekker LJM, Klip HG, Hollema H, Guryev V, Horvatovich PL, van der Zee AGJ, Bischoff R, Luider TM. Proteomic alterations in early stage cervical cancer. Oncotarget. 2018;9(26):18128-18147.

Güzel C, Govorukhina NI, Stingl C, Dekker LJM, Boichenko A, van der Zee AGJ, Bischoff RPH, Luider TM. Comparison of Targeted Mass Spectrometry Techniques with an Immunoassay: A Case Study for HSP90alpha. Proteomics Clin Appl. 2018;12(1).

Schol PB, Güzel C, Steegers EA, de Krijger RR, Luider TM. Trophoblast calcyclin is elevated in placental tissue from patients with early pre-eclampsia. Pregnancy Hypertens. 2014;4(1):7-10.

Güzel C, Ursem NT, Dekker LJ, Derkx P, Joore J, van Dijk E, Ligtvoet G, Steegers EA, Luider TM. Multiple reaction monitoring assay for pre-eclampsia related calcyclin peptides in formalin fixed paraffin embedded placenta. J Proteome Res. 2011;10(7):3274-3282.

Other publications

van den Berg CB, Duvekot JJ, Güzel C, Hansson SR, de Leeuw TG, Steegers EA, Versendaal J, Luider TM, Stoop MP. Elevated levels of protein AMBP in cerebrospinal fluid of women with preeclampsia compared to normotensive pregnant women. Proteomics Clin Appl. 2017;11(1-2).

Boichenko AP, Govorukhina N, Klip HG, van der Zee AG, Güzel C, Luider TM, Bischoff R. A panel of regulated proteins in serum from patients with cervical intraepithelial neoplasia and cervical cancer. J Proteome Res. 2014;13(11):4995-5007.

Liu NQ, Dekker LJ, Stingl C, Güzel C, De Marchi T, Martens JW, Foekens JA, Luider TM, Umar A. Quantitative proteomic analysis of microdissected breast cancer tissues: comparison of label-free and SILAC-based quantification with shotgun, directed, and targeted MS approaches. J Proteome Res. 2013;12(10):4627-4641.

Bliek BJ, Güzel C, de Klein A, Stingl C, Luider TM, Lindemans J, Steegers EA, Steegers-Theunissen RP. Peptide fingerprinting of folate-responsive proteins in human B lymphoblasts and orofacial clefting. Eur J Clin Invest. 2012;42(7):738-750.

Stingl C, van Vilsteren FG, Güzel C, Ten Kate FJ, Visser M, Krishnadath KK, Bergman JJ, Luider TM. Reproducibility of protein identification of selected cell types in Barrett's esophagus analyzed by combining laser-capture microdissection and mass spectrometry. J Proteome Res. 2011;10(1):288-298.

Kaletas BK, van der Wiel IM, Stauber J, Lennard JD, Güzel C, Kros JM, Luider TM, Heeren RM. Sample preparation issues for tissue imaging by imaging MS. Proteomics. 2009;9(10):2622-2633.

de Groot CJ, Güzel C, Steegers-Theunissen RP, de Maat M, Derkx P, Roes EM, Heeren RM, Luider TM, Steegers EA. Specific peptides identified by mass spectrometry in placental tissue from pregnancies complicated by early onset preeclampsia attained by laser capture dissection. Proteomics Clin Appl. 2007;1(3):325-335.

Dekker LJ, Burgers PC, Güzel C, Luider TM. FTMS and TOF/TOF mass spectrometry in concert: identifying peptides with high reliability using matrix prespotted MALDI target plates. J Chromatogr B Analyt Technol Biomed Life Sci. 2007;847(1):62-64.

de Groot CJ, Steegers-Theunissen RP, Güzel C, Steegers EA, Luider TM. Peptide patterns of laser dissected human trophoblasts analyzed by matrix-assisted laser desorption/ionisation-time of flight mass spectrometry. Proteomics. 2005;5(2):597-607.

Bliek JB, de Klein A, Luider TM, Lindemans J, Hulsman L, Güzel C, de Groot CJ, Steegers-Theunissen RP. New approach for the identification of folate-related pathways in human embryogenesis. Cell Mol Biol (Noisy-le-grand). 2004;50(8):939-944.

Portfolio

Name: Coşkun Güzel
Erasmus MC Department: Neurology
Research School: Molecular Medicine
PhD period: 2013-2018
Promoters: Prof. dr. P.A.E. Sillevis Smitt
Prof. dr. E.A.P. Steegers
Co-promoter: Dr. T.M. Luider

1. Training	Year	ECTS
General courses and Academic Skills		
• Basic Course on R, Erasmus MC	2010	0.3
• Course Biomedical Research Techniques, Erasmus MC	2010	0.6
Mass spectrometry courses		
• Ion Mobility, American Society for Mass Spectrometry, St. Louis, Missouri	2015	0.6
Conferences, seminars, workshops and meetings		
• Weekly neurology/clinical proteomics research meetings	2013-2018	2.0
• Weekly JNI scientific meetings	2013-2018	2.0
• American Society for Mass Spectrometry, Minneapolis, Minnesota	2013	1.5
• American Society for Mass Spectrometry, St. Louis, Missouri	2015	1.5
• Workshop Ingenuity Pathway Analysis (IPA, Erasmus MC)	2016	0.4
• 4th Daniel den Hoed Day & Kick Off Daniel den Hoed Cancer Core Facilities, Erasmus MC	2016	0.3
• 5th Daniel den Hoed Day, Erasmus MC	2016	0.3
• Validation of Biomarkers , de Doelen, Rotterdam	2017	0.3
• Erasmus MC Cancer Institute Research Day, Erasmus MC	2018	0.3
Oral presentations		
• Research meetings Neurology, Erasmus MC	2013-2018	4.5
• Research meetings Cervical Cancer, Rijksuniversiteit, Groningen	2013-2018	4.5
• Research meetings Obstetrics and Gynecology, Erasmus MC	2013	0.9
• Waters MS Technical Days, Utrecht	2015	1.5
• Fabian symposium, Janssen R&D, Beerse, Belgium	2016	1.5
Poster Presentations at (inter)national conferences		
• American Society for Mass Spectrometry, Minneapolis, Minnesota	2013	1.0
• American Society for Mass Spectrometry, St. Louis, Missouri	2015	1.0
• HUPO, Dublin, Ireland	2017	1.0
• Molecular Medicine Day, Rotterdam	2018	0.7

2. Teaching		
• Supervising Master students/HLO technicians	2013-2018	4.0
Total:		30.7

About the author

Coşkun Güzel was born on August 12, 1979 in Çayıralan (Turkey). After having completed his secondary laboratory education at the Reynevelt College in Delft in 1999, he continued his education at the Hogeschool Rotterdam. In 2002 he obtained his bachelor in Biology & Medical Laboratory Research after which he started working as a technician at the Pathology department of Erasmus MC. His work at the Department of Pathology was mainly routine, and soon he noticed that he wanted more challenges and also that he had an affinity for research using new technologies. In 2003 he obtained a position at the Department of Neurology as a research technician with a focus on mass spectrometry. Under the guidance of dr. Theo Luider, he conducted research on biomarkers related to the diseases preeclampsia (in collaboration with prof. dr. Eric Steegers) and cervical cancer (in collaboration with prof. dr. Rainer Bischoff). Not much later in 2004, his first article was published (co-author), followed by a second and third article in 2005 and 2007 (co-author). In 2007 his first publication on preeclampsia appeared with contributing first authorship. During this work, he was proposed to become a PhD student to write his dissertation. In 2013 he started his PhD research at the Department of Neurology, Clinical & Cancer Proteomics of the Erasmus MC. The goal of this research was to identify biomarker candidates in affected tissues related to preeclampsia and cervical cancer using laser capture microdissection and mass spectrometry. His first publication on cervical cancer appeared in 2014 (co-author). Both preeclampsia and cervical cancer studies ran parallel, the results of which are described in this thesis.